

Investigation of Heat Exchangers for a Solar Domestic Hot Water System

by

Elie Latouf

Submitted in partial fulfillment of the requirements
for the degree of Master of Applied Science

at

Dalhousie University
Halifax, Nova Scotia

October 2024

“Peace cannot be kept by force; it can only be achieved by understanding. Just as in nature, balance is achieved when energy flows freely, without unnecessary resistance.

Albert Einstein

TABLE OF CONTENTS

List of Tables	viii
List of Figures.....	ix
Abstract.....	xii
List of Abbreviations and Symbols Used.....	xiii
Acknowledgements	xvi
Chapter 1. Introduction	1
1.1. Background	1
1.2. Objective	3
1.3. Scope of the Study	4
Chapter 2. Literature Review	6
2.1. Previous Studies on Heat Exchangers.....	6
2.2. Shell and Tube	9
2.3. Shell and Twisted Tube	9
2.4. Brazed Plate	10
2.5. Shell and Four Coils Heat Exchanger (S4CHX).....	13
Chapter 3. Experimental Procedure	14

3.1. Introduction.....	14
3.2. Experimental System	14
3.2.1. Web Energy Logger.....	16
3.2.2. Glycol Loop	17
3.2.3. Pump	19
3.2.4. Electric Element.....	20
3.2.5. Flow Meter.....	20
3.2.6. Pulse Meter	21
3.2.7. Flow Meter Calibration.....	21
3.3. Heat Exchanger	22
3.3.1. Brazed Plate	23
3.3.2. Shell and Twisted Tube	24
3.3.3. Shell and Tube	25
3.4. Water Tank.....	26
3.5. Conclusion	27
Chapter 4. Theoretical Background.....	28
4.1. Introduction.....	28
4.2. General Considerations.....	28

4.3. Hydraulic Analysis.....	30
4.3.1. Flow in a Circular Duct.....	32
4.3.2. Flow Between Two Plates	33
4.3.3. Pressure Drop in Fittings	34
4.4. Thermal Analysis	36
4.4.1. Overall Heat Transfer Coefficient	36
4.4.2. Forced Convection	38
4.4.2.1. Shell and Tube	38
4.4.2.2. Brazed Plate Forced Convection.....	39
4.4.3. Natural Convection	40
4.4.3.1. Shell and Tube	41
4.5. Temperature Distribution in the Tank.....	42
4.6. Iterative Process	43
Chapter 5. Results.....	46
5.1. Introduction.....	46
5.2. Glycol Flow Rate	47
5.3. Temperature Distribution in the Water Tank.....	48
5.4. Water Flow Rate	51

5.4.1. Experimental and Analytical.....	51
5.4.2. Comparison between the Three Heat Exchangers	53
5.5. Flow Type in the Three Experiments.....	54
5.6. Comparing Data to the Manufacturer’s Specifications.....	55
5.6.1. Brazed Plate	55
5.6.2. Shell and Twisted Tube	58
5.7. Free and Forced Convection	60
5.8. UA Value Comparison.....	62
5.8.1. Analytical and Experimental Results of UA Value	63
5.8.2. UA Comparison of the Three Heat Exchangers	65
5.9. Overall Heat Transfer Coefficient	65
5.10. Comparison with Shell and Four Coils Heat Exchanger	66
Chapter 6. Conclusion and Summary.....	68
6.1. Summary.....	68
6.2. Conclusion	70
References.....	72
Appendix A.....	78
A.1. Code for Hydraulic Calculations.....	78

A.2. Code for Thermal Calculations	87
A.3. Code for Free and Forced Convection	92
A.4. Code for Catalogue Vs. Correlations	98
A.5. Code for Temperature Profile of Water Tank	105
Appendix B.....	109
B.1. Brazed Plate.....	109
B.2. Shell and Twisted Tube.....	110
B.3. Shell and Tube.....	111
B.4. Water Tank.....	112
Appendix C.....	113
C.1. Specific Heat of Propylene Glycol (40%).....	113
C.2. Thermal Conductivity of Propylene Glycol (40%)	114
C.3. Density of Propylene Glycol (40%).....	115
C.4. Dynamic Viscosity of Propylene Glycol (40/60).....	116
Appendix D.....	117
D.1. PL Heat Exchanger's Performance by SEC Ltd.	117
D.2. M14a Heat Exchanger's Performance by SEC Ltd.	118

LIST OF TABLES

Table 3.1 Experimental system apparatus	16
Table 3.2 Items of the glycol loop	19
Table 3.3 Brazed plate heat exchanger dimensions	23
Table 3.4 Shell and twisted tube dimensions.....	25
Table 3.5 Shell and tube dimensions	26
Table 4.1 K-value of fittings.....	35
Table 5.1 Glycol flow rate used in the experiment compared to literature.....	47
Table 5.2 Reynolds number at the glycol and water sides.....	54
Table 5.3 Reynolds number function of power and plates number	55
Table 5.4 Manufacture (SEC) specifications of different types of M14a.....	57
Table 5.5 Manufacture (SEC) specifications of PL-45.....	58
Table 5.6 Reynolds number of shell and twisted tube of SEC	59
Table 5.7 Error percentage between UA-values of the free and forced convection	62

LIST OF FIGURES

Figure 1.1 Heat exchangers: (a) Shell and Tube, (b) Shell and Twisted Tube, (c) Brazed Plate	1
Figure 2.1 Chevron (Corrugation) angle β	10
Figure 2.2 Symmetrical or asymmetrical arrangement of plates.	12
Figure 2.3 Glycol flow rate vs solar heat.....	13
Figure 3.1 Hot water solar system	14
Figure 3.2 Experimental system	15
Figure 3.3 Web logger device	17
Figure 3.4 Glycol loop	18
Figure 3.5 P24070M pump	20
Figure 3.6 Pulse meter	21
Figure 3.7 Flow rate of glycol in function of the pulses/min.....	22
Figure 3.8 Brazed plate heat exchanger	23
Figure 3.9 Shell and twisted tube.....	24
Figure 3.10 Shell and tube heat exchanger	25
Figure 3.11 Water tank	26
Figure 4.1 Glycol and water side of the system.....	29

Figure 4.2 General prespetive of the temperature profile in the system	31
Figure 4.3 Flow in a circlar pipe	32
Figure 4.4 Flow between two plates	33
Figure 4.5 Flow in a shell and tube heat exchanger.....	39
Figure 4.6 Flow in a brazed plate heat exchanger	40
Figure 4.7 Differential element of a cylindrical shap	42
Figure 4.8 The iterative process of the hydraulic analysis.....	44
Figure 4.9 The iterative process of the thermal analysis	45
Figure 5.1 Glycol flow rate of each experiment in function of electric power.....	48
Figure 5.2 Temperature distribution in the tank for the brazed plate	49
Figure 5.3 Temperature distribution in the tank for the shell and tube.....	50
Figure 5.4 Temperature distribution in the tank for the shell and twisted tube.....	50
Figure 5.5 Flow rate of water in the shell and tube	52
Figure 5.6 Flow rate of water in the shell and twisted tube	52
Figure 5.7 Flow rate of water in the brazed plate	53
Figure 5.8 Comparison of the water flow rate of the three experiments	54
Figure 5.9 UA-value of the brazed plate (SEC-Correlations).....	57
Figure 5.10 UA-value of the shell and twisted tube (SEC-Correlations)	59

Figure 5.11 UA of brazed plate at free and forced convection on water side.....	60
Figure 5.12 UA of shell and tube at free and forced convection on water side.....	61
Figure 5.13 UA of shell and twisted tube at free and forced convection on water side	61
Figure 5.14 Analytical and experimental UA-value of brazed plate heat exchanger ..	63
Figure 5.15 Analytical and experimental UA-value of shell and tube heat exchanger	64
Figure 5.16 Analytical and experimental UA-value of shell and twisted tube heat exchanger	64
Figure 5.17. UA-value of the three heat exchangers	65
Figure 5.18 U-value of the three heat exchangers	66
Figure 5.19 UA-value of the three heat exchangers, and the shell and 4-coils.....	67

ABSTRACT

This study evaluates the hydraulic and thermal performance of three heat exchangers used in hot water solar systems: shell and tube, shell and twisted tube, and brazed plate. The shell and tube heat exchanger is provided by Thermo Dynamics Ltd., while the brazed plate (type M14A) and shell and twisted tube (type PL45) models are supplied by SEC Ltd. SEC Ltd.'s data for the Brazed Plate and Shell and Twisted Tube heat exchangers are intended for high-power applications of 12 kW and above, however, this study investigates their performance at lower power levels, up to 3 kW.

In addition to these three heat exchangers, the study also includes a comparative analysis with a shell and coil heat exchanger, as studied by Gharbia (2010).

In the experimental setup, a 40% propylene glycol solution is circulated through one side of each heat exchanger, with water flowing through the other due to buoyancy-induced flow. The heat exchangers vary in surface area: Shell and Tube (0.36 m²), Shell and Twisted Tube (0.15 m²), Brazed Plate (0.14 m²).

The study indicates that the brazed plate heat exchanger has superior thermal performance compared to both the shell and twisted tube as well as shell and tube configurations. However, it exhibits lower performance in comparison to the shell and 4-coils heat exchanger, which is currently used by Thermo Dynamics Ltd. for hot water solar systems.

LIST OF ABBREVIATIONS AND SYMBOLS USED

<i>act</i>	Actual
<i>ave</i>	Average
<i>A</i>	Area, m ²
<i>C, n, x</i>	Constants
<i>CFD</i>	Computational fluid dynamics
<i>C_p</i>	Specific heat at constant pressure, $\frac{J}{kg.K}$
<i>D</i>	Diameter, m
<i>D_h</i>	Hydraulic tube diameter, m
<i>D_i</i>	Tube inner diameter, m
<i>D_o</i>	Tube outer diameter, m
<i>elec</i>	Electric
<i>EXP</i>	Experiment
<i>Gr</i>	Grashof number
<i>h</i>	Convection heat transfer coefficient, $\frac{W}{m^2.K}$
<i>K</i>	Thermal Conductivity, $\frac{W}{m.K}$

m	Mass, kg
Nu	Nusselt number
P	Pressure, Pa
\dot{Q}	Heat transfer rate, W
\dot{q}	Specific heat transfer rate, $\frac{W}{kg}$
t	Time, s
T	Temperature, °C
T_{hi}	Temperature inlet on the hot side, °C
T_{ho}	Temperature outlet on the hot side, °C
T_{ci}	Temperature inlet on the cold side, °C
T_{co}	Temperature outlet on the cold side, °C
\hat{u}	Specific internal energy, $\frac{kJ}{kg}$
u	Velocity, $\frac{m}{s}$
U	Overall heat transfer Coefficient, $\frac{W}{m^2.K}$
UA	Overall heat transfer coefficient-area product, $\frac{W}{K}$
V	Velocity, $\frac{m}{s}$

z	Height, m
β	Volumetric thermal expansion coefficient, K^{-1}
γ	Specific Weight, $\frac{N}{m^3}$
μ	Dynamic viscosity, $N \cdot \frac{s}{m^2}$
ν	Kinematic viscosity, $\frac{m^2}{s}$
ρ	Density, $\frac{kg}{m^3}$

ACKNOWLEDGEMENTS

I would like to express my deepest gratitude to my supervisor, **Dr. Peter Allen**, for his invaluable guidance, patience, and continuous support throughout the duration of this research. His expertise and encouragement were crucial in shaping this work and pushing me to achieve my best.

I would also like to extend my sincere thanks to my committee members, **Dr. Michal Cada** and **Dr. Ismet Ugursal**, for their insightful feedback, constructive suggestions, and valuable time. Their guidance has greatly contributed to the quality and depth of this thesis.

I am immensely grateful to **Paul Sajko, P.Eng**, for his invaluable assistance with the experiment, as well as to **Ed Russell** for his help in building the system. A special thanks goes to **Ross Stewart-Rankin** for his contributions, which were instrumental in completing this work.

I would like to thank my relatives in Halifax for their unwavering encouragement and support, and my parents in Lebanon for their constant love and belief in me. Their strength and encouragement, especially during the most challenging times, kept me motivated and focused throughout this journey.

Chapter 1. Introduction

1.1. Background

Solar systems for heating buildings and hot water tanks contribute to reducing operational expenses and achieving overall energy savings, by converting solar radiation into thermal energy.

A typical solar system uses heat exchangers to transfer the absorbed energy to the water. A heat exchanger is essential in such systems, as it plays a crucial role in transferring energy from one fluid to another.

In this study, the hydraulic and thermal performance of three heat exchangers. shell and tube, shell and twisted tube, and brazed plate—will be examined, as shown in Figure 1.1. Each type offers unique advantages and considerations, making them suitable for different applications in solar hot water systems.

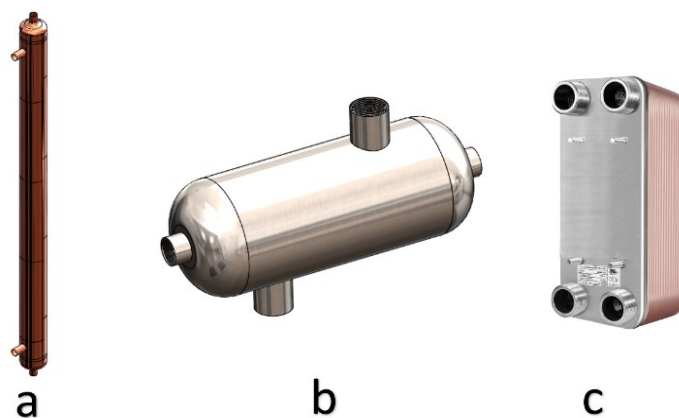


Figure 1.1 Heat exchangers: (a) Shell and Tube, (b) Shell and Twisted Tube, (c) Brazed Plate

Shell and tube heat exchangers are one of the most widely used heat exchanger designs in various industries, including solar hot water systems, Parent (1988). They consist of a large cylindrical shell with multiple smaller tubes running through it. For this study, we used a shell and tube heat exchanger manufactured by Thermo Dynamics Ltd.

In the context of heat transfer, twisted tube heat exchangers are an innovative design that offers enhanced thermal performance. These heat exchangers are designed similarly to shell and tube models, but they consist of twisted tubes instead of straight ones. Additionally, their compact design makes them suitable for installations with space limitations.

Brazed plate heat exchangers have been used in many applications due to their compact design and high heat transfer efficiency. They consist of a stack of corrugated plates that are brazed together.

In this study, the brazed plate and shell and twisted tube heat exchanger were produced by SEC Ltd.

In our investigation, the thermal and hydraulic behavior of the three heat exchangers will be analyzed by circulating a solution of 40% propylene glycol on one side of the heat exchanger and water on the other side. Propylene glycol will be pumped through the solar panels and heat exchanger, while water will circulate naturally due to the buoyancy-induced flow. The heat exchanger operates as a thermosyphon, providing natural convection to the water as the heated flow within it results in a lower density compared to the inlet flow. Consequently, this will lead to a difference in pressure between the extremities of the heat exchanger.

1.2. Objective

This research aims to conduct experimental analysis and analytical calculations to obtain and compare the hydraulic and thermal performance of three designs of heat exchangers: shell and tube, brazed plate, and twisted tube. The specific outlines are as follows:

1. **Comparison of heat exchanger designs:** the primary goal is to compare the thermal performance of the three heat exchangers in terms of the overall heat transfer coefficient-area (UA) product. The shell and tube have been provided by Thermo Dynamics (Ltd.), which is widely used in solar hot water systems. The brazed plat M14a-12 (12 Plates), and twisted tube PL 45 heat exchangers produced by SEC (Ltd.) represent a modern solution catering to high mass flow rates, which is not typical in hot water solar systems.
2. **Hydraulic Performance Analysis:** Another objective is to understand and analyze the hydraulic performance of the heat exchangers, particularly in terms of pressure drop, by measuring and analyzing pressure variations across the heat exchanger systems including the tank, pipes, and fittings. Additionally, we will determine the mass flow rate required to achieve at range of power output from 500 W to 3000 W. The brazed plate and twisted tube heat exchangers are designed for high power and mass flow rate applications, typically operating at around 70 Lpm and 60 kW, whereas our experimental setup entails a maximum power output of 3 kW and a flow rate less then 1.5 Lpm.

3. **Thermal Performance Analysis:** Through analytical calculations based on fundamental heat transfer principles, we endeavor to predict the thermal performance, specifically the UA-value, of the three heat exchanger configurations. By conducting analytical models and measuring the temperature and the mass flow rate across at the inlet and outlet of the three heat exchangers, we aim to investigate their heat transfer capabilities.
4. **Natural and Forced Convection Analysis:** Additionally, this research object is to evaluate the buoyancy -induced circulation of the water in the three heat exchangers.

1.3. Scope of the Study

Previous research has examined the efficacy of brazed plate and twisted tube heat exchangers in high-flow, high-power scenarios, Ibanez et al. (2019) and Naphon (2007). Parent (1988) conducted a comprehensive investigation, both experimental and numerical analyses of shell and tube heat exchangers in domestic water solar systems.

This investigation aims to evaluate the hydraulic and thermal performance of compact brazed plate and twisted tube heat exchangers in solar domestic hot water applications, where power and flow rates are constrained to less than 3 kW and 1-2 Lpm, respectively. The manufacturer of the brazed plate and shell and twisted tube heat exchangers, SEC Ltd., provided data for these models in high-power applications above 12 kW, as shown in Appendix D. However, this study focuses on performance under significantly lower power conditions, with a maximum of 3 kW. The performance of

these heat exchangers will be compared to the data sheets provided by SEC Ltd. to assess how well the findings align with the high-power data.

Furthermore, the performance of the brazed plate and twisted tube heat exchangers will be compared to the shell and tube exchanger. Additionally, all three heat exchangers will be evaluated against the shell and 4-coils heat exchanger, as studied by Gharbia (2010). This comparative analysis will offer insights into the thermal effectiveness and suitability of these heat exchangers for domestic hot water solar panel applications.

Chapter 2. Literature Review

2.1. Previous Studies on Heat Exchangers

Selbas et al. (2006) used an algorithm to find the appropriate heat exchanger design, while Leoni et al. (2017) reported in his paper that baffle clearances play an essential role in heat exchangers, by applying a numerical analysis in a shell and tube heat exchanger.

Shen et al. (2023) studied metal fluid as working fluid in helical-coiled heat exchangers. Subsequently, such fluids have a substantial thermal conductivity compared to the conventional ones, as it was declared by Shams et al. (2019) that “the thermal boundary layer is thicker than the momentum one”. Hoe et al. (1957) and Rickard et al. (1958) examined the thermal characteristics of mercury in a tube bank, which led them to find a correlation expression between Nusselt number and Peclet number.

Although Ibanez et al. (2019) set an experiment to examine the performance of a brazed plate heat exchanger using refrigerant as working fluid, a problem occurred during the experiment process which was presented by an ununiform distribution of fluid. Thus, this will affect the performance of the heat exchanger in case of using two-phase flow. Martins et al. (2022) investigated the structural behavior of two different geometry of plate heat exchanger to study the stress distribution of the pressure load. On the other hand, Adolfsson & Rashid (2016) detailed the failure of such systems, which occurred due to the high pressure and temperature gradient. In addition, Pelliccione (2019) studied the failure of titanium plate heat exchangers that are used for oil cooling by

water. Concerning the heat transfer phenomenon in such systems, Khanlari et al. (2019) analyzed numerically and experimentally using titanium and water nanofluid as working fluid. As results, the heat transfer coefficient enhanced by 6%.

Dagli & Ozbey (2023) studied the effect of hydrophobic coating on the thermal performance of the gasketed heat exchangers. They found that such coating led to better performance of heat exchange, while the average heat flux has been improved.

Kruthlventi et al. (2018) conducted an experimental and numerical study in coiled heat exchangers that focused mainly on the heat transfer between the two streams and the pressure drop inside the tubes, whereas Martynov & Krasnikova (1987) focused on the performance of three geometry of coiled tube that were differed by their coil diameter. The study showed that the heat transfer cannot be improved if the hydraulic-coil diameter ratio is less than 0.26.

A study conducted by Conté & Peng (2009) aimed to investigate the heat transfer behavior and the temperature distribution in a coil heat exchanger. While the study has been done on four straight pipes with 9, 15, 30 and 45 °s of inclination, the results were analyzed by changing Reynolds Number between 300 and 1400. This study was investigated numerically and experimentally, and it showed that the bundle tubes lead to turbulence without changing velocity.

CFD and experiment study done by Jayakumar et al. (2008) on a helical coil heat exchanger aimed to find the results error between both cases. The experiment was conducted at five different flow rates in the coil and three different temperatures on the helical side. The numerical and experimental results showed an acceptable error. Thus,

empirical correlations are used to find the pressure drop and the heat transfer coefficient in the inner tube.

Gupta et al. (2007) carried out an experimental study to determine heat transfer performance in a finned-tube heat exchanger. The experiment was conducted by applying a cross-counter flow and varying the Reynolds Number between 500 and 1900. The study investigated the values of the heat transfer coefficient for several mass flow rates and inlet temperatures.

To examine the convective heat transfer coefficient, an experiment was conducted by Coronel (2008) on a helical and straight tubular heat exchanger at turbulence. The used method allowed to find the overall heat transfer coefficient by monitoring the inlet and outlet temperature, and the mass flow rate. The correlations used for turbulence flow are verified, as they led to similar results as the experiment, under non-isothermal, and non-constant heat flux conditions. The fluid properties were calculated at the mean temperature, as well as Reynolds Number.

Hollands & Burnger (1991) carried out a study using an optimum flow rate in solar heating system by fixing the heat transfer coefficient (UA). On the other hand, Bojic et al. (2002) performed a simulation in aim to evaluate the solar fraction variation in function of the tank volume, hot water temperature needed and the consumption profile. Tanks with different volumes were used in this study, and the results showed that the systems with large volume of tanks need a higher solar fraction value. Thus, the results yield to show that the solar fraction and the water demand temperature are inversely proportional.

2.2. Shell and Tube

Maghsoudai et al. (2022) investigated shell and tube heat exchangers with low flow rates to improve the heat transfer coefficient in laminar streams. Their study compared three geometries: finless tubes, finned tubes, and optimized finned tubes. They found that adding fins increased the contact area and enhanced heat transfer.

Earlier research by Schlünder & Gaddis (1979) focused on the temperature distribution in shell and tube heat exchangers. Roppo & Ganl (1983) developed a transient model to assess thermal behavior over the time.

Leoni et al. (2017) emphasized the importance of baffle clearances in shell and tube heat exchangers. Milani et al. (2019) explored the role of wavy surfaces in enhancing heat exchanger performance.

2.3. Shell and Twisted Tube

Naphon (2007) experimentally investigated the performance of a shell and tube heat exchanger by incorporating twisted and finned tubes into the design, enhancing overall performance. Arani & Moradi (2019) examined the effects of different fin shapes, specifically triangular and circular, on the performance of shell and tube heat exchangers. Fazelpour et al. (2019) analyzed how the cross-sectional area affects the heat transfer coefficient and pressure drop in shell and tube heat exchangers, providing insights into optimizing their design.

2.4. Brazed Plate

Focke et al. (1985) established the relation between the inclination angle (Chevron angle, “ β ”) of the plate in the brazed plate heat exchanger and its thermohydraulic performance, as shown in Figure 2.1. Consequently, it has been proved that an angle of 80° can improve the fluid flow, as it passes through mainly the furrows of each plate. In the same paper, Focke et al. (1985) stated that the heat transfer and the pressure drop rise while β goes up to 60° , yet it decreases for a β angle between 60° and 80° . In addition, the flow patterns have been visualized at β angles of 45° , 80° and 90° . Hence, it is observed that the important notice was at $\beta = 90^\circ$, as the heat transfer at Reynolds number less than 300 is relatively small and it is referred to the small extra resistance that occurs due to the free shear layers.

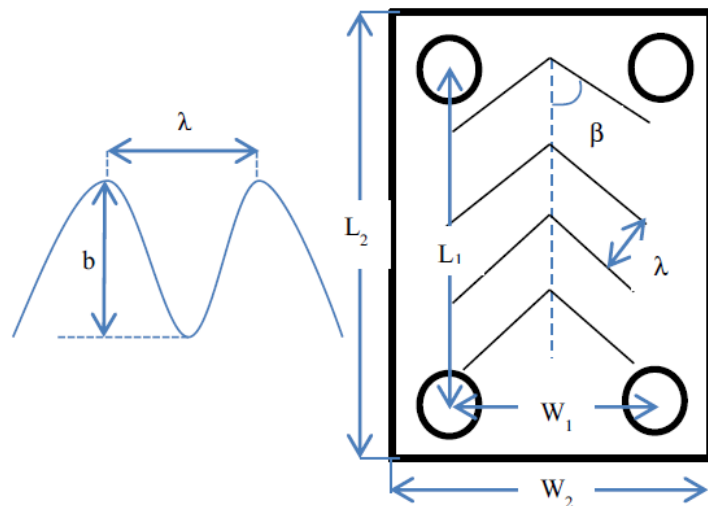


Figure 2.1 Chevron (Corrugation) angle β .

Mohebbi & Veysi (2019) stated several advantages of the pale heat exchanger, regarding the control of temperature, low cost, high durability, compactness, and high

efficiency. Although it has all these benefits, a brazed plate cannot operate at a temperature above 150°C. Brazed plate heat exchangers are known for their complex geometries due to the waved corrugated plates, which affect its the hydraulic-thermal behavior, based on Mohebbi & Veysi (2019). As it is mentioned in his paper, Mohebbi & Veysi (2019) shows that the chevron angle can be ranged between 30° and 60° with a symmetrical or asymmetrical arrangements, Figure 2.2. The apparatus of 60° chevron angle consists of 15 plates has been used with symmetrical geometry and made of stainless steel 316L. In the results, the heat transfer rate and the friction coefficient were obtained. During the experiment, the flow rate of the hot fluid changed, whereas that of the cold was at a constant value of 7 Lpm. The results showed that the thermal effectiveness was high at low Reynolds. With Reynolds increasing, the U increased, whilst “Q” remained steady. Mohebbi & Veysi (2019) declared that the heat transfer rate increased rapidly at a low Reynolds, however this phenomenon occurred due to the small exchanger size. The paper explained that with a high Reynolds number, the channels pass a high mass flow rate, and any increase in it will result a slight change in the heat transfer coefficient. In addition to the parameters that affected the hydrothermal efficiency, chevron angle and the corrugation aspect ratio have a crucial impact on the hydraulic-thermal behavior of compact brazed plate heat exchangers.

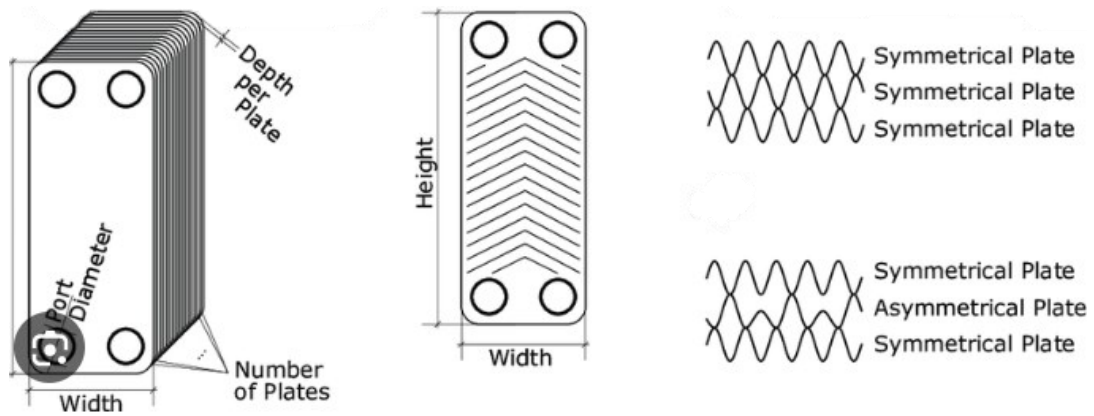


Figure 2.2 Symmetrical or asymmetrical arrangement of plates.

Saha & Khan (2020) studied numerically the thermohydraulic performance of a plate heat exchanger with a corrugation angle between 30° and 80° . In the same paper, it is observed that the pressure gradient increases with the Reynolds number and the corrugation angle. During this study, they used a stainless-steel apparatus with water and 70% propylene glycol as working fluids. Saha & Khan (2020) investigated the effect of the cross-corrugated angle (β) on the heat exchanger thermohydraulic performance by changing the angle between 30° and 80° . Subsequently, it is found that the friction factor drops with the increase of Reynolds number at the same corrugation angle. On the other hand, it increases with the increase of the corrugation angle at constant Reynolds. Moreover, the thermal efficiency leveled up from approximately 8% to 34% with increasing the corrugation angle from 30° to around 80° . The increase of thermal efficiency with the corrugation angle has been referred to the larger area and turbulent flow, (Saha & Khan, 2020).

2.5. Shell and Four Coils Heat Exchanger (S4CHX)

In a study conducted by Gharbia (2010), the thermal performance of a solar heat exchanger was analyzed with a focus on the glycol flow rate under varying conditions. The experiment was designed to simulate the operational dynamics of a solar collector system on a sunny day.

Gharbia (2010) methodology involved adjusting the power supplied to electrical heaters, beginning at 200 W and incrementally increasing to a maximum of 3000 W. The corresponding flow rates of glycol to each power value were varied and recorded, ranging from 0.90 Lpm at 200 W to 2.20 Lpm at 3000 W. Gharbia (2010) observed that higher heat transfer rates necessitated increased flow rates, which in turn enhanced the system's efficiency and resulted in greater temperature changes within the solar collector.

The experimental data, illustrated in Figure 2.3 of Gharbia (2010) work, shows the flow rate of glycol in function of the electric power.

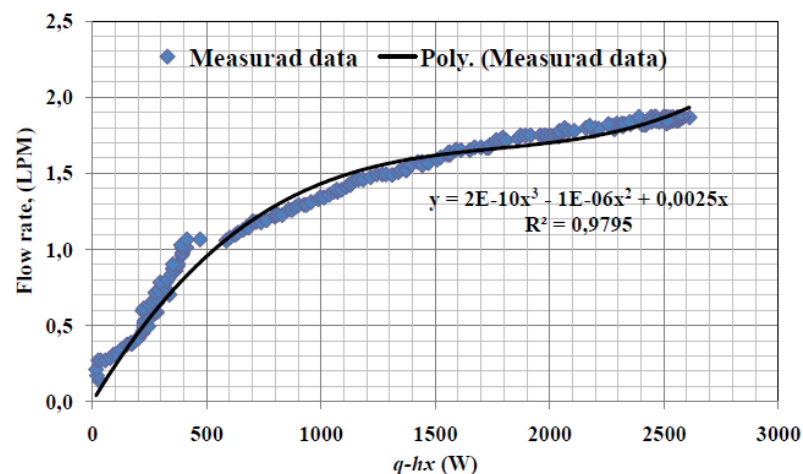


Figure 2.3 Glycol flow rate vs solar heat

Chapter 3. Experimental Procedure

3.1. Introduction

The setup includes two loops: one containing water and the other containing 40% propylene glycol. Water circulates through the heat exchanger due to buoyancy-induced flow, while the glycol is pumped through the other side of the heat exchanger. Figure 3.1 illustrates the key components commonly found in a typical domestic solar hot water system. To simulate the sun, an electric element will be used instead of the solar panel to power the system.

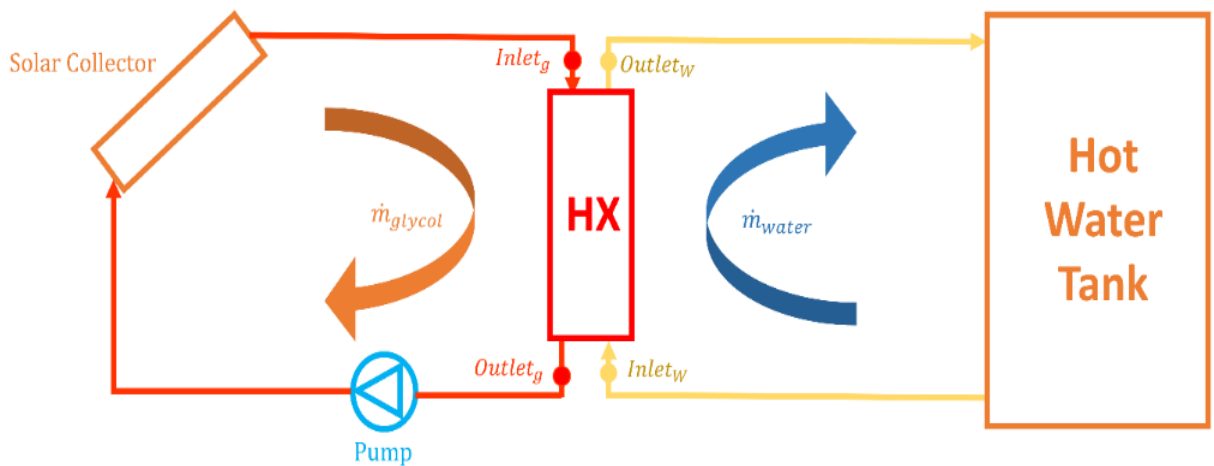


Figure 3.1 Hot water solar system

3.2. Experimental System

Figure 3.2 presents a schematic diagram of the experimental apparatus. In the schematic, solid red lines represent the working fluid, glycol, flowing from the electric element to the heat exchanger. The glycol system is connected to the heat exchanger by

nylon pipes. Blue dash-dotted lines indicate the wiring of the web energy logger connected to the temperature sensors, while dashed orange lines indicate the electrical connections between the variable transformer and the electric heater. The connection of all temperature sensors to a web energy logger facilitates the monitoring of both temperature variations and the flow pulse. All the components of the scheme are detailed in Table 3.1.

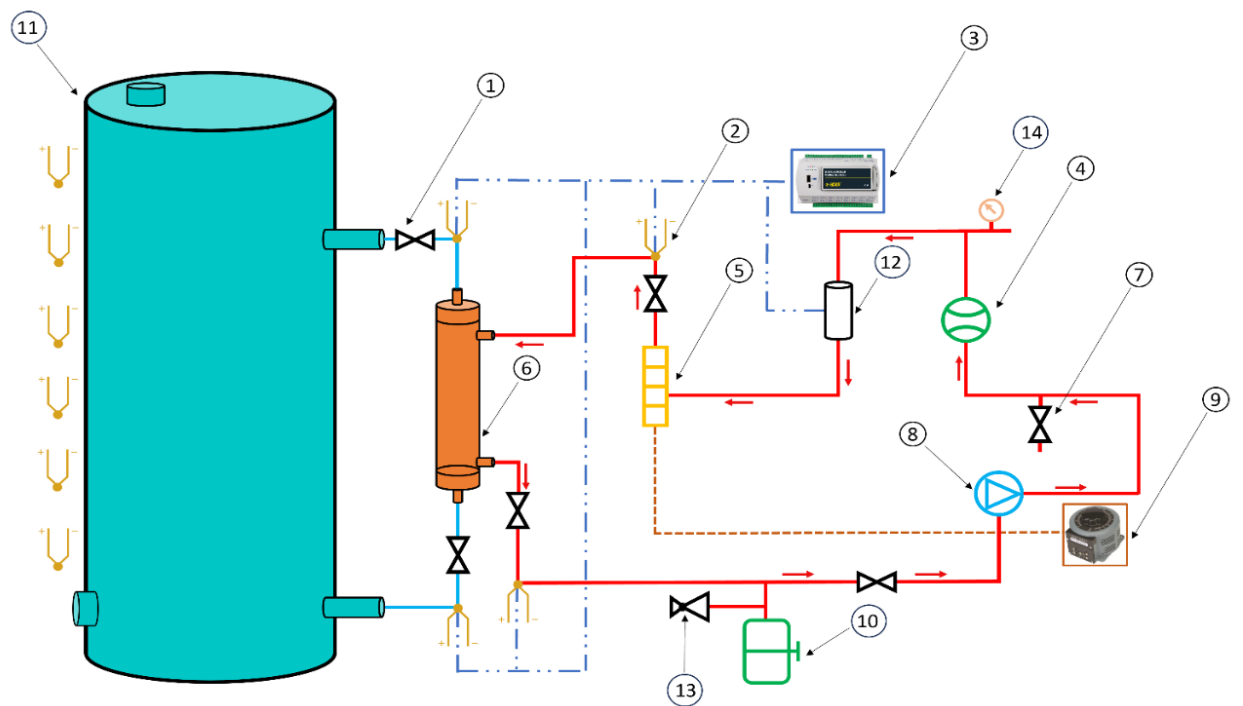


Figure 3.2 Experimental system

Item No.	Part	QTY.
1	Ball Valve	5
2	Temperature Sensor	10
3	Data Logger	1
4	Flow Meter	1
5	Electric Heating Element	1
6	Heat exchanger	1
7	Globe Valve	1
8	Pump	1
9	Variable Transformer	1
10	Expansion Tank	1
11	Water Tank	1
12	Pulse Meter	1
13	Expansion Valve	1
14	Pressure Gauge	1

Table 3.1 Experimental system apparatus

3.2.1. Web Energy Logger

The Web Energy Logger (WEL) from *OurCoolHouse.com* is designed to monitor and log a building's energy consumption. In this study, the WEL is utilized to measure the

temperatures of the water and the glycol, as well as the pulses from a flow meter on the glycol side. The WEL unit (Figure 3.3) is capable of reading numerous networked sensors (temperature and contact closure), six pulse-output devices (such as a wattmeter or flow meter), eight local contact closures, and two 0-10V analog inputs. The filtered data is presented on web pages hosted directly on the WEL and is also posted to the *WELServer.com* website via a standard 10-baseT Ethernet connection.

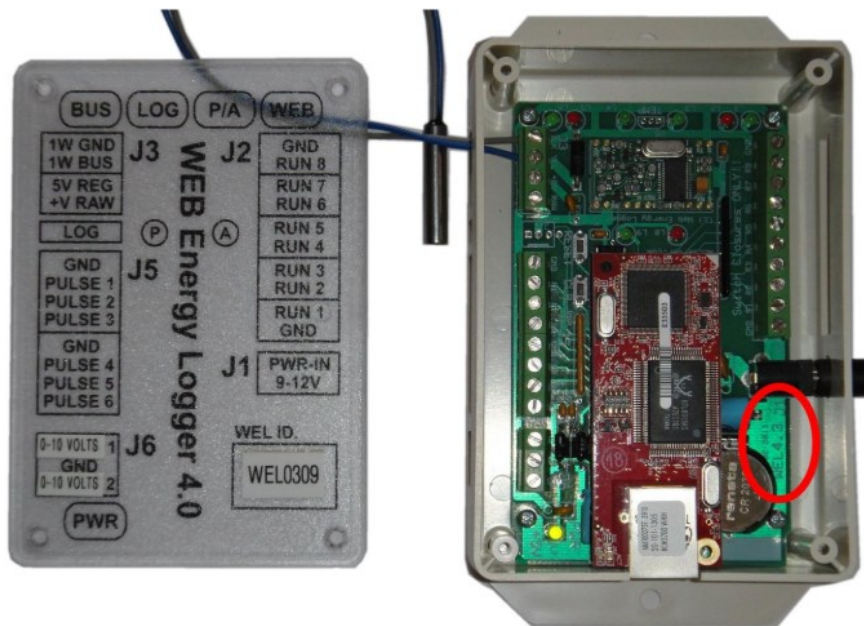


Figure 3.3 Web logger device

3.2.2. Glycol Loop

A 40% propylene glycol solution is pumped by a sliding-vane pump into an electric heater to heat the fluid. Figure 3.4 illustrates the detailed system, and Table 3.2 shows the description of each part.

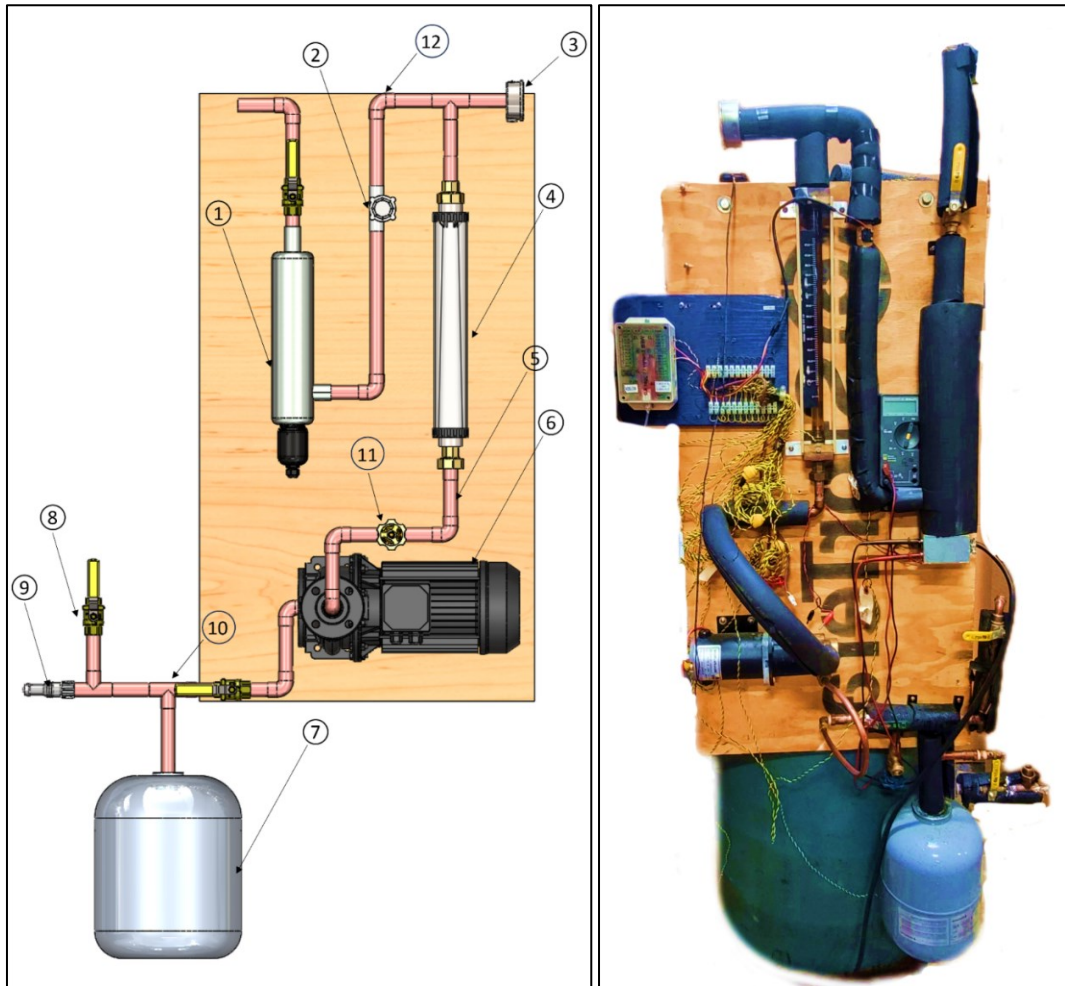


Figure 3.4 Glycol loop

The flow meter, positioned before the heater, measures the volumetric flow rate of the glycol. Two thermocouples are located at the extremities of the heat exchanger to monitor the temperature at the inlet and outlet. Four ball valves are used to control the flow rate and allow for the switching of heat exchangers during the experiment. An expansion tank, equipped with a pressure relieve valve (PRV), is installed to manage thermal expansion of the glycol and prevent excessive pressure.

Item No.	Part	Description	QTY.
1	Electric Element	3000 W	1
2	Pulse meter	½” Dia.	1
3	Pressure Gauge	½” Dia.	1
4	Flow Meter	½” Dia.	1
5	Pipe	½” Dia. - Type L	13
6	Pump	0.3 – 1.2 Lpm	1
7	Expansion Tank	-	1
8	Globe Valve	½” Dia.	1
9	Expansion Valve	½” Dia.	1
10	Tee	½” Dia.	3
11	Gate Valve	½” Dia	1
12	Elbow	1/2” Dia. - 90 Degree	8

Table 3.2 Items of the glycol loop

3.2.3. Pump

The pump is a model P24070M manufactured by Thermo Dynamics Ltd. (Figure 3.5) offering a flow rate range from 0.3 Lpm to 12 Lpm and a pressure up to 3.5 bar. This model incorporates a rotary vane pump driven by a DC motor, circulating a 40% glycol solution through the heat exchanger loop. The pump motor is powered by A DC power with variable voltage and current controls.

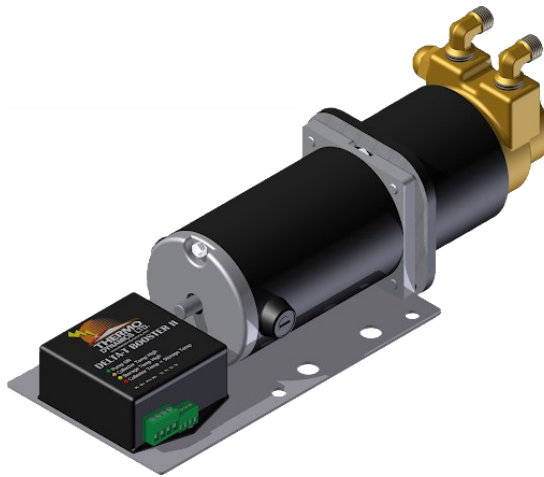


Figure 3.5 P24070M pump

3.2.4. Electric Element

An electric heating element served as the “solar collector” for heating the glycol solution. The electric element was powered with a variable transformer, allowing the capability to adjust its power output within a range of 100W to 3000W

3.2.5. Flow Meter

To measure the flow rate of glycol, a rotameter was used to record the gallons passing through per minute. This measurement was crucial for calculating the heat transfer rate discussed in Chapter 4.

3.2.6. Pulse Meter

A pulse meter (Figure 3.6) was also used to measure the glycol flow rate in terms of pulses per minute and was connected to the web energy logger (WEL). The calibration process for the pulse meter is detailed in the following paragraph.



Figure 3.6 Pulse meter

3.2.7. Flow Meter Calibration

The calibration of the flow meter was performed by running a glycol solution consisting of propylene glycol, 40% by volume, in water through the flow meter at different rates and measuring the flow rate by recording the time needed to collect a certain volume of glycol.

The flow meter, calibrated in GPM, was used to measure the total flow rates of the working fluid, with a flow measurement range of 0.01-1.00 GPM. The calibration plot

is shown in Figure 3.7 linear behavior of the flow in GPM as a function of the pulses per minute was observed, as shown in equation (3.1):

$$\text{GPM} = 5 \times 10^{-4} \frac{\text{Pulsed}}{\text{min}} + 0.153 \quad (3.1)$$

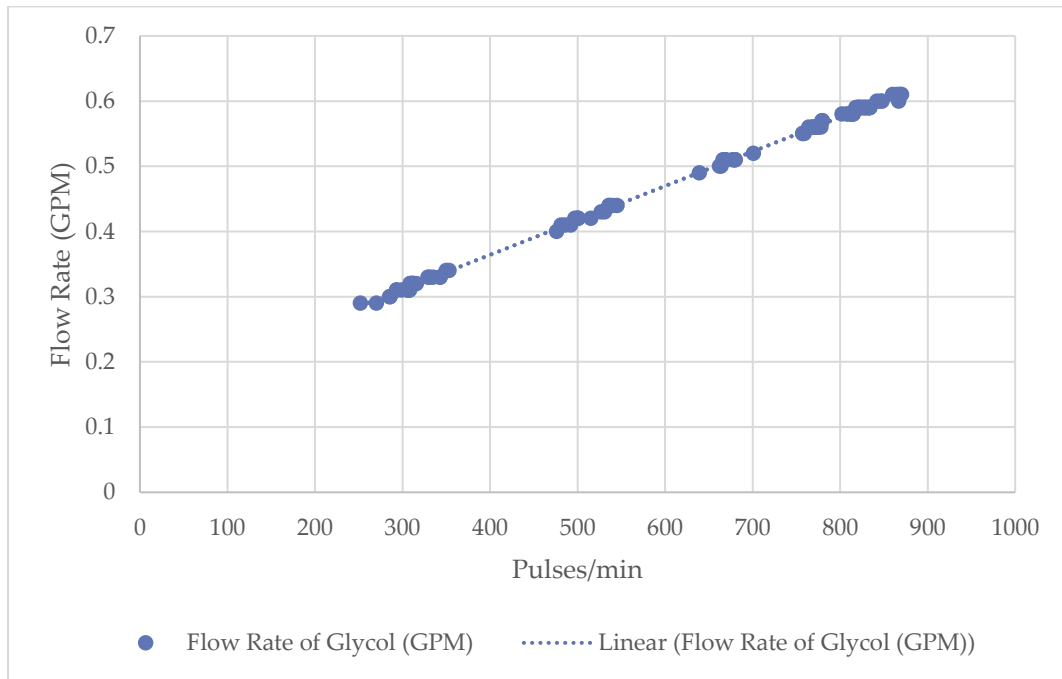


Figure 3.7 Flow rate of glycol in function of the pulses/min

3.3. Heat Exchanger

In this experiment, three heat exchangers will be evaluated both thermally and hydraulically. The brazed plate heat exchanger and the shell and twisted tube heat exchanger, both manufactured by SEC Ltd., are designed for high-power applications. The third heat exchanger, a shell and tube model made by Thermo Dynamics Ltd., is primarily intended for solar domestic hot water systems.

3.3.1. Brazed Plate

The brazed plate heat exchanger, model M14a-12 and manufactured by SEC Ltd., consists of 12 plates made of AISI 316 stainless steel and is designed primarily for 6 kW to 43 kW applications, as it is indicated in Appendix D Appendix D.2. In this experiment, its hydraulic and thermal performance will be tested for applications below 3 kW. Figure 3.8 and Table 3.3 show the geometry of the brazed heat exchanger.

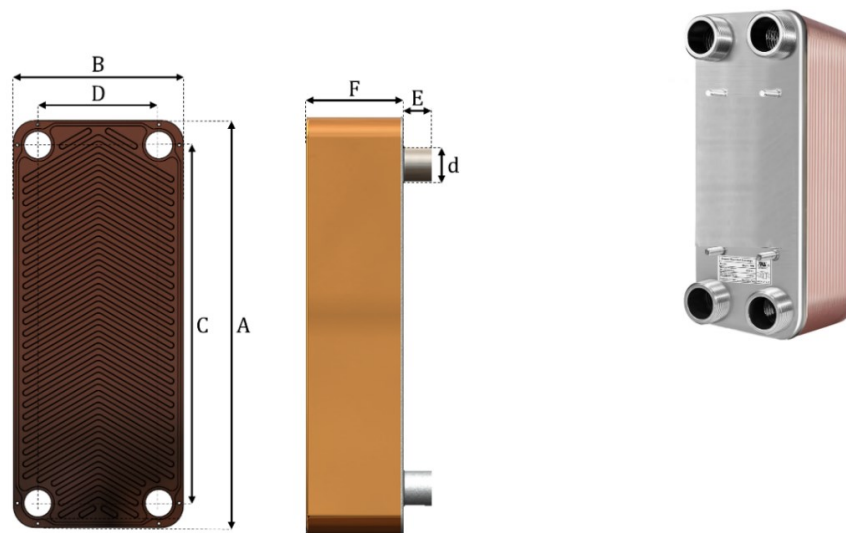


Figure 3.8 Brazed plate heat exchanger

	A	B	C	D	E	F	Np	d	Surface Area
Dimensions (in)	7.6	3.1	6.1	1.6	3/4	6.6	12	3/4" NPT	A = 0.15 m ²
Dimensions (mm)	193	79	155	40.6	19	168			

Table 3.3 Brazed plate heat exchanger dimensions

3.3.2. Shell and Twisted Tube

The shell and twisted tube heat exchanger, model PL-45 (Figure 3.9), is constructed from 316 stainless steel. It features 37 inner twisted tubes through which water circulates, while glycol flows through the outer shell. This type of heat exchanger is typically used for swimming pool applications with power requirements exceeding 13 to 290 kW, Appendix D.1. Figure 3.9 illustrates the geometry of the PL-45 heat exchanger. Table 3.4 shows the dimensions of the shell and twisted tube heat exchanger.

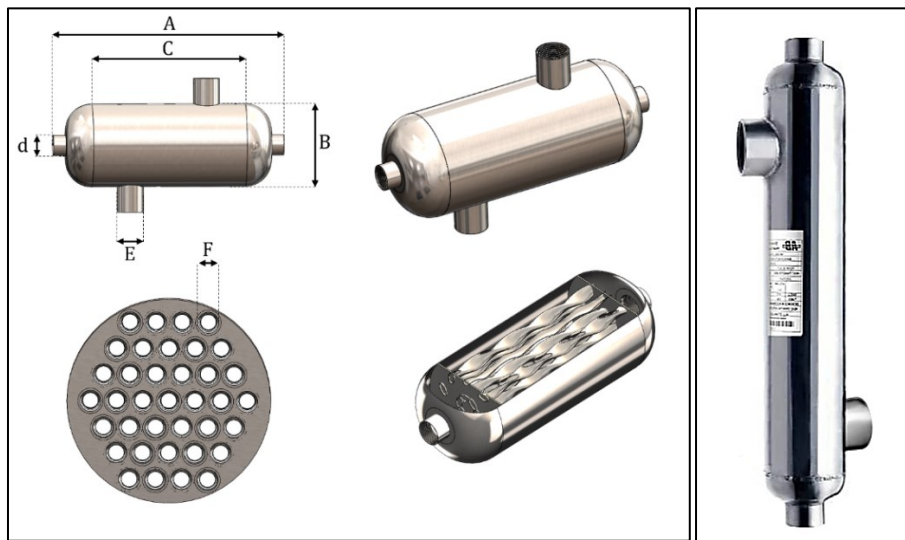


Figure 3.9 Shell and twisted tube

	A	B	C	D	E	F	d	Surface Area
Dimensions (in)	12	3.15	6	1.6	1" NPT	0.23	3/4" NPT	$A_i = 0.15 \text{ m}^2$
Dimensions (mm)	305	80	152	40.6	19	6		$A_o = 0.17 \text{ m}^2$

Table 3.4 Shell and twisted tube dimensions

3.3.3. Shell and Tube

The Shell and Tube heat exchanger, manufactured by Thermo Dynamics Ltd., features copper tubes and has a length of 130 cm. It includes an outer pipe with a nominal diameter of 2 inch and seven inner tubes, each with a diameter of $\frac{1}{2}$ inch. Water flows through the inner tubes, while glycol circulates in the shell. This heat exchanger is primarily designed for solar domestic hot water applications, facilitating heat transfer from glycol to a water tank. Figure 3.10 and Table 3.5 show the detailed geometry of the shell and tube heat exchanger.

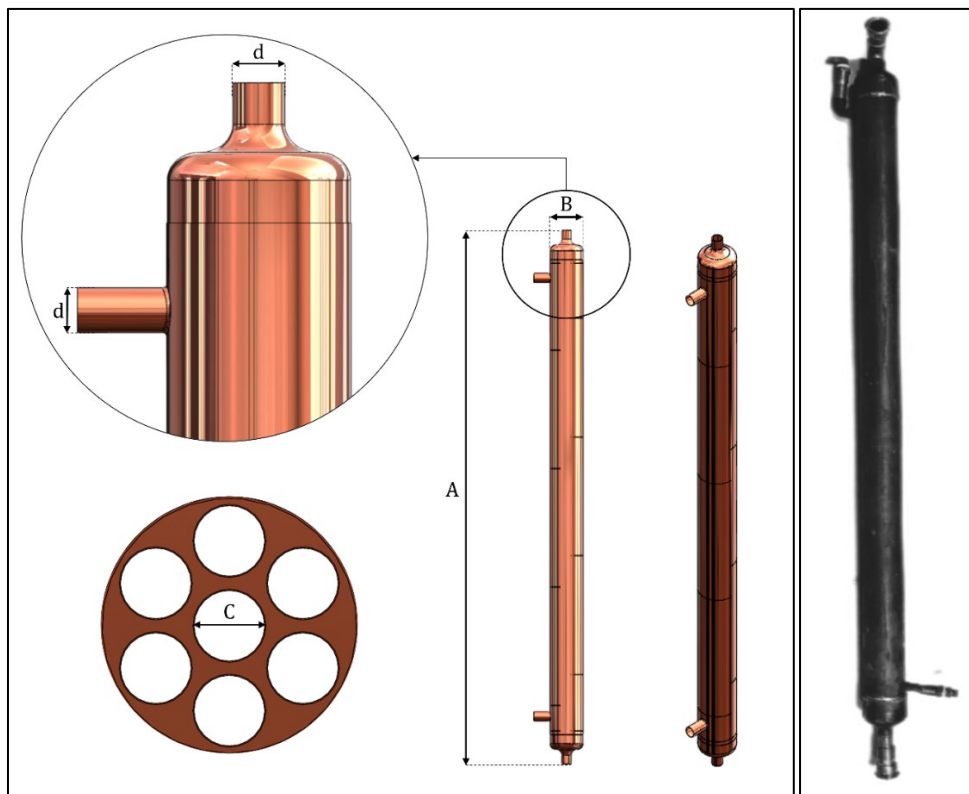


Figure 3.10 Shell and tube heat exchanger

	A	B	C	d	Surface Area
Dimensions (in)	52	2	½"	¾"	$A_i = 0.37 \text{ m}^2$
Dimensions (mm)	305	51	13	19	$A_o = 0.39 \text{ m}^2$

Table 3.5 Shell and tube dimensions

3.4. Water Tank

The water (Figure 3.11) tank has a capacity of 454 liters (120 US gallons) and is used to store hot water. Water flows from the bottom of the tank to the heat exchanger and then returns to the top of the tank.

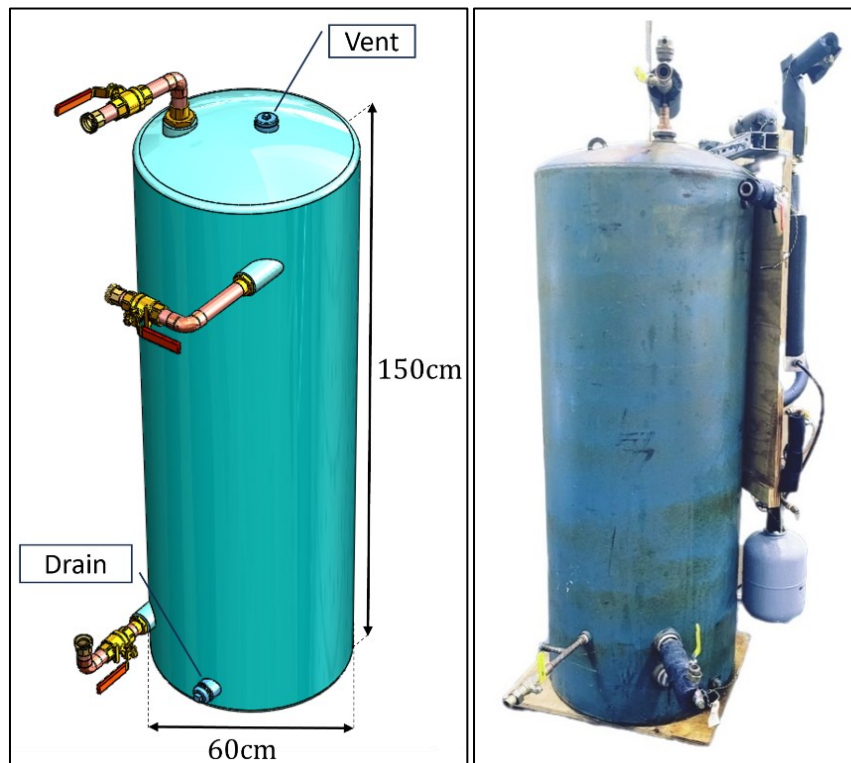


Figure 3.11 Water tank

3.5. Conclusion

The experimental procedure involved collecting critical data to evaluate the performance of three heat exchangers: brazed plate, shell and tube, and shell and twisted tube. This included recording the temperature profile of the water tank at six points and measuring the flow rate of the glycol. These steps were essential for assessing the thermal performance of each heat exchanger. The data gathered will be analyzed in Chapter 5. This procedure effectively sets the stage for a thorough evaluation of the heat exchangers' efficiency and their performance for the solar domestic hot water system.

Chapter 4. Theoretical Background

4.1. Introduction

This chapter establishes correlations describing the thermal and hydraulic characteristics of each heat exchanger. Evaluating the performance involves employing various correlations derived from literature and prior research. These correlations are utilized to derive analytical results and compare them with experimental findings. The analytical calculations and results were performed using a programming language with the iterative method (Appendix A).

Several assumptions were adopted to facilitate the evaluation of the heat exchangers:

- i. Steady-state conditions are assumed.
- ii. The interior surface of the wall maintains uniform temperatures.
- iii. The external wall is well-insulated.
- iv. Thermophysical properties are uniform across the water cross-sectional area.
- v. Thin wall is assumed

4.2. General Considerations

The thermal and hydraulic analysis of three heat exchangers assumes a steady state with a constant mass flow rate of water. The inlet water temperature and electric element power (P_{elec}) are held constant throughout the study. The water and glycol sides of the

system (Figure 4.1) are treated as closed cycles (White, 2009), ensuring mass flow rate conservation and enabling the application of continuity equations (4.1), and (4.2).

$$\frac{\partial}{\partial z}(\rho v_z) = 0 \quad (4.1)$$

$$\sum_i (\rho UA)_{in} = \sum_i (\rho UA)_{out} \quad (4.2)$$

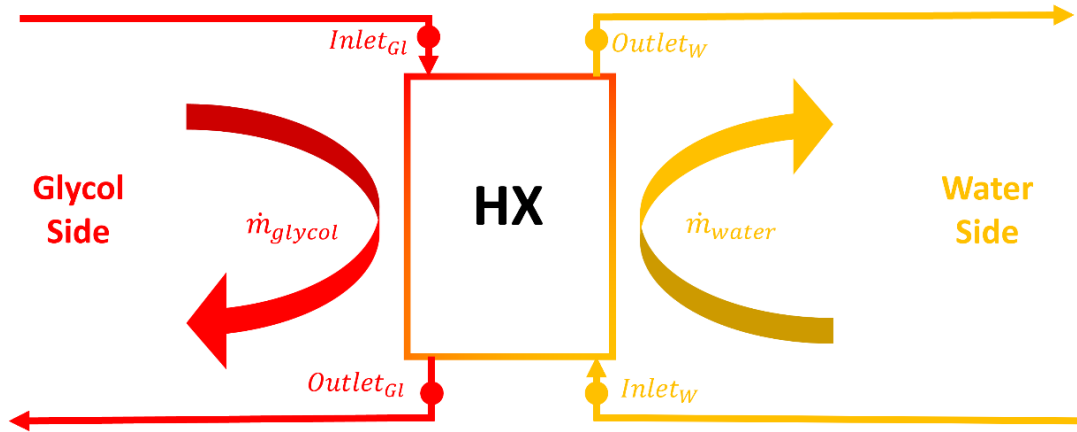


Figure 4.1 Glycol and water side of the system

To analyze the thermal performance of the heat exchangers, the energy equation (4.3) was used and expanded into equation (4.4), where the change in potential energy is considered, (Reisel, 2016).

$$d\dot{Q} = \frac{dm}{dt} \left(\hat{u} + \frac{P}{\rho} + gz \right) \quad (4.3)$$

$$\left(\frac{P}{\rho} + gz \right)_{in} = \left(\frac{P}{\rho} + gz \right)_{out} + (\hat{u}_2 - \hat{u}_1) + dq \quad (4.4)$$

The heat is transferred to the water through the heat exchanger and the flow is driven by buoyancy natural circulation. Thus, the shear head loss h_f , equation (4.5), is due to the change in internal energy and heat transfer:

$$\frac{\hat{u}_2 - \hat{u}_1 + dq}{g} = h_f \quad (4.5)$$

Now, the general equation (4.6) can be written as, (White, 2009):

$$\left(\frac{P}{\gamma} + z\right)_{in} = \left(\frac{P}{\gamma} + z\right)_{out} + h_f \quad (4.6)$$

4.3. Hydraulic Analysis

A hydraulic analysis was conducted on the water side to determine the flow rate and outlet temperature of the water. The pressure-drop across the entire system (ΔP) is the sum of the drag force imposed by the heat exchanger surfaces on the flowing fluid and the hydrostatic head, which depends on the density of the water, as shown in equation (4.7).

$$\oint dP = h_f + \int_0^H \rho(z)gdz \quad (4.7)$$

The solution of equation (4.8) is as following:

$$\Delta P = \rho gH + \frac{64 L_e V^2}{Re D 2g} \quad (4.8)$$

Where: $h_f = f \frac{L_e V^2}{D 2g}$

Considering a laminar flow: $f = \frac{64}{Re}$

At any instant the total pressure difference will be equal to zero (equation (4.9):

$$\oint dP = 0 \Rightarrow \Delta P = 0 \quad (4.9)$$

Now, equation (4.10) is a general formula that describes the hydrologic behavior of the flow in the heat exchangers pipes and fittings.

$$\rho g H + \frac{64 L_e V^2}{Re D 2g} = 0 \quad (4.10)$$

For accurate results, the system was divided into three temperature regions: inlet, outlet, and heat exchanger, as shown in Figure 4.2 The properties of water were determined at the temperature of each region.

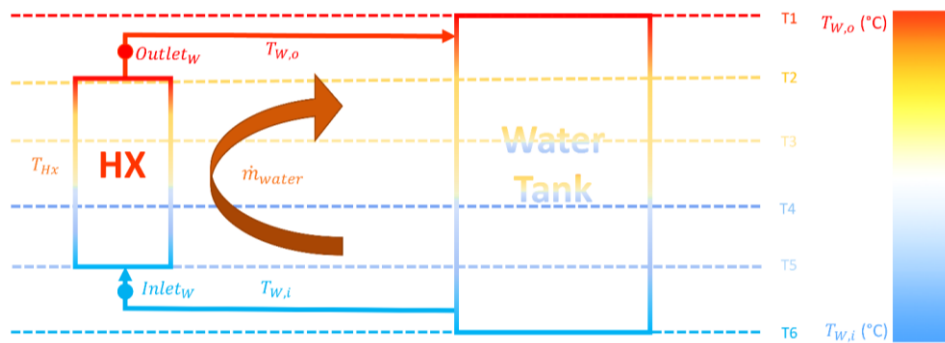


Figure 4.2 General perspective of the temperature profile in the system

4.3.1. Flow in a Circular Duct

The system consists of circular pipes, and two of the heat exchangers are of the shell-and-tube type, necessitating a study of the pressure drop in a circular pipe. Figure 4.3 shows the velocity profile in a pipe.

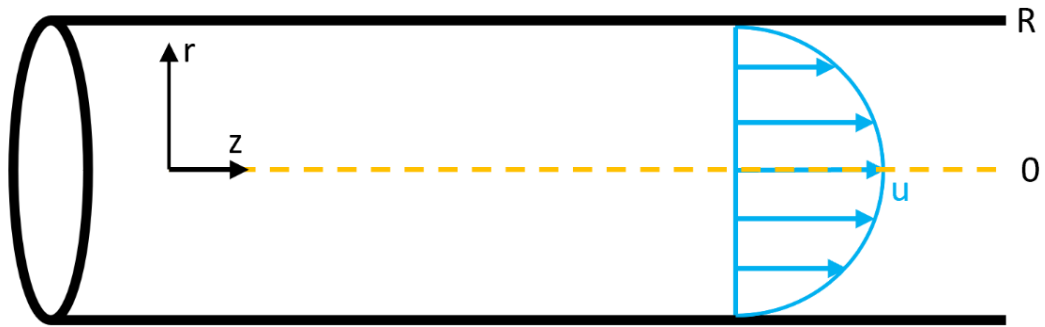


Figure 4.3 Flow in a circular pipe

Equation (4.11) describes the velocity profile of the flow in cylindrical form.

$$u(r) = \frac{-dP}{dz} \frac{R^2}{4\mu} \left(1 - \frac{r^2}{R^2}\right) \quad (4.11)$$

Where:

$$\frac{\Delta P}{l} = -\frac{dp}{dz}$$

On the other hand, the volumetric flow rate is written as follows:

$$\dot{V} = \pi R^2 V = \int_A U dA = \int_0^R 2\pi U r dr \quad (4.12)$$

Equation (4.13) is the solution to equation (4.12), which describes the pressure drop in a circular duct.

$$\Delta P = \rho \frac{64 l V^2}{Re D 2} \quad (4.13)$$

4.3.2. Flow Between Two Plates

In addition to the circular pipes, a brazed plate heat exchanger was studied, which necessitated a study of the pressure drop for flow between two plates. Equation (4.14) describes the velocity profile of a flow between two plates, as follows:

$$u(y) = -\frac{t}{2\mu} \frac{dP}{dx} y \left(1 - \frac{y}{t}\right) \quad (4.14)$$

Where:

$$\frac{\Delta P}{l} = -\frac{dp}{dx}$$

Figure 4.4 shows the velocity shape in one channel of brazed plate heat exchanger of a gap width t between two plates.

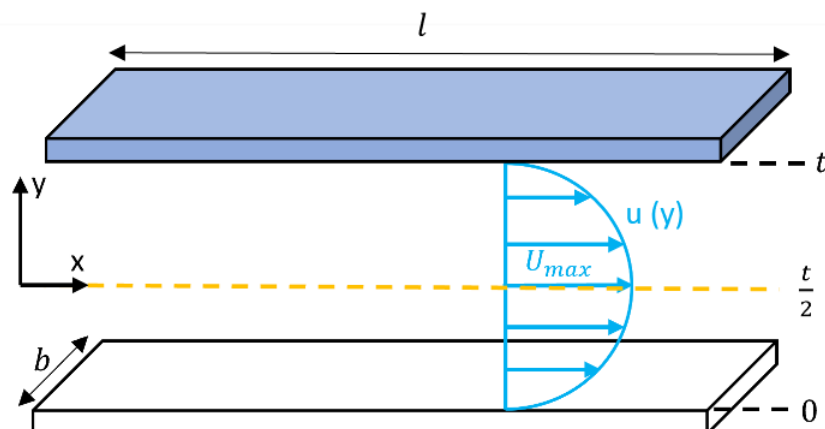


Figure 4.4 Flow between two plates

On the other hand, the volumetric flow rate is written as follows, equation (4.15):

$$\dot{V} = tU_{av} = \int_A U dA = \int_0^t U dy \quad (4.15)$$

Equation (4.16) describes the pressure drop between two plates:

$$\Delta P = \frac{12U_{av}\mu l}{t^2} \quad (4.16)$$

The hydraulic diameter between two plates can be considered as: $D_h = \frac{4bt}{2(b+t)} \cong 2t$

4.3.3. Pressure Drop in Fittings

To calculate the pressure, drop in each fitting the effective length, equation (4.17), must be considered as follows:

$$L_e = K \times \frac{\dot{m}}{16\pi * \mu} \quad (4.17)$$

Each fitting has a specific K value obtained form White (2009), as shown in Table 4.1.





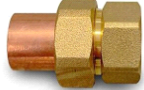



Item		Type	K
Pipe to Tank			1
Tank to Pipe			0.5
Ball Valve		3/4"-Nominal Diameter	0.19
90° Elbow		90°	0.9
Union			0.04
Reducer		3/4"-1/2"	0.5
Bushing		1/2"-3/4"	0.22
Pipe		Type-L	0.45
HX inlet			1
HX Outlet			0.5

Table 4.1 K-value of fittings

Then the pressure drop can be calculated as follows:

$$\Delta P = 128\mu \frac{\dot{m}l_e}{\pi\rho D^4} \quad (4.18)$$

4.4. Thermal Analysis

The thermal analysis determined the outlet temperature of the glycol and the overall heat transfer coefficient by knowing the flow rate of the glycol and the power of the solar panel. To study the flow type, the Reynolds number will be analyzed as follows:

$$Re = \frac{UD_h}{\nu} \quad (4.19)$$

Based on literature and previous studies, the heat transfer coefficient for each heat exchanger can be calculated by determining the specific Nusselt number. The Nusselt number, an empirical and dimensionless form of the heat transfer coefficient, is found experimentally and is unique to each heat exchanger geometry.

The general formula, equation (4.20), of Nusselt number is as follows:

$$Nu = \frac{hD_h}{k} \quad (4.20)$$

4.4.1. Overall Heat Transfer Coefficient

The mean inside heat transfer coefficient, h is a measure of the heat transfer performance on the inside surface of the tube and this coefficient cannot be measured

directly during heat exchanger operation. Newton's law of cooling shown in equation (4.21) states that:

$$\dot{q} = hA(T_w - T_\infty) \quad (4.21)$$

For a counterflow concentric tube heat exchanger, with inlet and outlet temperatures known, LMTD method, where the heat transfer rate is stated in equation (4.22):

$$\dot{q} = UA\Delta T_{log} \quad (4.22)$$

Where:

$$\Delta T_{log} = \frac{(T_{h,i} - T_{c,o}) - (T_{h,o} - T_{c,i})}{\ln \frac{T_{h,i} - T_{c,o}}{T_{h,o} - T_{c,i}}}$$

Solving for, UA and are presented in equations (4.23) and (4.24), respectively:

$$UA = \frac{\dot{q}}{\Delta T_{Log}} \quad (4.23)$$

$$U = \frac{1}{\frac{1}{h_c} + \frac{1}{h_h}} \quad (4.24)$$

The inside surface area of this tube exposed to the fluid is calculated given the tube geometry. The rate of heat transfer in equation (4.25), (\dot{q}), is the product of the mass flow rate on hot and cold side are as following:

$$\dot{q} = (\dot{m}Cp\Delta T)_c = (\dot{m}Cp\Delta T)_h \quad (4.25)$$

4.4.2. Forced Convection

Understanding convection associated with external forced flow, such as that driven by a pump, compressor, or fan, is crucial for comparing its effects to natural convection. This analysis helps determine the system's performance characteristics under external influences, in order to understand the thermal performance of the system.

4.4.2.1. Shell and Tube

For shell and tube heat exchangers, Figure 4.5, Thulukkanam (2013) found a specific Nusselt number for both the pipe and shell sides.. Equation (4.26) presents the empirical correlation that describes the dimensionless heat transfer behavior of the flow inside the pipes.

For $Re < 500$:

$$0.5 < C < 1$$

$$Nu_t = C \left(Re \times \frac{D_p}{l} \right)^{0.5} \times Pr^{\frac{5}{6}} \times \left(\frac{\mu_b}{\mu_{wall}} \right)^{0.14} \quad (4.26)$$

While on the shell side the Nusselt number is as shown in equation (4.27):

For, $Re < 100$:

$$C = 1 \text{ and } n = -0.694$$

For, $100 < Re < 1000$:

$$C = 0.717 \text{ and } n = -0.574$$

$$Nu_s = C \times Re^{1+n} \times Pr^{\frac{1}{3}} \times \left(\frac{\mu_b}{\mu_{wall}} \right)^{0.14} \quad (4.27)$$

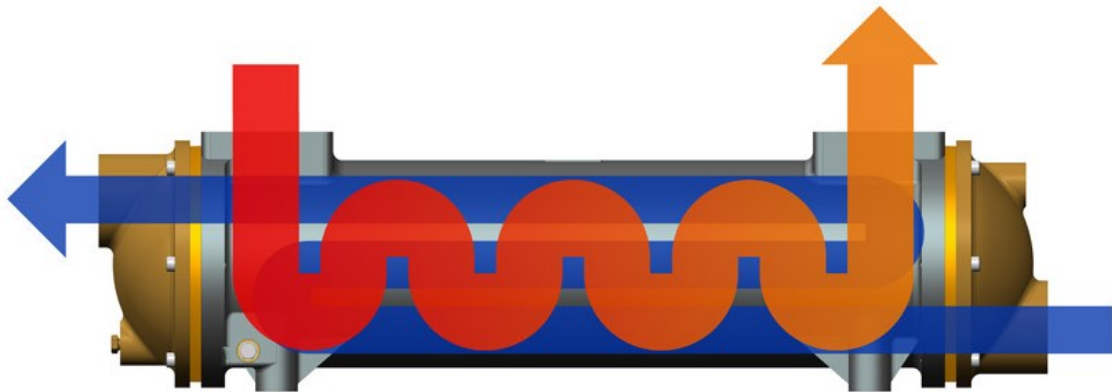


Figure 4.5 Flow in a shell and tube heat exchanger

The previous correlations are applicable for the twisted tube- shell and tube heat exchanger.

4.4.2.2. Brazed Plate Forced Convection

For brazed plate heat exchangers, shown in Figure 4.6, Thulukkanam (2013) determined a specific Nusselt number for both the hot and cold sides. Equation (4.28) presents Nusselt number within two plates.

For, $10 < Re < 720$:

$$0.1 < C < 1$$

$$Nu = C \times Re^{0.75} Pr^{0.4} \quad (4.28)$$

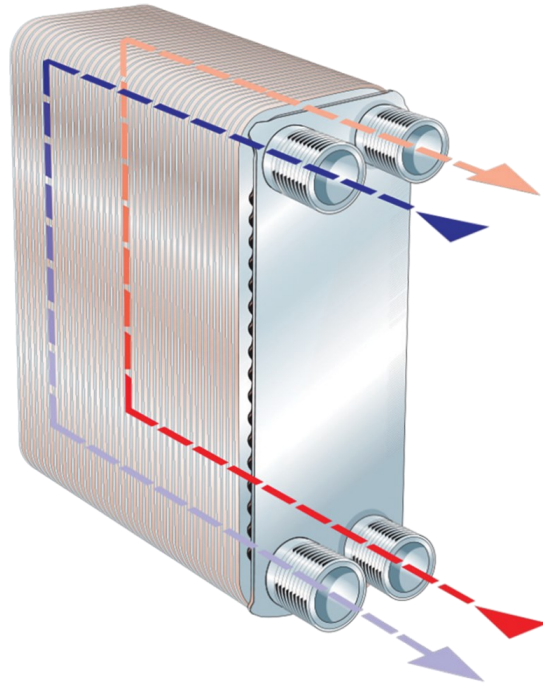


Figure 4.6 Flow in a brazed plate heat exchanger

4.4.3. Natural Convection

Convection associated with buoyancy-induced flow occurs when warmer, less dense fluid rises while cooler, denser fluid descends, creating continuous circulation. Understanding buoyancy-induced convection is essential for comparing its effects to those of forced convection. This comparison helps determine whether the system operates under forced or natural (free) convection, allowing for accurate assessment and optimization of thermal performance. The Grashof and Rayleigh number, equation (4.29), is particularly useful in determining the natural convection phenomena and the flow behavior in situations where fluid motion is driven by density differences due to temperature variations.

$$Gr = \beta g(T_m - T_s) \frac{t^3}{\nu^2} \quad (4.29)$$

$$Ra = Gr.Pr$$

4.4.3.1. Shell and Tube

For shell and tube heat exchangers, Ohk & Chung (2017) found a specific Nusselt number for on the pipe side where the natural convection occurs. Equation (4.30) presents the empirical correlation that describes the Nusselt number of a natural convection phenomenon of inside the pipes.

For, $10 < Ra < 500$:

$$0.1 < C < 0.6$$

$$Nu = C(Gr.Pr)^{0.25} \quad (4.30)$$

4.4.3.2. Brazed Plate

For brazed plate heat exchangers, equation (4.31) found by Ahmadi & Fakkor-Pakdaman (2015) presents the empirical correlation that describes the Nusselt number for natural convection phenomena occurring between two plates.

For, $10 < Ra < 500$:

$$Nu = 0.414(Gr.Pr)^{0.414} \quad (4.31)$$

4.5. Temperature Distribution in the Tank

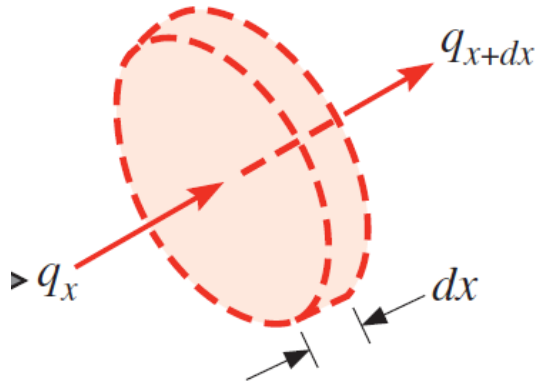


Figure 4.7 Differential element of a cylindrical shap

In this study, accurately determining the temperature profile within the water tank was essential. To accomplish this, six temperature sensors were installed at different points within the tank to monitor temperature variations. The temperature distribution within the tank was analyzed using Fourier's law, equation (4.32), of heat conduction, which is expressed as follows, (Bergman & Lavine, 2017):

$$q_x \int_0^x \frac{dx}{A(x)} = - \int_{T_0}^T K(T) dT \quad (4.32)$$

The general solution of equation (4.32) is presented in equation (4.33)

$$\theta(x) = C e^{mx} - C e^{-mx} \quad (4.33)$$

Where:

$$C = \frac{T_{w,o} - T_{w,i}}{e^{mH} - e^{-mH}} \text{ and } m = \left(\frac{4h}{KD_t} \right)^{\frac{1}{2}}$$

4.6. Iterative Process

The analytical calculation relies on certain assumptions and the defined geometry of each heat exchanger. It involves two main steps: first, a hydraulic analysis of the system on the water side only, and second, a thermal analysis on the glycol side.

- **Hydraulic Analysis**

The hydraulic analysis was conducted on the water side, primarily to determine the outlet temperature of the water, the pressure drop, and the water flow rate. The analysis begins by setting the inlet temperature of the water and assuming the water flow rate. Defining the geometry of the heat exchanger, as well as the system's piping and fittings, is crucial to determining the static and shear pressure drop. An iterative process is then employed, adjusting the mass flow rate of the water until the two pressure drops become equal. Figure 4.8 illustrates the steps involved in the hydraulic analysis.

- **Thermal Analysis**

After obtaining all the data from the hydraulic analysis, the thermal analytical calculations can be conducted on the glycol side. By using the water temperature difference and mass flow rate at each heat transfer rate, along with the relationship between electric power and glycol flow rate in addition to the empirical correlation described in paragraph 4.4, the overall heat transfer coefficient can be calculated. The iteration process shown in Figure 4.9 begins by assuming the outlet temperature of the glycol and stops when the $UA\Delta T_{log}$ becomes equal the electric power of the heater.

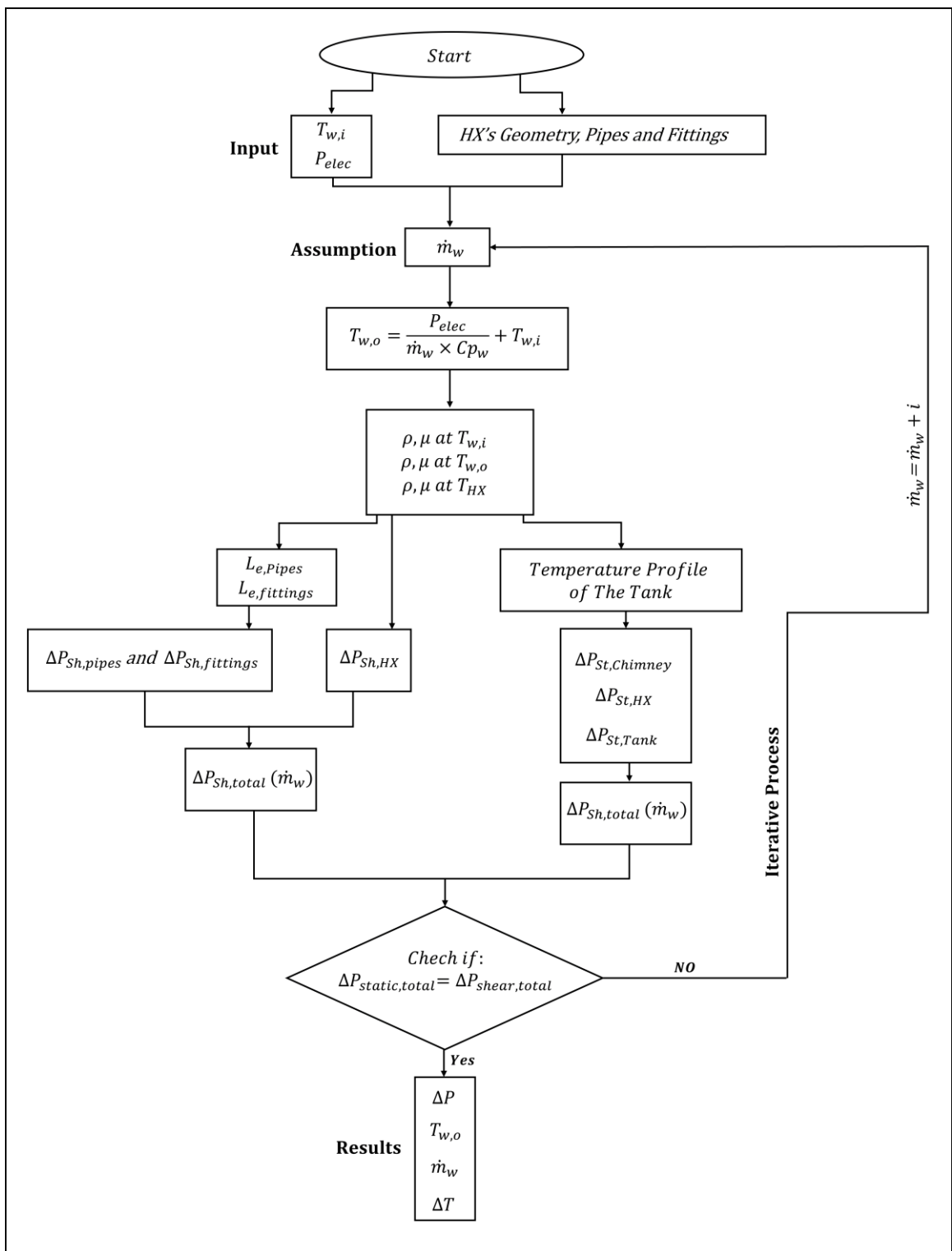


Figure 4.8 The iterative process of the hydraulic analysis

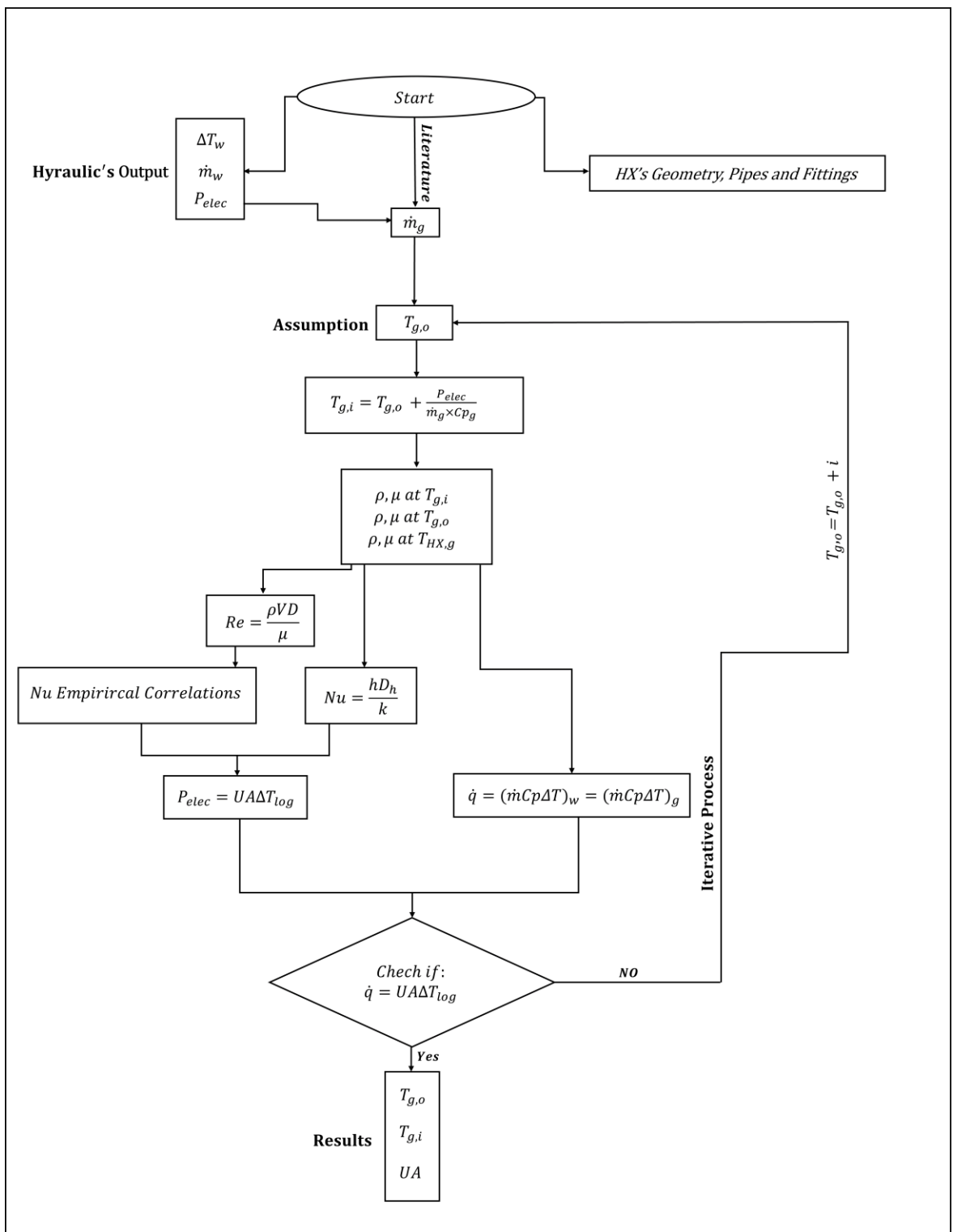


Figure 4.9 The iterative process of the thermal analysis

Chapter 5. Results

5.1. Introduction

In this chapter, the hydrothermal performance of each heat exchanger is evaluated by calculating various parameters. The experimental results are compared with analytical results obtained using the empirical correlations, thermal, and hydraulic expressions discussed in the previous chapter.

The analysis includes comparing these results with experimental data collected at typical glycol flow rates of an actual system where the DC motor pump is powered by a photovoltaic solar panel.

The overall heat transfer coefficient, pressure drop (ΔP), and the relationship between the mass flow rate of water \dot{m}_w and the heat transfer rate (\dot{q}) are examined. Each heat exchanger's performance is assessed by comparing the overall heat transfer coefficient per unit area and other parameters across the three heat exchangers.

The analysis of the results also examines the data collected at glycol flow rates specified by Gharbia (2010) to compare the performance of the three heat exchangers with the shell and coil heat exchangers analyzed in his study. The data for the brazed plate and shell and twisted tube heat exchangers are compared to the specifications provided in the data sheet by the manufacturer, SEC Ltd.

5.2. Glycol Flow Rate

The glycol flow rate was analyzed as a function of the electrical power (W) to ensure that the three heat exchangers operated under the same conditions.

Table 5.1 indicates that, in general, the experimental flow rates for the different heat exchangers are close to the literature values, with relatively low percentage errors. The errors are generally within a few percentage points, indicating that the experimental setup aligns well with the literature data. The shell and tube heat exchanger consistently shows the lowest percentage errors, while the brazed plate and shell and twisted tube exchangers exhibit slightly higher deviations at certain power levels.

Power(W)	Literature	Shell and Tube		Brazed Plate		Shell and Twisted Tube	
	Lpm	Lpm	Error (%)	Lpm	Error (%)	Lpm	Error (%)
500	0.81	0.9	11.11	0.8	1.23	0.8	1.23
1000	1.08	1.1	1.85	1.1	1.85	1.1	1.85
1500	1.29	1.3	0.78	1.3	0.78	1.3	0.78
2000	1.42	1.4	1.41	1.4	1.41	1.4	1.41
3000	1.52	1.5	1.32	1.6	5.26	1.5	1.32

Table 5.1 Glycol flow rate used in the experiment compared to literature

In addition, Figure 5.1 illustrates that the glycol flow rate (Lpm) changed logarithmically as a function of the electric power. Additionally, it is observed that the glycol flow rates across the three experiments are considerably similar.

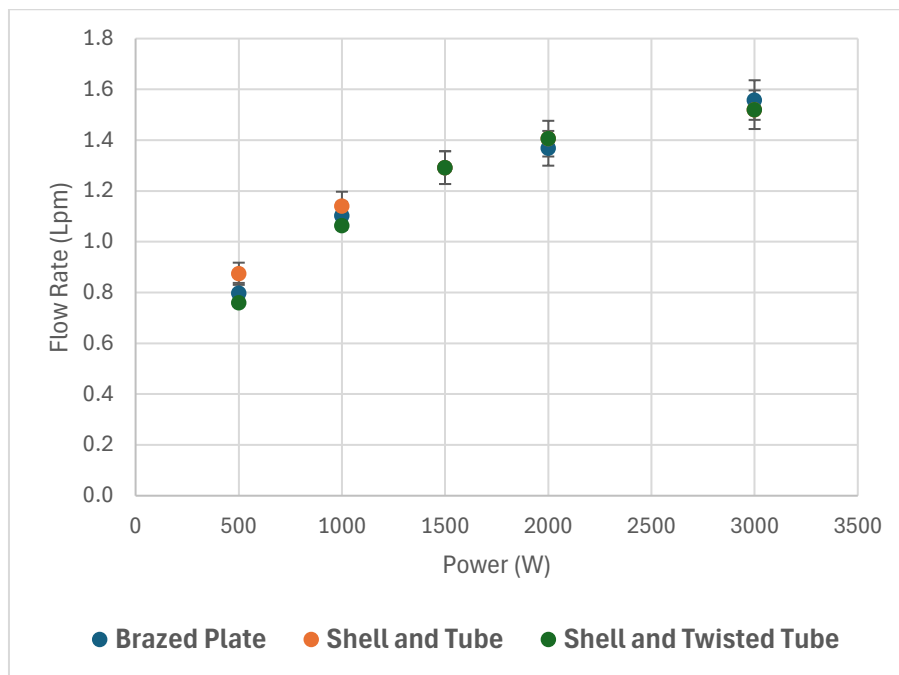


Figure 5.1 Glycol flow rate of each experiment in function of electric power

The uncertainty occurs in this experiment due to the reading errors, the potential fluctuation in the power output of the electric element, and precision in measuring the volumetric flow rate of glycol. Additionally, uncertainties in the measurements of the flow rate of the working fluids and the temperature will lead to some errors in calculation and it will be seen in this chapter later.

5.3. Temperature Distribution in the Water Tank

The temperature distribution within the water tank was analyzed through cylindrical shape charts plotted by using Python, covering the three experiments regarding: brazed plate, shell and tube, and shell with twisted tube heat exchangers.

In each case, the temperature distribution within the tank was visually represented and compared to the corresponding analytical data derived from the correlations in Chapter 4.

The temperature distribution in the water tank observed in the brazed plate heat exchanger experiment (Figure 5.2) ranged between 20°C and 58°C. This aligned closely with the analytical results, with minor variations noted but within acceptable limits.

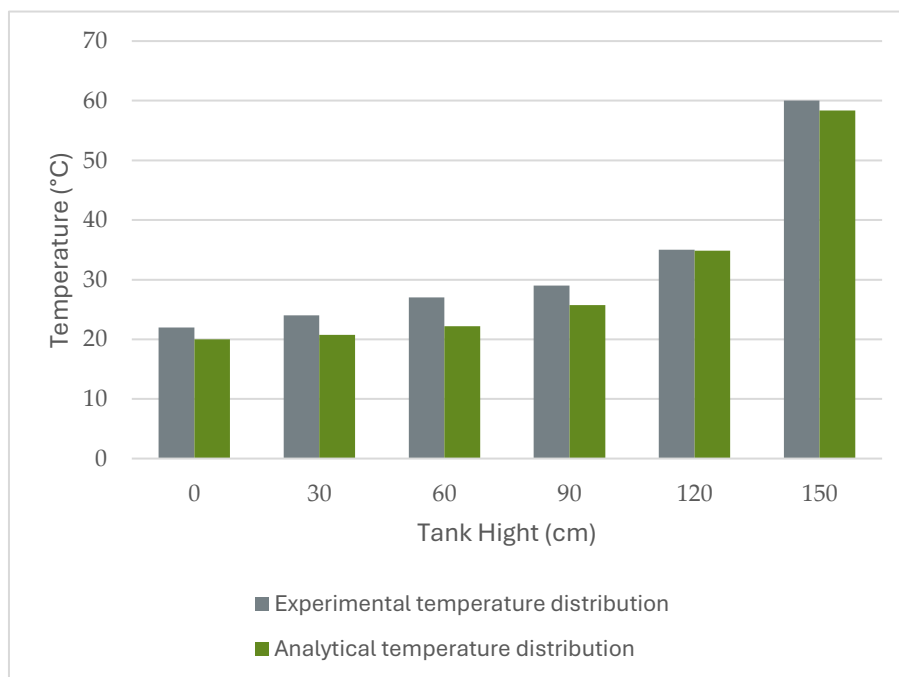


Figure 5.2 Temperature distribution in the tank for the brazed plate

In the shell and tube heat exchanger (Figure 5.3), the temperature distribution ranged between 20°C and 55°C, showing good agreement with the analytical predictions. Minor deviations were observed but remained within acceptable tolerances.

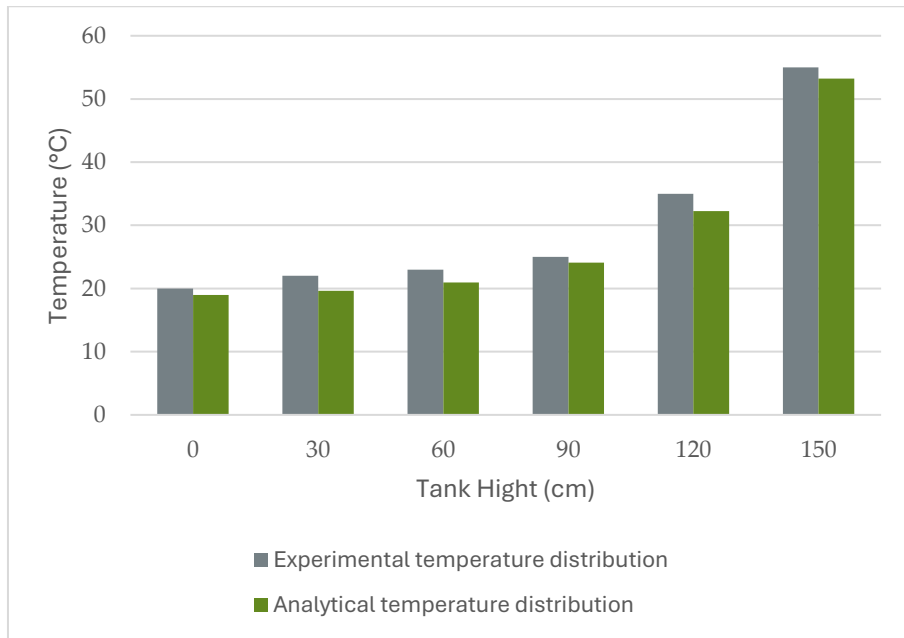


Figure 5.3 Temperature distribution in the tank for the shell and tube

Concerning the shell and twisted tube experiment, the observed temperature distribution ranged between 20°C and 50°C, as shown in Figure 5.4

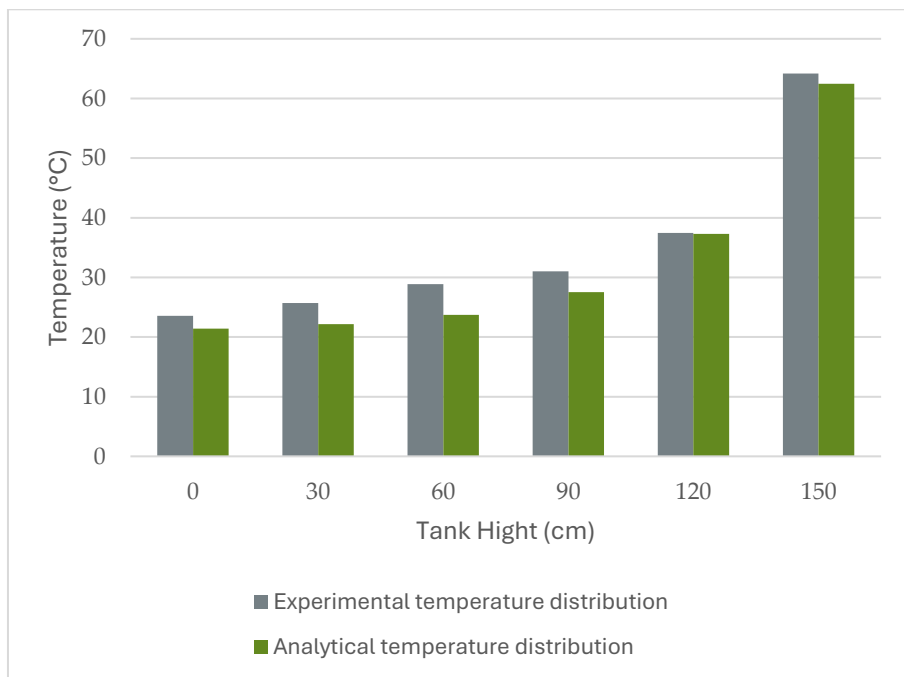


Figure 5.4 Temperature distribution in the tank for the shell and twisted tube

These comparisons confirm that the correlations established in Chapter 4 are verified, demonstrating the accuracy and reliability of the analytical models in predicting the thermal behavior within the water tank.

5.4. Water Flow Rate

The water flow in the system is driven by buoyancy-induced forces, a phenomenon often referred to as natural convection. In this process, differences in temperature within the fluid result in density variations, creating a natural circulation loop.

5.4.1. Experimental and Analytical

Figure 5.5, Figure 5.6, and Figure 5.7 illustrates the variation in the volumetric flow rate of water over a range of power inputs from 500 W to 3000 W for the three heat exchangers: shell and tube, shell and twisted tube, and brazed plate. The figure shows a logarithmic relationship between the flow rate and the heat transfer rate. The data indicates that the hydraulic correlations used to model the behavior of each heat exchanger provide a good approximation of the system's performance. The comparison between experimental and analytical results confirms the model's accuracy across the tested range.

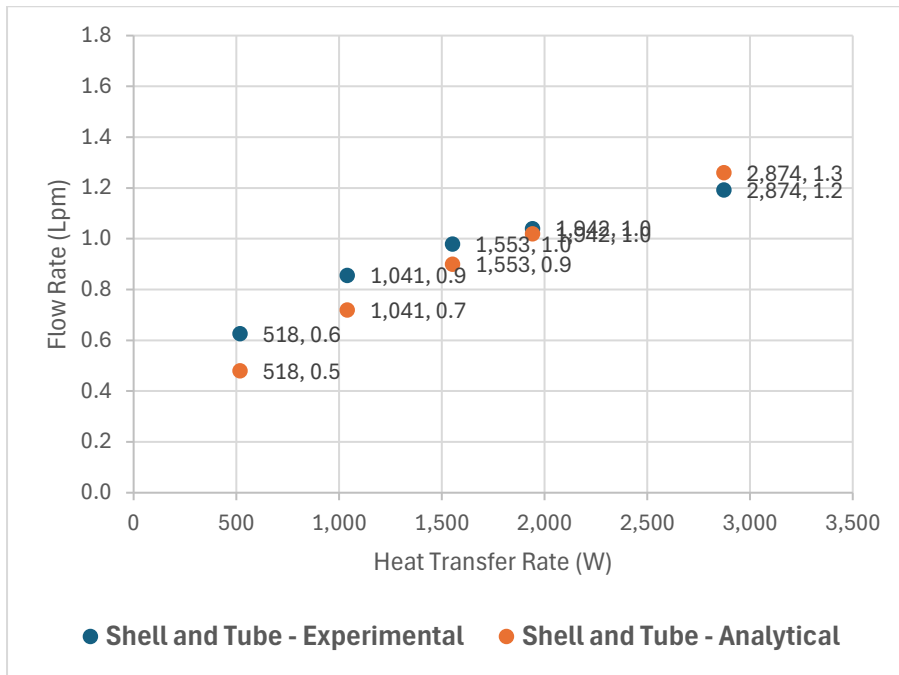


Figure 5.5 Flow rate of water in the shell and tube

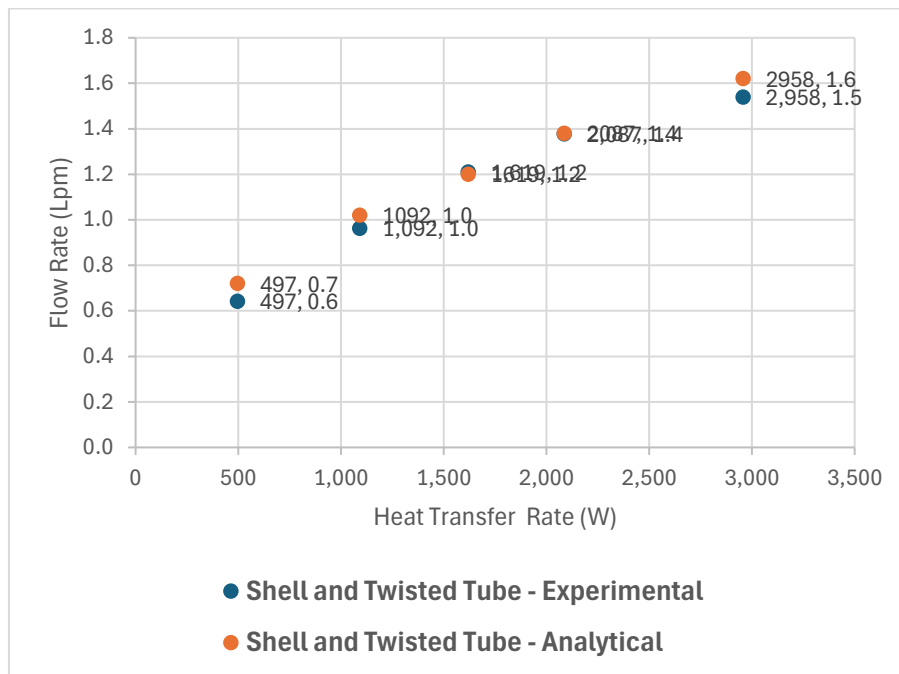


Figure 5.6 Flow rate of water in the shell and twisted tube

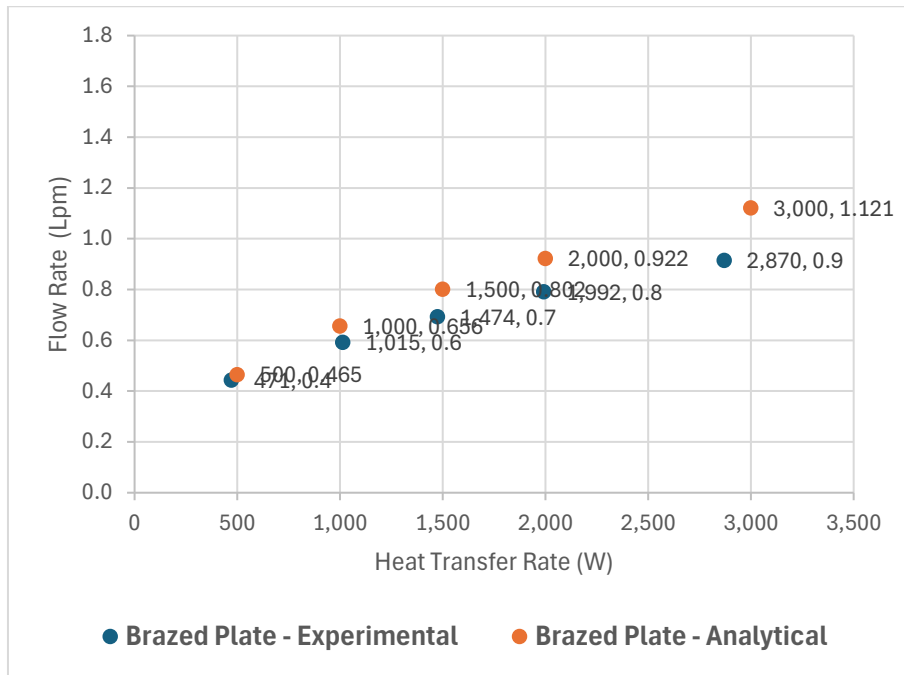


Figure 5.7 Flow rate of water in the brazed plate

5.4.2. Comparison between the Three Heat Exchangers

Figure 5.8 shows the flow rate for each type of heat exchanger. The shell and twisted tube heat exchanger has the highest water flow rate, while the brazed plate heat exchanger consistently has the lowest pressure drop across all power levels. The flow rates of the shell and tube and shell and twisted tube heat exchangers are approximately equal at 500W.

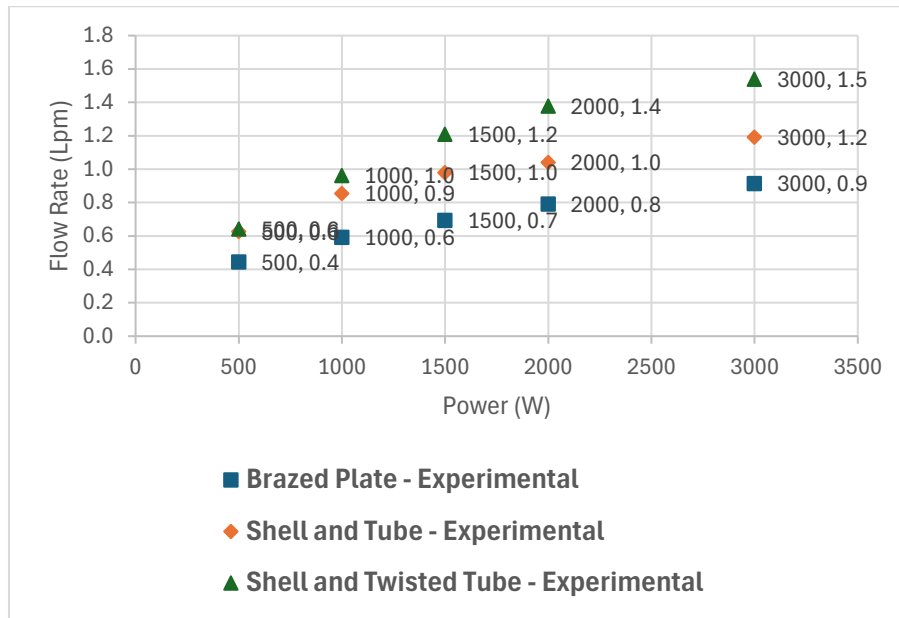


Figure 5.8 Comparison of the water flow rate of the three experiments

5.5. Flow Type in the Three Experiments

q(W)	Brazed Plate		Shell and Tube		Shell and Twisted Tube	
	Re _w	Re _g	Re _w	Re _g	Re _w	Re _g
500	24	38	185	229	67	130
1,000	48	55	270	384	108	278
1,500	68	69	330	587	140	384
2,000	82	84	368	720	164	449
3,000	106	107	461	935	197	649

Table 5.2 Reynolds number at the glycol and water sides

Analyzing the Reynolds number results for the glycol and water flow reveals that both scenarios flow in a pipe and flow between two plates show characteristics of laminar flow. For the flow in a pipe, the Reynolds number falls well below the critical value of 2300, indicating that the flow regime is laminar. Similarly, for the flow between two plates, the Reynolds number is also within the laminar range, confirming that the fluid behavior remains orderly and predictable in this configuration. Consequently, the

results shown in Table 5.2 support the application of laminar flow analysis techniques for both scenarios.

5.6. Comparing Data to the Manufacturer's Specifications

5.6.1. Brazed Plate

In this study, we focus on low-power applications and evaluate the UA values by comparing our correlations with those for high-power applications, as presented in the manufacturer's datasheet (Appendix D) based on the power, inlet and outlet temperatures, and the number of plates. The brazed plate heat exchanger used in this study is an M14A type, manufactured by SEC Ltd.

Water, instead of glycol, is used as the working fluid in this analysis. In this analysis, the correlation outlined in Chapter 4 is extended to account for a flow conditions, where (Re) exceeds a value of 2000, as the manufacturer specifies these heat exchangers for higher flow rates (> 3 Lpm) and power outputs (> 12 kW). as shown in Table 5.3.

N - plates	P(kW)	P (BTU/hr)	Re_{cold}	Re_{hot}
10	12	40,000	336	5,022
10	15	50,000	420	6,441
20	17	60,000	252	2,918
20	20	70,000	294	3,509
20	24	90,000	336	4,135
30	37	120,000	351	4,110
30	40	130,000	392	4,747

Table 5.3 Reynolds number function of power and plates number

To characterize the Nusselt number under turbulent flow between two plates, equation (5.1) is used.

For turbulent flow:

For $Re > 2000$:

$$0.15 < C < 0.4; 0.05 < x < 0.2; 0.3 < m < 0.45; 0.65 < n < 0.85$$

$$Nu = C \times Re^n \times Pr^m \times \left(\frac{\mu_b}{\mu_w}\right)^x \quad (5.1)$$

The same code was used to compare the overall heat transfer coefficient provided by the manufacturer with the analytical results. This comparison aimed to investigate the performance of the brazed plate heat exchanger in a low-power application. The code calculated the inlet and outlet temperatures on the hot side and the overall heat transfer coefficient, using the same flow rate and power conditions specified in the manufacturer's data sheet.

Table 5.4 shows the flow rates of both hot and cold water, as well as the inlet and outlet temperatures for multiple M14a heat exchangers with 10, 20, and 30 plates, based on the company's data sheet.

M14a-10						
P (kW)	Cold Water			Hot Water		
	In (°C)	Out (°C)	Flow Rate (Lpm)	In (°C)	Out (°C)	Flow Rate (Lpm)
12000	4.5	60	3	82	71	15
15000	4.5	60	3.8	82	71	19
M14a-20						
P (kW)	Cold Water			Hot Water		
	In (°C)	Out (°C)	Flow Rate (Lpm)	In (°C)	Out (°C)	Flow Rate (Lpm)
17	4.5	60	4.5	82	71	23
20	4.5	60	5	82	71	27
24	4.5	60	6	82	71	30
M14a-30						
P (kW)	Cold Water			Hot Water		
	In (°C)	Out (°C)	Flow Rate (Lpm)	In (°C)	Out (°C)	Flow Rate (Lpm)
37	4.5	60	9	82	71	48
40	4.5	60	10	82	71	54

Table 5.4 Manufacture (SEC) specifications of different types of M14a

Figure 5.9 demonstrate that the empirical UA values in the company manual closely match the data calculated using the empirical correlations.

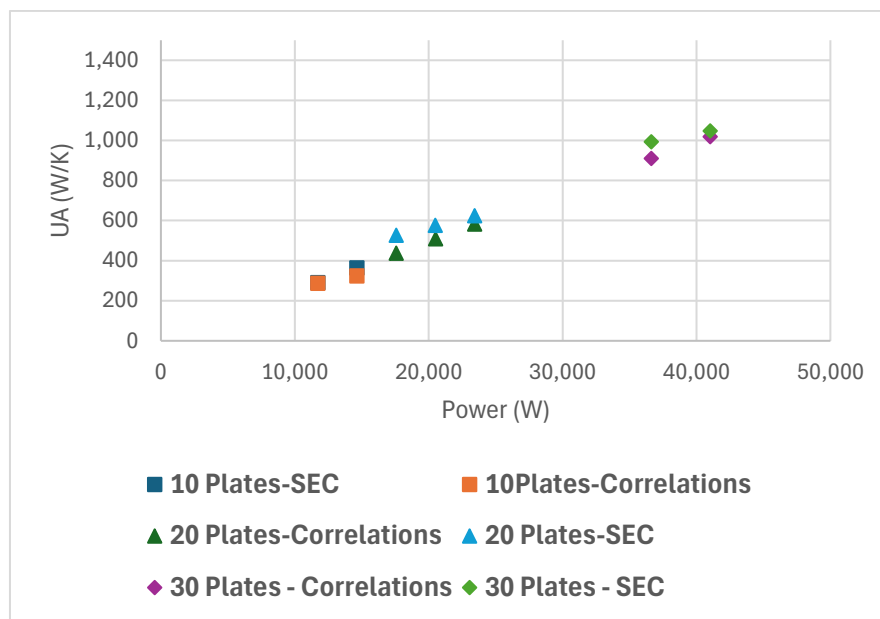


Figure 5.9 UA-value of the brazed plate (SEC-Correlations)

5.6.2. Shell and Twisted Tube

Following the evaluation of the brazed plate heat exchanger, the focus now shifts to the shell and twisted tube heat exchanger. Similar to the brazed plate model, the UA values are assessed by comparing them with those provided in the manufacturer's datasheet (Appendix D) for high-power applications. The data in Table 5.5. were used to determine the overall heat transfer coefficient for each PL heat exchanger, as specified by the manufacturer, considering a temperature difference of 60°C between the hot and cold inlet flows.

PL-45			
		Cold Water	Hot Water
P (kW)	P (BTU/hr)	Flow Rate (Lpm)	Flow Rate (Lpm)
13	45,000	150	23
PL-70			
		Cold Water	Hot Water
P (kW)	P (BTU/hr)	Flow Rate (Lpm)	Flow Rate (Lpm)
20	70,000	170	25
PL-130			
		Cold Water	Hot Water
P (kW)	P (BTU/hr)	Flow Rate (Lpm)	Flow Rate (Lpm)
38	130,000	200	27

Table 5.5 Manufacture (SEC) specifications of PL-45

The same correlation from Chapter 4 is applied, taking into account the flow conditions specified by the manufacturer for higher flow rates and corresponding high Reynolds numbers on both cold and hot sides (Table 5.6). Additionally, heat exchangers of types of PL-45, PL-70, and PL-130, with diameters of 150mm, 250mm, and 350mm,

respectively, are compared to further analyze performance differences across these configurations and to verify if the correlations are valid for both high-power and low-power applications

Type	Power (kW)	Re _{cold}	Re _{hot}
PL-45	13	4000	17000
PL-70	20	12000	15000
PL-130	38	48000	32000

Table 5.6 Reynolds number of shell and twisted tube of SEC

The results shown in Figure 5.10, and Table 5.6 ensure that the correlations accurately predict the performance across a range of operating conditions.

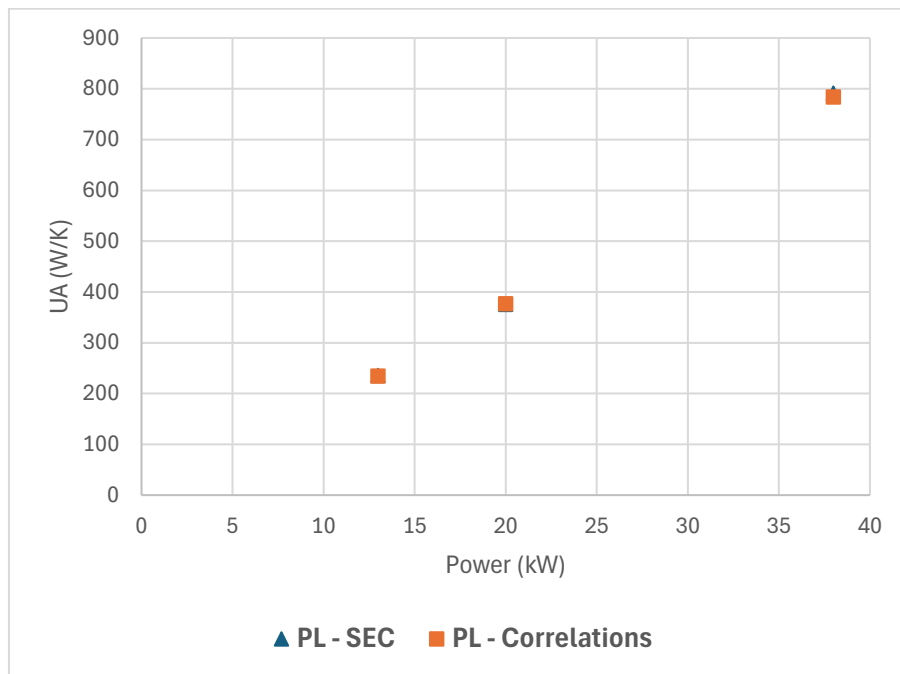


Figure 5.10 UA-value of the shell and twisted tube (SEC-Correlations)

5.7. Free and Forced Convection

In this study, we compare the results obtained from forced and natural convection analyses. As discussed earlier, the water side experienced a thermosyphon effect, driven by buoyancy-induced flow. Consequently, a natural convection investigation is essential to ascertain the heat transfer coefficient on the water side for each type of heat exchanger. Figure 5.11, Figure 5.12, and Figure 5.13 illustrate the variations in the overall heat transfer coefficients for brazed plate, shell and tube, and shell and twisted tube heat exchangers, respectively.

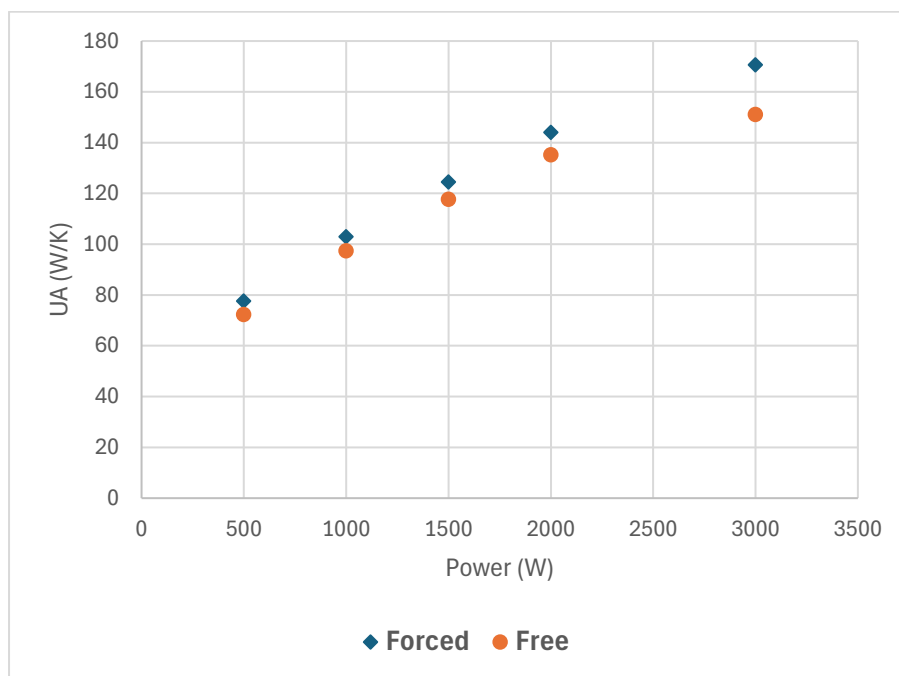


Figure 5.11 UA of brazed plate at free and forced convection on water side

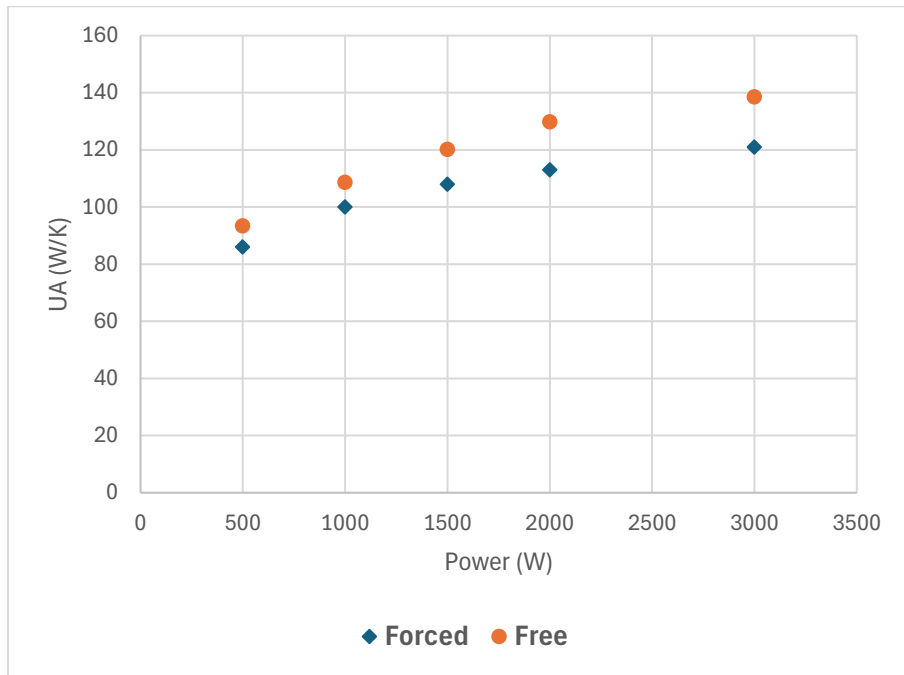


Figure 5.12 UA of shell and tube at free and forced convection on water side

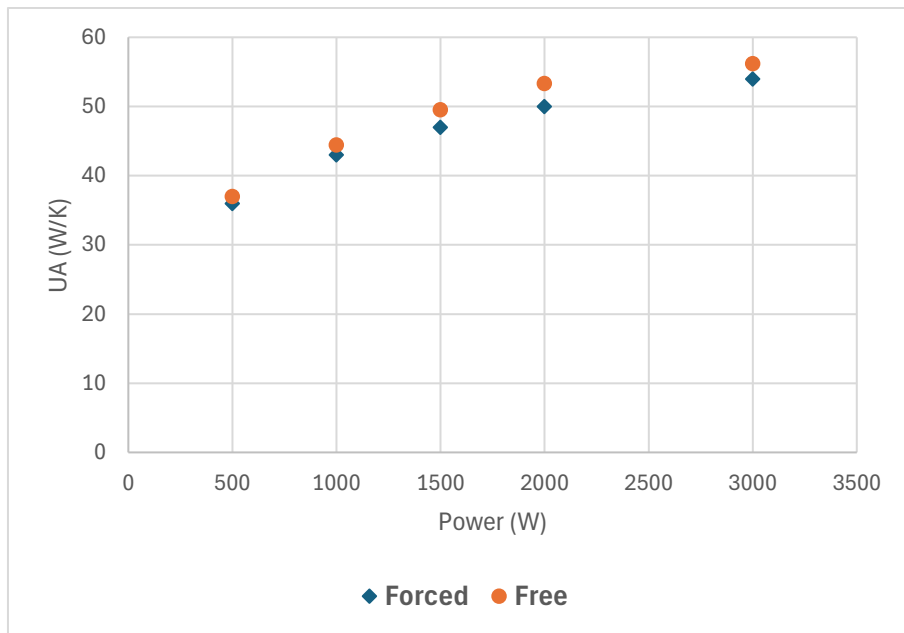


Figure 5.13 UA of shell and twisted tube at free and forced convection on water side

Table 5.7 presents the percentage differences between forced and free convection for all three heat exchangers remain within a relatively small range. For the brazed plate

exchanger, the difference varies between 5% and 11%, while the shell and tube heat exchanger show differences between 9% and 15%. The shell and twisted tube heat exchanger has the smallest percentage differences, ranging from 3% to 7%.

This indicates that either forced or free convection can be used without significantly compromising the accuracy of the UA values and overall heat exchanger performance.

Power (W)	Brazen Plate			Shell and Tube			Shell and Twisted Tube				
	UA (W/K)		Error (%)	Power (W)	UA (W/K)		Error (%)	Power (W)	UA (W/K)		Error (%)
	Forced	Free			Forced	Free			Forced	Free	
500	78	72	7	500	86	93	9	500	36	37	3
1000	103	97	5	1000	100	109	9	1000	43	44	3
1500	125	118	6	1500	108	120	11	1500	47	50	5
2000	144	135	6	2000	113	130	15	2000	50	53	7
3000	171	151	11	3000	121	139	14	3000	54	56	4

Table 5.7 Error percentage between UA-values of the free and forced convection

5.8. UA Value Comparison

Evaluating the UA-value of each heat exchanger provides a method to compare their performance. In the following paragraph, both analytical and experimental UA values will be presented to validate empirical correlations against experimental results.

Additionally, the overall heat transfer coefficient for each heat exchanger will be detailed. The glycol flow rate was systematically adjusted to simulate the conditions of a typical day, with electrical power used to ensure consistent conditions across all three experiments.

5.8.1. Analytical and Experimental Results of UA Value

Figure 5.14 presents a comparison between the experimental and analytical overall heat transfer coefficients at various power levels, ranging from 500 W to 3000 W.

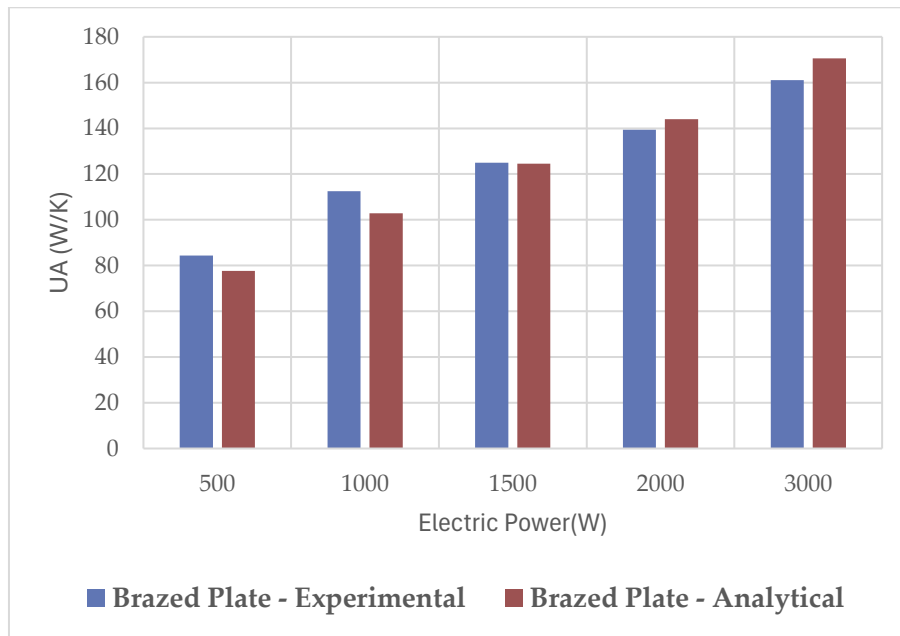


Figure 5.14 Analytical and experimental UA-value of brazed plate heat exchanger

Similarly, Figure 5.15, and Figure 5.16 compares the experimental and analytical overall heat transfer coefficients for shell and tube heat exchangers. The close alignment of the results in all three figures indicates that the Nusselt number correlations provided in Chapter 4 are reliable approximations, effectively describing the thermal behavior across these different types of heat exchangers.

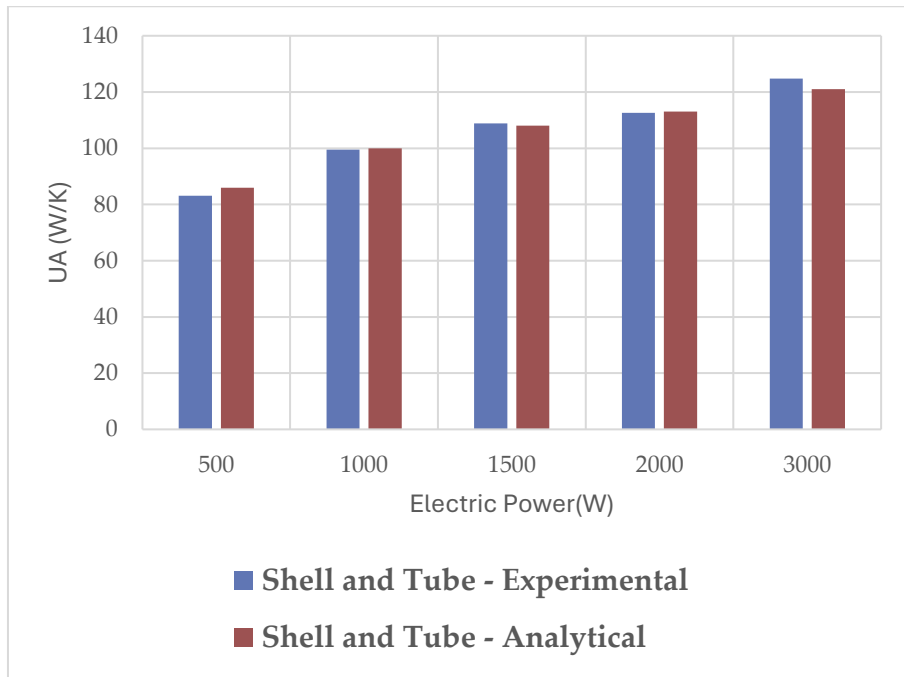


Figure 5.15 Analytical and experimental UA-value of shell and tube heat exchanger

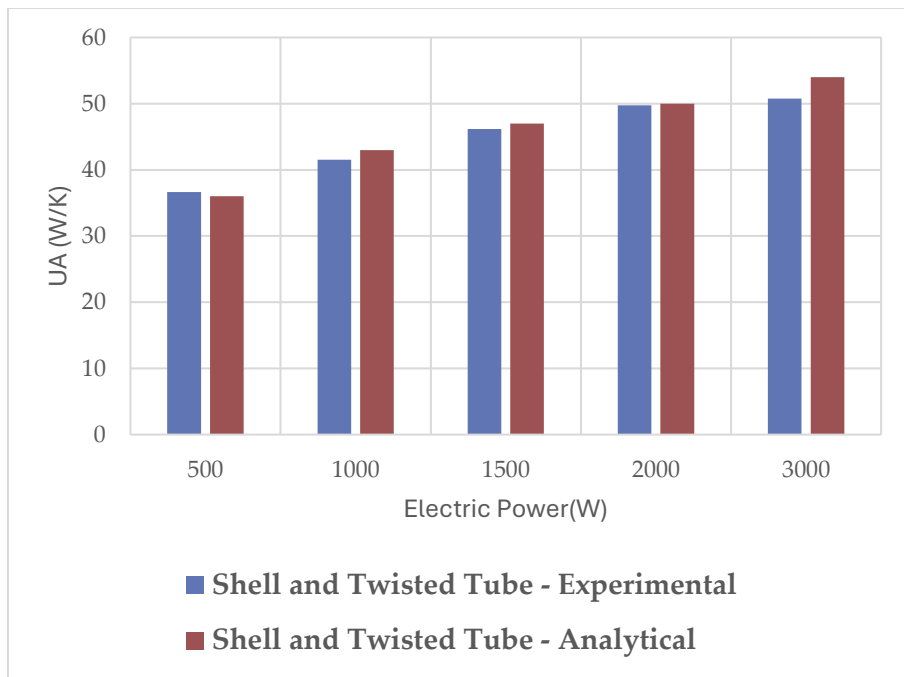


Figure 5.16 Analytical and experimental UA-value of shell and twisted tube heat exchanger

5.8.2. UA Comparison of the Three Heat Exchangers

After discussing the comparison between the experimental and analytical results, it is evident that the data aligns well with the theoretical predictions. Figure 5.17 shows that the brazed plate heat exchanger reaches the highest UA value of approximately 170 W/K at a heat transfer rate of around 3000 W, while the twisted shell and tube exchanger has the lowest UA value of about 40 W/K at a heat transfer rate below 500 W. The shell and tube exchanger falls in the middle range.

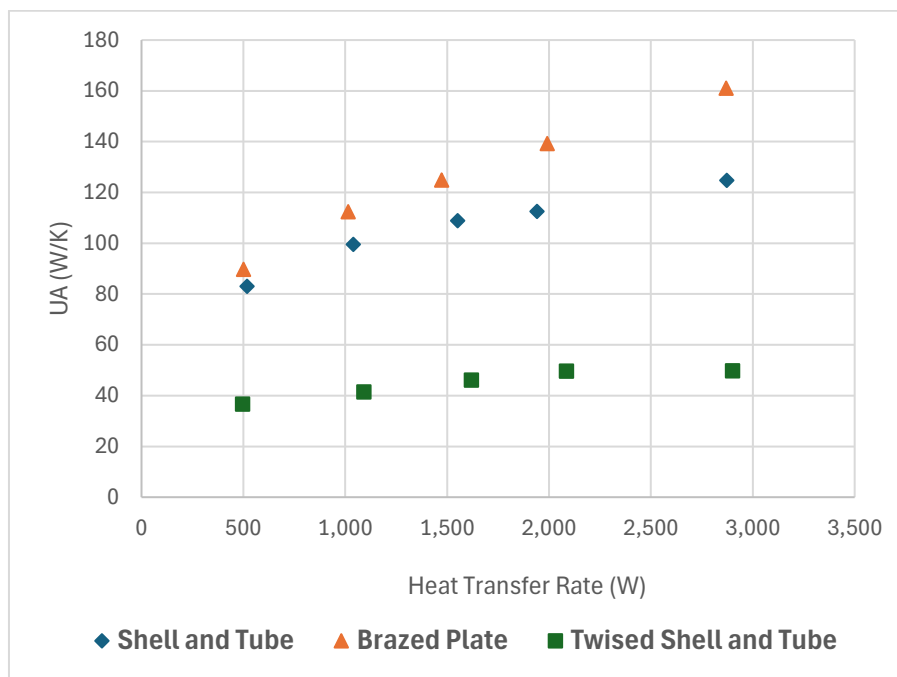


Figure 5.17. UA-value of the three heat exchangers

5.9. Overall Heat Transfer Coefficient

After completing the analysis of the UA-values for each heat exchanger, this section focusses on the overall heat transfer coefficient (U), by considering that the surface area

of each heat exchangers are as follows: $A_{shell} = 0.36 \text{ m}^2$, $A_{twisted} = 0.15 \text{ m}^2$, and $A_{brazed} = 0.14 \text{ m}^2$. Figure 5.18 indicates that, the brazed plate demonstrates the highest U-values. In contrast, the shell and twisted tube exhibits intermediate performance with relatively stable U-values between, while the shell and tube shows the lowest U-values. The larger surface area of a shell and tube exchanger, despite its lower U-value, doesn't guarantee higher efficiency. Alternatively, the brazed plate heat exchanger, with its smaller surface area, achieves higher performance, highlighting the important role of both UA-value in determining heat exchanger efficiency.

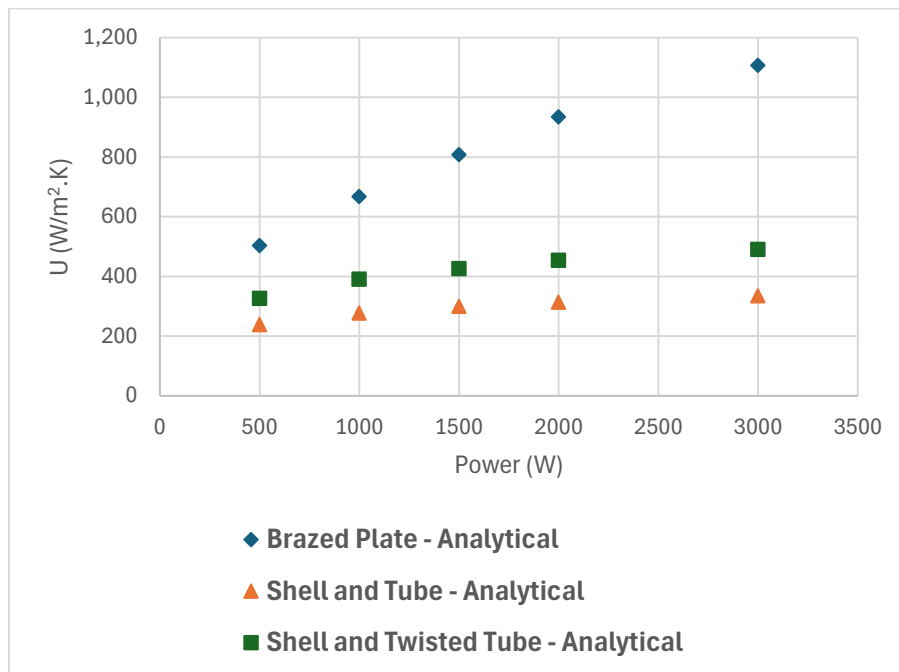


Figure 5.18 U-value of the three heat exchangers

5.10. Comparison with Shell and Four Coils Heat Exchanger

Figure 5.19 illustrates the UA-value for three types of heat exchangers, brazed plate, shell and tube, and shell and twisted tube, as well as the shell and 4-coils heat exchanger

studied by (Gharbia, 2010). The performance of these heat exchangers is measured based on the glycol flow rate specified by (Gharbia, 2010) and presented in the literature. As power increases, UA values rise for all heat exchangers. The brazed plate exchangers reach UA values of up to 250 W/K at approximately 3000 W, while shell and tube exchangers peak around 200 W/K. Shell and Twisted Tube exchangers achieve a maximum of about 100 W/K. The Shell and 4-Coils system, used by Thermo Dynamics Ltd. for solar hot water systems reaches a peak of around 150 W/K.

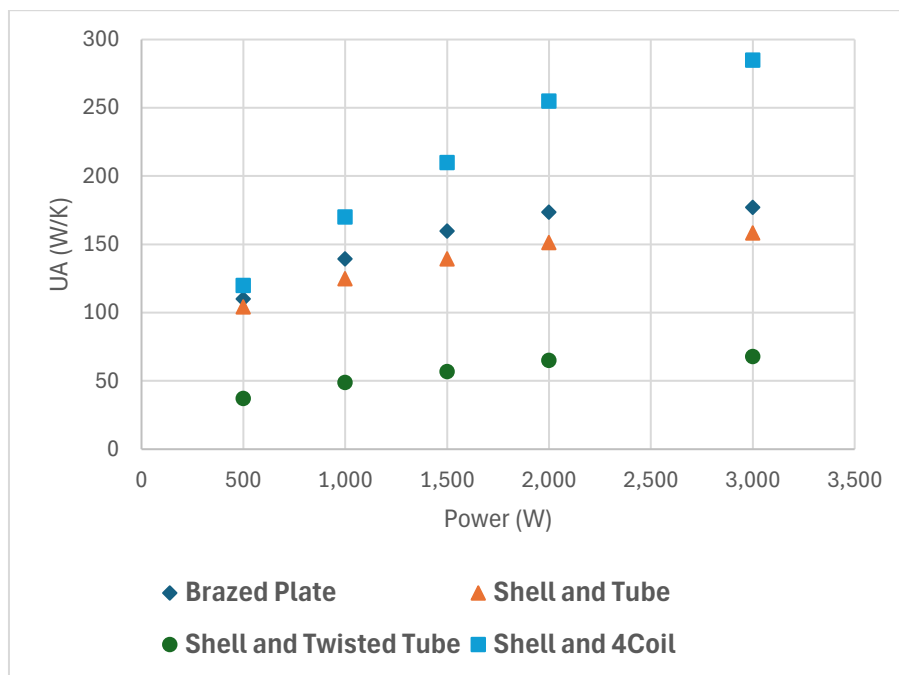


Figure 5.19 UA-value of the three heat exchangers, and the shell and 4-coils

Chapter 6. Conclusion and Summary

6.1. Summary

This chapter provides a comprehensive evaluation of the hydrothermal performance of three different heat exchangers: brazed plate, shell and tube, and shell and twisted Tube. The assessment combines experimental data with analytical calculations to validate the accuracy of empirical correlations and theoretical models. Here's a detailed summary of the findings:

- **Temperature Distribution:**

The temperature profiles observed in the water tanks for each type of heat exchanger were consistent with analytical predictions. For the brazed plate heat exchanger, temperatures ranged between 20°C and 58°C, closely matching the analytical results with minor deviations. The shell and tube heat exchanger showed a temperature range of 20°C to 55°C, while the shell and twisted tube had a range of 20°C to 50°C. These results confirm the reliability of the thermal behavior predictions based on the correlations established in Chapter 4.

- **Water Flow Rate and Reynolds Numbers:**

The water flow rates demonstrated a logarithmic relationship with the power, influenced by natural convection driven by buoyancy-induced forces. The Reynolds number analysis indicated that the flow in both pipe and plate configurations remained within the laminar range, suggesting predictable and orderly fluid behavior. This

supports the use of laminar flow analysis techniques for both the shell and plate heat exchangers.

- **Comparison with Manufacturer Specifications:**

The empirical UA values for the brazed plate and shell and twisted Tube heat exchangers were compared with manufacturer data. The analysis extended to high-power applications, confirming that the empirical correlations accurately predict performance under both laminar and turbulent flow conditions. The comparison revealed that the manufacturer's specifications for both the brazed plate and shell and Twisted Tube heat exchangers were closely matched by the empirical data.

- **Free vs. Forced Convection Analysis:**

A comparison between forced and free convection showed that the differences in overall heat transfer coefficients (UA-values) were relatively small. The brazed plate heat exchanger had the highest percentage differences between forced and free convection conditions, ranging from 5% to 11%. The shell and tube and shell and twisted tube heat exchangers exhibited smaller differences, indicating that either convection method provides comparable accuracy for performance predictions.

- **UA-value and Overall Heat Transfer Coefficient:**

The brazed plate heat exchanger demonstrated the highest UA-value, reaching approximately 170 W/K at 3000 W of heat transfer. This indicates superior thermal performance compared to the shell and tube and shell and twisted tube heat exchangers. The shell and tube heat exchanger, despite its larger surface area, showed lower UA-

values, emphasizing that a larger surface area does not necessarily equate to higher efficiency. The shell and twisted tube heat exchanger provided intermediate performance with relatively stable U-values across power levels.

- **Comparison with Shell and 4-Coils Heat Exchanger:**

The performance of the three heat exchangers was compared to the shell and 4-coils heat exchanger studied by Gharbia (2010). The brazed plate heat exchanger outperformed the others, achieving the highest UA-values at higher power levels. The shell and 4-coils system reached a peak UA-value of around 150 W/K, which was higher than any other heat exchanger examined in this study.

6.2. Conclusion

In conclusion, this study studies the hydrothermal performance of brazed plate, shell and tube, and shell with twisted tube heat exchangers within a hot water solar system. While manufacturers provided performance data for the brazed plate and shell with twisted tube heat exchangers at high power and flow rates, this research focused on evaluating their performance for a water solar system at low power.

Circulation on the water side is due to buoyancy-induced flow, while glycol is forced on the other side of each heat exchanger. The analytical calculations initially considered forced flow on the water side, and the results matched experimental data. Later, free convection was also examined, producing results consistent with those from the forced convection setup, showing reliable consistency and only minor discrepancies.

The analysis shows that the brazed plate heat exchanger demonstrates a superior thermal efficiency, particularly at higher power levels. Although the shell and tube and shell with twisted tube heat exchangers also performed effectively, they were less efficient compared to the brazed plate. The shell and tube exchanger, despite its larger surface area, had intermediate performance with lower U-values. In contrast, the shell with twisted tube heat exchanger showed stable performance but had the lowest UA-values.

Additionally, when compared to the shell and 4-coils heat exchanger from Thermo Dynamics Ltd., it was found to outperform the other three heat exchangers in the study.

References

- Adolfsson, M., & Rashid, S. (2016). Life Cycle Assessment and Life Cycle Cost of Heat Exchangers: A Case for Inter Terminals Sweden AB Located in Port of Gothenburg. *Master's Thesis Chalmers University of Technology, Gothen.*
- Ahmadi, M., & Fakkor-Pakdaman, M. (2015). Natural convection from vertical parallel plates: An integral method solution. *JOURNAL OF THERMOPHYSICS AND HEAT TRANSFER*, 239–247. doi:0.2514/1.T4308
- Aonghus, M., & Killian, S. (2012, July 4). Efficient drain water heat recovery in horizontal domestic shower drains.
- Arani, R., & Moradi, R. (2019). Shell and tube heat exchanger optimization using new baffle and tube configuration,. *Appl. Therm. Eng.*, 113736. doi:https://doi.org/10.1016/j.applthermaleng.2019.113736
- Avina, J. (1995). *The Modelling of a Natural Convection heat Exchnager in a Solar Domestic Hot Water System*. Wisconsin: University of Wisconsin-Masdison.
- Azher, A. M., Hasan, M., & Hussein , Z. (2012, September 12). Numerical analysis of flow and heat transfer enhancement in a horizontal pipe with P-TT and V-Cut twisted tape. *Case Studies in Thermal Engineering*, pp. 749-758.
- Bergman , T. L., & Lavine, A. S. (2017). *Fundamentals of heat and mass transfer*. Los Angeles: John Wiley & Sons, Inc.
- Bojic, M., Kalogirou, S., & Petronijevec, K. (2002). Simulation of a solar domestic water heating system using a time marching model. *Renewable Energy* 27(3), 441-452.
- Chiesa, G., Simonetti, M., & Grosso, M. (2014). A 3-field earth-heat-exchanges ystem for a school build in Imola, Italy: monitoring results. *Renew Energy*, 563-70.
- Cipolla, & Maglionico, M. (2014). Heat recovery from urban wastewater: Analysis of the variability of flow rate and temperature. *Energy and Buildings*,, 69.122-130. doi:https://doi.org/10.1016/j.enbuild.2013.10.017
- Conté, I., & Peng, X. F. (2009). Numerical and experimental investigations of heat transfer performance of rectangular coil heat exchangers. *Appl. Therm. Eng* 29(8-9), 1799-1808.
- Coronel, P. (2008). Heat transfer coefficient in helical heat exchangers under turbulent flow conditions. *International Journal of Food Engineering* 4(1), 302-310.

- Cullen, J., & Allwood, M. (2010). The efficient use of energy: tracing the global flow of energy. *Energy Policy*, 75-81.
- Dagli, S., & Ozbey, M. (2023). Experimental investigation of the effect of hydrophobic coating on heat transfer and gasketed plate heat exchanger performance. *Process mechanical engineering*, 1-12. doi:sagepub.com/journals-permissions/DOI:10.1177/09544089231156309/journals.sagepub.com/home/pie
- Dong, X., Jin, X., Li, P., Bi, Q., Gui, M., & Wang, T. (2020). Experimental research on heat transfer and flow resistance properties in spiral twisted tube heat exchanger. *Applied Thermal Engineering*, 1359-4311. doi:https://doi.org/10.1016/j.applthermaleng.2020.115397
- Fazelpour, F., Saffarian, M., & Sham, M. (2019). Numerical study of shell and tube heat exchanger with different cross-section tubes and combined tubes. *Int. J. Energy Environ. Eng*, 33–46. doi:https://doi.org/10.1007/s40095-019-0297-9
- Focke, W., Zachariades, J., & Oliver, I. (1985). *The effect of the corrugation inclination angle on the thermohydraulic performance of plate heat exchangers*. Great Britain: Pergamon Press Ltd.
- Gharbia (2010), I. (2010). *A Theoretical and Experimental Investigation of a Shell and Coil Heat Exchanger for a Solar Domesitic Hot Water System*. Halifax, Nova Scotia: Dalhousie University.
- Gupta, P., Kusha, K., & Tiwari, A. (2007). Design and optimization of coil finned-tube heat exchangers for cryogenic applications. *Cryogenics* 47(5-6), 322-332.
- Hoe, R., Dwyer, O., & Dropkin, D. (1957). Heat transfer rates to crossflowing mercury in a staggered Tube Bank. *Trans. Am. Soc. Mech. Eng.*, 79, 899–905.
- Hollands, K., & Burnger, A. (1991). Optimum flow rates in solar water heating systems with a counterflow exchanger. *Solar Energy Vol. 48, Issue 1*, 15.
- Howard, Hasan, N., & Knudsen, P. (2021). Thermal-Hydraulic Characterization of Shell-Side Flow in a Cryogenic Coiled Finned-Tube Heat Exchanger. *Journal of Heat Transfer*, 143. doi:https://doi.org/10.1115/1.4049961
- Ibanez, J., Navarro, A., Toledo, J., & Tendero, J. (2019, June 12). Experimental analysis of the refrigerant flow maldistribution in braze plate heat exchanger. *XI National and II International Engineering Thermodynamics Congress*, pp. 978-84-09-11635-5.

- Ibrahim, G. (2010). *A Theoretical and Experimental Investigation of a Shell-and-Coil Heat Exchanger for a Solar Domestic Hot Water System*. Halifax, Nova Scotia: Dalhousie University.
- Jarvis , A., Jarvis, S., & Hewitt, N. (2014). Resource acquisition. *Distttribution and use of energy efficiency and growth of industrial society*, 44-90.
- Jayakumar, J., Mahajani, S., Mandal, J., Vijayan, P., & Bhoi, R. (2008). Experimental and CFD estimation of heat transfer in helically coiled heat exchangers. *Chem. Eng. Res. Design* 86(3), 221-232.
- Kays, W., & London, A. (1984). Compact Heat Exchangers. *Book Company, Stanford:McGraw-Hill*, 14-20.
- Khanlari, A., Sozen, A., & Variyenli, H. (2019). Simulation and experimental analysis of heat transfer characteristics in the plate type heat exchangers using TiO₂/water. *HFF* 29 (n° 4), 1343-1362.
- Kruthlventi, S., Rasu, G., & Rao, Y. (2018). COILED TUBE HEAT EXCHANGERS - A REVIEW. *ResearchGate*, 895-904. doi:<https://www.researchgate.net/publication/323277798>
- Kuppan, T. (2000). *Heat Exchanger Design Handbook*. Colombus, Ohio: Colombus Division, Battlele Memorial Institute and Department of Mechanical Engineering, the Ohio State University .
- Lee, J., & Mudawar, I. (2006, August 6). Assessment of the effectiveness of nanofluids for single-phase and two-phase heat transfer in micro-channels.
- Lee, K. P., Tom , C., & Mattia, D. (March 2011). A review of reverse osmosis membrane materials for desalination—Development to date and future potential. *Journal of Membrane Science*, 1-22.
- Leinonen, H., & Hanninen, H. (1999). SCC susceptibility of nitrogen alloyed stainless steels in 50% CaCl₂ solution[J]. *High Nitrogen Steel* 98., 545-549.
- Leoni, G., Klein, T., & Medronho, R. (2017). Assessment with computational fluid dynamics of the effects of baffle clearances on the shell side flow in a shell and tube heat exchanger. *Appl Therm*, 112:497–506.
- Li, B., & Haneklaus, N. (2022). Reducing CO₂ emissions in G7 countries. *The role of clean energy consumption, trade openness and urbanization*, pp. 704-713. Retrieved from <https://www.sciencedirect.com/science/article/pii/S2352484722002384>

- Maghsoudai, Y., Rastegarkoutenaeei, A., & Bandpy, M. (2022). Investigation of the effect of using the finned tubes on the performance of shell and tube heat exchanger by 3D modeling. *Journal of Energy Storage*, 16. doi:<https://doi.org/10.1016/j.est.2022.106031>
- Manouchehri, R., & Collins, M. R. (2016, March 29). An experimental analysis of the impact of temperature on falling film drain water heat recovery system effectiveness. *Solar Thermal Research Laboratory, Department of Mechanical and Mechatronics Engineering, University of Waterloo, 200 University Avenue West*.
- Martins, G., Santiago, R., Beckedorff, L., Possamai, T., Oliveira, J., de Oliveira, A., & Paiva, K. (2022). Structural analysis of gasketed plate heat exchangers. *International Journal of Pressure Vessels and Piping*, 197 (2022) 104634. doi:<https://doi.org/10.1016/j.ijpvp.2022.104634>
- Martynov, V., & Krasnikova, O. (1987). Thermal hydrodynamic characteristics of coil heat exchangers of throttle stage of cryogenic helium plants. *Chemical and Petroleum engineering.*, 24-28.
- Mayer, P. W., & DeOreo, W. B. (1999). Residential End Uses of Water. *New York: AWWA Research Foundation*, 99-101.
- McNabola, A., & Killian, S. (2012). Efficient drain water heat recovery in horizontal domestic shower drains. *Energy and Buildings*, 6.
- MG, F. (1986). *Corrosion Engineering*, 4-5.
- Milani, S., Momourian, M., & Esfahani, J. A. (2019). Experimental study on thermal analysis of a novel shell and tube heat exchanger with corrugated tubes. *Journal of Thermal Analysis and Calorimetry*, 138:1583–1606.
- Mohammed, T., Otsuki, N., & Hamada, H. (2003). Corrosion of Steel Bar in Cracked Concrete Under Marine Environment . *ASCE, Journal of Material in Civil Engineering*, 15:460-469.
- Mohebbi, S., & Veysi, F. (2019). *An experimental investigation on the heat transfer and friction coefficients of a small plate heat exchanger with chevron angle*. Springer-Verlag: Springer-Verlag GmbH Germany, part of Springer Nature 2019.
- Naphon, P. (2007). Thermal performance and pressure drop of the helical-coil heat exchangers with and without helically crimped fins. *Int. Commun. Heat Mass Transfer*, 321-330. doi:<https://doi.org/10.1016/j.icheatmasstransfer.2006.11.009>

- Ohk, S.-M., & Chung, B.-J. (2017). Natural convection heat transfer inside an open vertical pipe: Influences of length, diameter and Prandtl number. *International Journal of Thermal Sciences*, 54-64. Retrieved from www.elsevier.com/locate/ijts
- Padwal, A. (2022, March 1). *Cove.tool*. Retrieved from Cove.tool: <https://help.covetool.com/en/articles/2625583-what-is-necb>
- Parent, M. G. (1988). *Natural Convection Heat Exchnagers: Theory and Experiment*. Waterloo, Ontario: Waterloo, Ontario.
- Pelliccione, A. (2019). Failure analysis of a titanium plate heat exchanger mechanical fatigue. *Eng. Fail. Anal.* 105, 1172–1188.
- Reisel, J. R. (2016). *Principles of engineering thermodynamics*. Boston : Cengage Learning, Inc.
- Revie, R. W., & Uhlig, H. H. (1972). Further evidence regarding the dezincification mechanism[J]. *Corr Sci*, 669-671.
- Rickard, C., Dwyer, O., & Dropkin, D. (1958). Heat-Transfer Rates to Cross-Flowing Mercury in a Staggered Tube Bank. *I. Trans. Am. Soc. Mech. Eng* , 80, 646–65.
- Roppo, M., & Ganl, E. (1983). Time-dependent heat exchanger modeling. *Heat Transfer Eng.* 4, 42-46. doi:<https://doi.org/10.1080/01457638108939600>
- Saha, S., & Khan, A. (2020). Numerical study on the effect of corrugation angle on thermal performance of cross corrugated plate heat exchangers. *Thermal Science and Engineering Progress*, 2451-9049. doi:100711
- Saunders , H. (2015). Recent evidence for large rebound: elucidating the drivers and their implications for climate change models. *Energy Journal*, 23-48.
- Schlünder, E., & Gaddis, E. (1979). Temperature distribution and heat exchange in multipass shell-and-tube exchangers with baffles. *Heat Transfer Eng.* 1, 43-52. doi:<https://doi.org/10.1080/01457637908939548>
- Selbas, R., Kızılkın, O., & Reppich, M. (2006). new design approach for shell-and-tube heat exchangers using genetic algorithms from economic point of view. *Chem. Eng. Process. Process Intensif.* 45 (4), 268-275.
- Seyedzadeh, P. F. (2021). *Data-Driven Modelling of Non-Domestic Building Energy Performance*. Springer International Publishing AG.

- Shams, A., Santis, D., & Roelofs, F. (2019). An overview of the AHFM-NRG formulations for the accurate prediction of turbulent flow and heat transfer in low-Prandtl number flows. *Nucl. Eng. Des.*, 355, 238-258.
- Shen, C., Liu, L., Xu, Z., Gu, H., & Liu, M. (2023). Influence of helix angle on flow and heat transfer characteristics of lead–bismuth flow in helical-coiled tube bundles. *Annals of Nuclear Energy*, 109483. doi:<https://doi.org/10.1016/j.anucene.2022.109483>
- Thulukkanam, K. (2013). *Heat exchnagers design handbook*. Ohio: Taylor & Francis Group.
- Van Rossum, N. J. (1990). *Natural Convection in Vertical Circular Tubes With and Without Twisted Tape Inserted*. Halifax: Technical University of Nova Scotia.
- Wallin, & Claesson, J. (2014). Investigating the efficiency of a vertical inline drain water heat recovery heat exchanger in a system boosted with a heat pump. *Energy and Buildings*, 80,7-16. doi:<https://doi.org/10.1016/j.enbuild.2014.05.003>
- White, F. M. (2009). *Fluid Mechanics*. New York: Raghathan Srinivasan.
- Zaloum, C., Lafrance, M., & Gusdorf, J. (2007). Drain Water Heat Recovery Characterization and Modeling. *Ottawa: Sustainable Buildings and Communities Natural Resources Canada*, 38-40.

APPENDIX A.

A.1. CODE FOR HYDRAULIC CALCULATIONS

```
# Finding the mass flow rate of the water side of the Brazed  
Plate HX  
  
# Tank and heat exchanger dimensions are not accurate  
  
# Items used:  
  
# Shear Pressure:  
  
# 2x Ball valve 3/4"  
  
# 3x 90 elbow 3/4"  
  
# 2x Union 3/4"  
  
# 1x Reducer 2" to 3/4"  
  
# 1x Bushing 3/4" to 2"  
  
# 3/4" Pipe of length tank to pipe"  
  
# 3/4" Pipe of length pipe to tank"  
  
# 3/4" Pipe of length pipe A, B and C"  
  
# Other friction (shear) Losses:  
  
# 1. Contraction  
  
# 2. Expansion  
  
  
# The Brazed plate Heat exchanger is a model of M14A-12, which  
means it has 12 plates. Number of cold channels are 6 and the  
hot one are 5./  
  
# in total of 11 channels  
  
import CoolProp.CoolProp as CP  
  
import numpy as np  
  
import math
```

```

from decimal import Decimal
import matplotlib.pyplot as plt
import xlwings as xw
from scipy import integrate

# Shear Pressure due to the fittings and losses in the system
elements

# Static pressure due to the change of temperature in the tank
and heat exchanger

#  $\Delta P = \rho \cdot g \cdot H$ 

# Define an average definition
def sqrt(number):
    sqareroot = number**0.5
    return sqareroot

def av(sequence):
    total = sum(sequence)
    count = len(sequence)
    average = total / count
    return average

# Initial conditions:
size = 5
print('Size of: ', int(size))
m_dot_w = np.zeros(int(size))
TCo = np.zeros(int(size))
V = np.zeros(int(size))
Delta_P_Hx = np.zeros(int(size))
Delta_P_sh = np.zeros(int(size))
Delta_P = np.zeros(int(size))
Re_w = np.zeros(int(size))

```

```

Delta_P_T = np.zeros(int(size))
Delta_T = np.zeros(int(size))
Tci = np.zeros(int(size))
Pr_w = np.zeros(int(size))
K_w = np.zeros(int(size))
Nu_w = np.zeros(int(size))
h_w = np.zeros(int(size))
vis_w = np.zeros(int(size))
# Initial Assumptions
# in Kg/s initial assumed mass flow
M_w = np.full(int(size), 0.0009)
Tci = 20+273.15
# number of plate and channels
n_P = 12
nc = 12-1
ncc = n_P/2
nch = (n_P-2)/2
P = np . array ([500, 1000, 1500, 2000, 3000])
# Iteration
for j in range(size):
    while M_w[j] < 1:
        # input:
        fluid_1 = "water"
        quality = 0
        g = 9.81 # Gravitational acceleration
        pi = math.pi
        cp = CP.PropsSI('C', 'T', Tci, 'Q', 0, fluid_1)

```



```

Factor = 2
K = 1
# outlet temperature of based on the P[j] and the
inlet temperature
TCo[j] = Tci+P[j]/(M_w[j]*cp)
# Diameter of all components
D_pipe = 0.019
D_elbow = 0.019
D_valve = 0.019
D_reducer = 0.019
D_bushing = 0.019
D_Union = 0.019
# Dimensions in m
L_HX = 0.15 # length of the heat exchanger
t = 0.00189 # m
L_Pipe1 = 0.41
D_in = 0.0127 # diameter of the inner pipe of HX
L_Tank = 1.5 # length of the tank
w = 0.079 # length of HX
Area_ch = t*w # m^2
Dh = 2*t
# Change of temperature and density with tank height
(temperature distribution in the Tank ):
rho = np.zeros(6)
vis = np.zeros(6)
H_Tank = np.linspace(0, L_Tank, 6)
Tc = np.full(6, 273.15)
for i in range(6):

```

```

Tc[i] = (TCo[j]-Tci)*H_Tank[i]/L_Tank + \
        Tci # based on a linear relation

# Finding density at each height
rho[i] = CP.PropsSI('D', 'T', Tc[i], 'Q', quality,
fluid_1)
vis[i] = CP.PropsSI('V', 'T', Tc[i], 'Q', quality,
fluid_1)
rho_av = av(rho)
vis_av = av(vis)

# effective length and pressure drop of fittings:
# @ inlet:
L_tank_exit = 0.5*M_w[j]/(16*pi*vis[0])
Delta_P_tank_exit = 128*vis[0]*M_w[j] * \
        L_tank_exit/(rho[0]*pi*pow(D_pipe, 4))
L_valve_inlet = 0.19*M_w[j]/(16*pi*vis[0])
Delta_P_valve_inlet = 128*vis[0]*M_w[j] * \
        L_valve_inlet/(rho[0]*pi*pow(D_valve, 4))
L_elbow_inlet = 0.9*M_w[j]/(16*pi*vis[0])
Delta_P_elbow_inlet = 128*vis[0]*M_w[j] * \
        L_elbow_inlet/(rho[0]*pi*pow(D_elbow, 4))
L_Union_inlet = 0.04*M_w[j]/(16*pi*vis[0])
Delta_P_Union_inlet = 128*vis[0]*M_w[j] * \
        L_Union_inlet/(rho[0]*pi*pow(D_Union, 4))
L_HX_inlet = 1.0*M_w[j]/(16*pi*vis[0])
Delta_P_HX_inlet = 128*vis[0]*M_w[j] * \
        L_HX_inlet/(rho[0]*pi*pow(D_pipe, 4))
L_pipe_inlet = 0.32

```

```

Delta_P_pipe_inlet = 128*vis[0]*M_w[j] * \
    L_pipe_inlet/(rho[0]*pi*pow(D_pipe, 4))
# @ exit:
L_HX_exit = 0.5*M_w[j]/(16*pi*vis[5])
Delta_P_HX_exit = 128*vis[5]*M_w[j] * \
    L_HX_exit/(rho[5]*pi*pow(D_pipe, 4))
L_elbow_exit = 0.9*M_w[j]/(16*pi*vis[5])
Delta_P_elbow_exit = 128*vis[5]*M_w[j] * \
    L_elbow_exit/(rho[5]*pi*pow(D_elbow, 4))
L_Union_exit = 0.04*M_w[j]/(16*pi*vis[5])
Delta_P_Union_exit = 128*vis[5]*M_w[j] * \
    L_Union_exit/(rho[5]*pi*pow(D_Union, 4))

L_valve_exit = 0.19*M_w[j]/(16*pi*vis[5])
Delta_P_valve_exit = 128*vis[5]*M_w[j] * \
    L_valve_exit/(rho[5]*pi*pow(D_valve, 4))
L_pipe_exit = 1.2
Delta_P_pipe_exit = 128*vis[5]*M_w[j] * \
    L_pipe_exit/(rho[5]*pi*pow(D_pipe, 4))
L_tank_inlet = 1.0*M_w[j]/(16*pi*vis[5])
Delta_P_tank_inlet = 128*vis[5]*M_w[j] * \
    L_tank_inlet/(rho[5]*pi*pow(D_pipe, 4))

# Heat exchanger pressure drop:
rho_hx = CP.PropsSI('D', 'T', (Tc[0]+Tc[5])/2, 'Q',
quality, fluid_1)
vis_hx = CP.PropsSI('V', 'T', (Tc[0]+Tc[5])/2, 'Q',
quality, fluid_1)

```

```

    K_hx = CP.PropsSI('L', 'T', (Tc[0]+Tc[5])/2, 'Q',
quality, fluid_1)

```

```

    V[j] = M_w[j]/(rho_hx*Area_ch*ncc)

```

```

    Delta_P_Hx[j] = K*4*V[j]*vis_hx*L_HX/t**2

```

```

# Total Shear Pressure:

```

```

    Delta_P_sh = Delta_P_tank_exit + L_valve_inlet +
2*Delta_P_elbow_inlet + \

```

```

        L_Union_inlet + Delta_P_HX_inlet +
Delta_P_pipe_inlet

```

```

    Delta_P_sh = Delta_P_sh + Delta_P_HX_exit +
3*Delta_P_elbow_exit + \

```

```

        Delta_P_Union_exit + Delta_P_valve_exit + \

```

```

        Delta_P_pipe_exit + Delta_P_tank_inlet

```

```

    Delta_P_sh = Factor*(Delta_P_sh + Delta_P_Hx[j])

```

```

# Pressure Drop in the Tank:

```

```

    C1 = -2.8054253*10**(-10)

```

```

    C2 = 1.0556302*10**(-7)

```

```

    C3 = -4.6170461*10**(-5)

```

```

    C4 = -0.0079870401

```

```

    C5 = 16.945176

```

```

    C6 = 999.83952

```

```

    C7 = 0.01687985

```

```

def f1(Z):

```

```

    T = (TCo[j]-Tci)*(Z-L_Tank)/L_Tank+TCo[j]-273.15

```

```

    rho =

```

```

((((((C1*T+C2)*T+C3)*T+C4)*T+C5)*T+C6)/(1+C7*T)

```

```

    Delta_P_Tank = rho*g

```

```

    return Delta_P_Tank

```

```

        Delta_P_Tank, error1 = integrate.quad(f1, 0, L_Tank)
# Pressure Drop in the Hx:
def f2(Z):
    T = (TCo[j]-Tci)*(Z-L_HX)/L_HX+TCo[j]-273.15
    rho =
((((((C1*T+C2)*T+C3)*T+C4)*T+C5)*T+C6)/(1+C7*T)
    Delta_P_HX = rho*g
    return Delta_P_HX
    Delta_P_HX, error2 = integrate.quad(f2, 0, L_HX)
# Total Static Pressure:
# print (Delta_P_Tank, rho[0]*g*L_Tank,TCo[j])
Delta_P_st = Delta_P_Tank - Delta_P_HX - \
    rho[0]*g*L_Pipe1 - rho[5]*g*(L_Tank-L_Pipe1-L_HX)
# finding the mass flow rate
if Delta_P_sh < Delta_P_st+0.01*Delta_P_st and
Delta_P_sh > Delta_P_st-0.01*Delta_P_st:
    print("Mass Flow Rate= ", f"{M_w[j]:.4f}",
        "Kg/s", "=", f"{60*M_w[j]:.4f}", "Lpm")

Re_w[j] = rho_hx*V[j]*Dh/vis_hx
Delta_P_T[j] = Delta_P_Tank
Delta_P[j] = Delta_P_st
Delta_T[j] = TCo[j] - Tci
K_w[j] = K_hx
Pr_w[j] = vis_hx*cp/K_w[j]
vis_w[j] = CP.PropsSI('V', 'T', (Tci+TCo[j]) /
                        2, 'Q', quality, fluid_1)

```

```

# print ('P=', P, 'W')
# print (P[j], mass)
j += 1
if j <= size-1:
    M_w[j] = M_w[j-1]
    print("Loading:",
f"{int((j+1)*100/int(size)):.2f}", "% -----")
    print(P, Tci-273.15, TCo-273.15, M_w)
    break
if Delta_P_sh != Delta_P_st:
    M_w[j] += 0.00001
print(P, M_w, TCo-273.15)

```

A.2. CODE FOR THERMAL CALCULATIONS

```
from BrazedPlateSP import M_w # type: ignore
from BrazedPlateSP import Pr_w
from BrazedPlateSP import Re_w # type: ignore
from BrazedPlateSP import P # type: ignore
from BrazedPlateSP import vis_w # type: ignore
from BrazedPlateSP import TCo # type: ignore
from BrazedPlateSP import K_w
from BrazedPlateSP import Tci
from BrazedPlateSP import ncc
from BrazedPlateSP import nch
from BrazedPlateSP import nc
from BrazedPlateSP import n_P
from BrazedPlateSP import L_HX
from BrazedPlateSP import Delta_P_Hx
from BrazedPlateSP import Delta_P
from BrazedPlateSP import Dh

import numpy as np
import math
import pandas as pd
from BrazedPlateSP import size # type: ignore
import CoolProp.CoolProp as CP
import matplotlib.pyplot as plt
import xlwings as xw
# Input and dimensions:
```

```

t = 0.00189 # m
L = 0.156 # m # flow length
A = 0.014 # m2 area a plate = surface area
w = 0.079 # m
Twi = Tci
Two = TCo

# definitions:

m_dot_g = np.zeros(int(size))
Tgo = np.zeros(int(size))
T_wall = np.zeros(int(size))
vis_wall = np.zeros(int(size))
Nu_w = np.zeros(int(size))
h_w = np.zeros(int(size))
rho_g = np.zeros(int(size))
V_g = np.zeros(int(size))
Nu_g = np.zeros(int(size))
vis_g = np.zeros(int(size))
K_g = np.zeros(int(size))
Pr_g = np.zeros(int(size))
Re_g = np.zeros(int(size))
h_g = np.zeros(int(size))
DeltaT1 = np.zeros(int(size))
DeltaT2 = np.zeros(int(size))
DeltaPH = np.zeros(int(size))
DeltaTlog = np.zeros(int(size))

```



```

q_UA = np.zeros(int(size))
U = np.zeros(int(size))
Cp_g = np.zeros(int(size))
Tgi = np.zeros(int(size))
log = np.zeros(int(size))
m_dot_g = np.linspace(0.2, 0.41, size)
C = 0.1/0.49/0.95/0.99
# Loop 1:
for i in range(size):
    # m_dot_g [i] = -4 * 10**(-8) * P [i]**2 + 0.0002 * P [i]
    + 0.108 #GPM
    m_dot_g[i] = m_dot_g[i] * 3.8 / 60
    # Assume:
    Tgi[i] = Two[i] + 1
    # loop 2:
    while Tgi[i] < 300 + 273.15:
        Tgav = (Tgi[i] + Tgo[i]) / 2
        # m_dot_g[i] = 0.1606 * math.log(P[i]) - 0.6821 #GPM
        Cp_g[i] = 2.3205 * (Tgi[i] - 273.15) + 3731.4
        Tgo[i] = Tgi[i] - P[i] / (m_dot_g[i] * Cp_g[i])
        T_wall[i] = (Tgo[i] + Tgi[i] + Two[i] + Twi) / 4
        # water side:
        vis_wall[i] = CP.PropsSI('V', 'T', T_wall[i], 'Q', 0,
"water")
        # Nu_w [i] = C * (Re_w[i] * Pr_w[i] * 2 * t / L)**
0.333 * (vis_w[i] / vis_wall[i])**0.14
        Nu_w[i] = C * Re_w[i]**0.75 * Pr_w[i]**0.4 # 10 < Re
< 720
        # Nu_w [i] = 1.05 * Re_w [i]**0.64 * Pr_w [i]**0.5

```

```

h_w[i] = K_w[i]*Nu_w[i] / (2 * t)

# Glycol side:
rho_g[i] = -1.532 * 10**(-3) * (Tgav - 273.15)**2 - \
          5.336 * 10 ** (-1) * (Tgav - 273.15) + 1.043 *
10**3
vis_g[i] = -2.904 * 10**(-8) * (Tgav - 273.15)**3 +
6.001 * 10 ** (-6) * (
          Tgav - 273.15) ** 2 - 4.240 * 10 ** (-4) * (Tgav -
273.15) + 1.138 * 10**(-2)
K_g[i] = 7.001 * 10**(-8) * (Tgav - 273.15)**3 - 1.313
* 10 ** (-5) * (
          Tgav - 273.15)**2 + 1.268 * 10 ** (-3) * (Tgav -
273.15) + 3.793 * 10**(-1)
Pr_g[i] = vis_g[i] * Cp_g[i]/K_g[i]
V_g[i] = m_dot_g[i] / (nch * rho_g[i] * t * w)
Re_g[i] = (rho_g[i] * V_g[i] * 2 * t) / vis_g[i]
# Nu_g [i] = C * (Re_g[i] * Pr_g[i] *2 * t / L)**0.333
* (vis_g[i] / vis_wall[i])**0.14
Nu_g[i] = C * Re_g[i]**0.75 * Pr_g[i]**0.4
# Nu_g [i] = 1.05 * Re_g [i]**0.64 * Pr_g [i]**0.5
h_g[i] = K_g[i] * Nu_g[i] / (2 * t)
# pressure drop:
DeltaPH[i] = 4*vis_g[i]*V_g[i]*L_HX/(t**2)
DeltaT1[i] = Tgi[i] - Two[i]
DeltaT2[i] = Tgo[i] - Twi
log = math.log(DeltaT1[i] / DeltaT2[i])
DeltaTlog[i] = (DeltaT1[i] - DeltaT2[i]) / (log)
U[i] = 1 / (1 / h_g[i] + 1 / h_w[i])
q_UA[i] = U[i] * (n_P-2) * A * DeltaTlog[i]

```

```

        if q_UA[i] < P[i] + 0.0005 * P[i] and q_UA[i] > P[i] -
0.0005 * P[i]:
            print(Tgi[i] - 273.15, P[i])
            break
    if q_UA[i] != P[i]:
        Tgi[i] = Tgi[i] + 0.01
        # print (Tgi[i]-273.15)
print(Tgi, U*nc*A, q_UA, " Done!", Dh)

Twi = np. full(size, Twi-273.15)

data = np.array([q_UA, Tgi - 273.15, Tgo - 273.15, Tgi-Tgo,
Twi, Two - 273.15, Two - Twi -273.15 , M_w, m_dot_g,
                DeltaT1, DeltaT2, DeltaTlog, U*A* (n_P-2),
Delta_P_Hx, Delta_P, DeltaPH,h_w, h_g, Re_w, Re_g, Nu_w,
Nu_g])

Tansposed_data= data.T

df = pd.DataFrame(data.T, columns=['q(w)', 'Tgi(C)', 'Tgo(C)',
'DeltaTg', 'Twi(C)', 'Two(C)', 'DeltaTw',
                                'mW (Kg/s)', 'mg (Kg/s)',
'DeltaT1', 'DeltaT2', 'DeltaTlog',
                                'UA(w/k)', 'DeltaPHX_w(Pa)',
'DeltaP_w(Pa)', 'DeltaPHX_g(Pa)', 'h_w', 'h_g', 'Re_w' ,
'Re_g', 'Nu_w', 'Nu_g'])

df.to_excel('HeatTransfer.xlsx', index=False)

plt.plot (DeltaTlog, Tgi - Tgo )

plt.show()

```

A.3. CODE FOR FREE AND FORCED CONVECTION

```
from BrazedPlateSP import M_w # type: ignore
from BrazedPlateSP import Pr_w
from BrazedPlateSP import Re_w # type: ignore
from BrazedPlateSP import P # type: ignore
from BrazedPlateSP import vis_w # type: ignore
from BrazedPlateSP import TCo # type: ignore
from BrazedPlateSP import K_w
from BrazedPlateSP import Tci
from BrazedPlateSP import ncc
from BrazedPlateSP import nch
from BrazedPlateSP import nc
from BrazedPlateSP import n_P
from BrazedPlateSP import L_HX
from BrazedPlateSP import Delta_P_Hx
from BrazedPlateSP import Delta_P
from BrazedPlateSP import cp as cp_w
import numpy as np
import math
import pandas as pd
from BrazedPlateSP import size # type: ignore
import CoolProp.CoolProp as CP
import matplotlib.pyplot as plt

# Input and dimensions:
t = 0.00189 # m
```

```

L = 0.156 # m # flow length
A = 0.014 # m2 area a plate = surface area
w = 0.079 # m
Twi = Tci
Two = TCo
fluid_1 = "water"
# definitions:

m_dot_g = np.zeros(size)
Tgo = np.zeros(size)
T_wall = np.zeros(size)
vis_wall = np.zeros(size)
Tgav =np.zeros(size)
Nu_w = np.zeros(size)
h_w = np.zeros(size)
Gr = np.zeros(size)
rho_g = np.zeros(size)
V_g = np.zeros(size)
Nu_g = np.zeros(size)
vis_g = np.zeros(size)
K_g = np.zeros(size)
Pr_g = np.zeros(size)
Re_g = np.zeros(size)
h_g = np.zeros(size)
DeltaT1 = np.zeros(size)
DeltaT2 = np.zeros(size)
DeltaPH = np.zeros(size)

```

```

DeltaTlog = np.zeros(size)
q_UA = np.zeros(size)
U = np.zeros(size)
Cp_g = np.zeros(size)
Tgi = np.zeros(size)
log = np.zeros(size)
rho_w = np.zeros(size)
alfa_w = np.zeros(size)
Ra = np.zeros(size)
Twav = np.zeros(size) # mean temperature for water side
m_dot_g = np.linspace(0.2, 0.41, size)
g = 9.81 #m/s2
beta = np.zeros(size)
C = 0.1/0.49/0.95/0.99

C1 = 576
C2 = 2.87
# Loop 1:
for i in range(size):
    # m_dot_g [i] = -4 * 10**(-8) * P [i]**2 + 0.0002 * P [i]
    + 0.108 #GPM

    m_dot_g[i] = m_dot_g[i] * 3.8 / 60
    # Assume:

    Tgi[i] = Two[i] + 1
    # loop 2:
    while Tgi[i] < 100 + 273.15:

```

```

Tgav[i]= (Tgi[i] + Tgo[i]) / 2
Twav[i] = (Twi [i] + Two [i]) / 2
# m_dot_g[i] = 0.1606 * math.log(P[i]) - 0.6821 #GPM

Cp_g[i] = 2.3205 * (Tgi[i] - 273.15) + 3731.4
Tgo[i] = Tgi[i] - P[i] / (m_dot_g[i] * Cp_g[i])
T_wall[i] = (Tgo[i] + Tgi[i] + Two[i] + Twi[i]) / 4
vis_wall[i] = CP.PropsSI('V', 'T', T_wall[i], 'Q', 0,
"water")

# water side - Natural Convection:

beta[i] = CP.PropsSI('ISOBARIC_EXPANSION_COEFFICIENT',
'T', Twav [i], 'Q', 0, fluid_1)

rho_w [i] = CP.PropsSI('D', 'T', Twav [i], 'Q', 0 ,
fluid_1)

alfa_w [i] = cp_w [i] / (K_w [i] * rho_w [i])

Gr [i] = g * beta [i] * (T_wall [i] - Twav [i]) *
t**3 / ((vis_w [i]/ rho_w [i])**2)

Ra [i] = Gr [i] * Pr_w [i]

#Nu_w[i] = ((24 / Ra [i]) **2 + (1 / ( 0.59 * Ra
[i]**0.25 )) **2 ) ** (-0.5)

#Nu_w [i] = 1/24 * Ra [i] * t/L_HX * (1 - math.exp (-
35/(Ra [i]*t/L_HX))) ** 0.75

Nu_w [i] = 0.414 * Ra [i]** 0.414
h_w[i] = K_w[i]*Nu_w[i] / (2 * t)

# Glycol side:
rho_g[i] = -1.532 * 10**(-3) * (Tgav[i]- 273.15)**2 -
\

```

```

5.336 * 10 ** (-1) * (Tgav[i]- 273.15) + 1.043 *
10**3
vis_g[i] = -2.904 * 10**(-8) * (Tgav[i]- 273.15)**3 +
6.001 * 10 ** (-6) * (
Tgav[i]- 273.15) ** 2 - 4.240 * 10 ** (-4) *
(Tgav[i]- 273.15) + 1.138 * 10**(-2)
K_g[i] = 7.001 * 10**(-8) * (Tgav[i]- 273.15)**3 -
1.313 * 10 ** (-5) * (
Tgav[i]- 273.15)**2 + 1.268 * 10 ** (-3) *
(Tgav[i]- 273.15) + 3.793 * 10**(-1)

Pr_g[i] = vis_g[i] * Cp_g[i]/K_g[i]
V_g[i] = m_dot_g[i] / (nch * rho_g[i] * t * w)
Re_g[i] = (rho_g[i] * V_g[i] * 2 * t) / vis_g[i]

# Nu_g [i] = C * (Re_g[i] * Pr_g[i] *2 * t / L)**0.333
* (vis_g[i] / vis_wall[i])**0.14
Nu_g[i] = C * Re_g[i]**0.75 * Pr_g[i]**0.4
# Nu_g [i] = 1.05 * Re_g [i]**0.64 * Pr_g [i]**0.5
h_g[i] = K_g[i] * Nu_g[i] / (2 * t)

# pressure drop:
DeltaPH[i] = 4*vis_g[i]*V_g[i]*L_HX/(t**2)

DeltaT1[i] = Tgi[i] - Two[i]
DeltaT2[i] = Tgo[i] - Twi [i]
log = math.log(DeltaT1[i] / DeltaT2[i])
DeltaTlog[i] = (DeltaT1[i] - DeltaT2[i]) / (log)
U[i] = 1 / (1 / h_g[i] + 1 / h_w[i])
q_UA[i] = U[i] * (n_P-2) * A * DeltaTlog[i]

```



```

        if q_UA[i] < P[i] + 0.005 * P[i] and q_UA[i] > P[i] -
0.005 * P[i]:
            print(Tgi[i] - 273.15, P[i])

            break

        if q_UA[i] != P[i]:
            Tgi[i] = Tgi[i] + 0.01
            print (Nu_g [i], Nu_w[i], q_UA [i] , P[i])

print(Tgi, U*nc*A, q_UA, " Done!", Ra/Re_w**2)

data = np.array([q_UA, Tgi - 273.15, Tgo - 273.15, Tgi-Tgo,
Twi -273.15, Two - 273.15, Two - Twi, M_w*60, m_dot_g*60,
                DeltaT1, DeltaT2, DeltaTlog, U*A*nc,
Delta_P_Hx, Delta_P, DeltaPH, beta, Ra, h_w, h_g, Gr, Pr_w])
Tansposed_data= data.T

df = pd.DataFrame(data.T, columns=['q(w)', 'Tgi(C)', 'Tgo(C)',
'DeltaTg', 'Twi(C)', 'Two(C)', 'DeltaTw',
                                'mW (Lpm)', 'mg (Lpm)',
'DeltaT1', 'DeltaT2', 'DeltaTlog',
                                'UA(w/k)', 'DeltaPHX_w(Pa)',
'DeltaP_w(Pa)', 'DeltaPHX_g(Pa)', ' beta', 'Ra', 'h_w',
'h_g', 'Gr', 'Pr_w'])

df.to_excel('HeatTransfer.xlsx', index=False)

```

A.4. CODE FOR CATALOGUE VS. CORRECTIONS

```
# Computinh for PL heat exchanher at 3 points - PL 45 - PL 70
- PL 130

import numpy as np
import math
import pandas as pd
import CoolProp.CoolProp as CP
import matplotlib.pyplot as plt
# Input and dimensions:
A = np.array([0.15, 0.246, 0.339])
n_p = 37 # number of internal pipes
l = np.array([0.15, 0.25, 0.35]) # m # pipe length
D_HX = 0.0075 # m Nominal
D_HX_inner = 0.00635 # m
D_HX_outer = 0.0086 # m
D_HX_s = 0.08 # m
D_HX_h = (D_HX_s**2 - n_p * D_HX_outer**2)**0.5

# power input:
P = [13000, 20000, 38000]
size = len(P)

# definitions:

# hot fluid prop
Nu_h = np.zeros(size)
vis_h = np.zeros(size)
```

```
K_h = np.zeros(size)
Pr_h = np.zeros(size)
Re_h = np.zeros(size)
h_h = np.zeros(size)
rho_h = np.zeros(size)
V_h = np.zeros(size)
cp_h = np.zeros(size)

# cold fluid Prop
Nu_c = np.zeros(size)
vis_c = np.zeros(size)
K_c = np.zeros(size)
Pr_c = np.zeros(size)
Re_c = np.zeros(size)
h_c = np.zeros(size)
rho_c = np.zeros(size)
V_c = np.zeros(size)
cp_c = np.zeros(size)
vis_c = np.zeros(size)

# wall prop
vis_w = np.zeros(size)
T_w = np.zeros(size)

# temperatures
Thi = np.zeros(size)
Tho = np.zeros(size)
```

```

Tci = np.zeros(size)
Tco = np.zeros(size)
DeltaT1 = np.zeros(size)
DeltaT2 = np.zeros(size)
DeltaTlog = np.zeros(size)
DeltaPH = np.zeros(size)
q_UA = np.zeros(size)
U = np.zeros(size)

# Pressure drop on the hot side
DeltaPH = np.zeros(size)

log = np.zeros(size)

m_dot_h = [23, 25, 27]
m_dot_c = [150, 170, 200]
# math
pi = math.pi
A_c = pi*D_HX_inner**2 / 4
A_h = pi * D_HX_h**2 / 4
# loop for m_dot from lpm to kh/s
for i in range(size):
    m_dot_h[i] = m_dot_h[i]/60
    m_dot_c[i] = m_dot_c[i]/60
fluid_1 = "water"
# Loop 1:
for i in range(size):

```

```

# Assume:

Tci[i] = 10 + 273.15

# loop 2:
while Tci[i] < 500 + 273.15:

    Thi[i] = Tci[i] + 60
    cp_c[i] = CP.PropsSI('C', 'T', Tci[i], 'Q', 0,
fluid_1)
    Tco[i] = Tci[i]+P[i]/(m_dot_c[i]*cp_c[i])
    cp_h[i] = CP.PropsSI('C', 'T', Thi[i], 'Q', 0,
fluid_1)
    Tho[i] = Thi[i] - P[i] / (m_dot_h[i] * cp_h[i])
    Thav = (Thi[i] + Tho[i]) / 2
    Tcav = (Tci[i] + Tco[i]) / 2

    # thermo

    T_w[i] = (Tho[i] + Thi[i] + Tco[i] + Tci[i]) / 4

    # wall
    vis_w[i] = CP.PropsSI('V', 'T', T_w[i], 'Q', 0,
fluid_1)

    # cold side:
    rho_c[i] = CP.PropsSI('D', 'T', Tcav, 'Q', 0, fluid_1)
    vis_c[i] = CP.PropsSI('V', 'T', Tcav, 'Q', 0, fluid_1)
    K_c[i] = CP.PropsSI('L', 'T', Tcav, 'Q', 0, fluid_1)

```

```

Pr_c[i] = vis_c[i] * cp_c[i]/K_c[i]
V_c[i] = m_dot_c[i]/(rho_c[i]*A_c*n_p)
Re_c[i] = rho_c[i]*V_c[i]*D_HX_inner/vis_c[i]
Nu_c[i] = 0.027 * (Re_c[i])** (4/5) * Pr_c[i] ** (1/3)\
        * (vis_c[i] / vis_w[i])**0.14

h_c[i] = K_c[i] * Nu_c[i] / (D_HX_inner)

# hot side:
rho_h[i] = CP.PropsSI('D', 'T', Thav, 'Q', 0, fluid_1)
vis_h[i] = CP.PropsSI('V', 'T', Thav, 'Q', 0, fluid_1)
K_h[i] = CP.PropsSI('L', 'T', Thav, 'Q', 0, fluid_1)
Pr_h[i] = vis_h[i] * cp_h[i]/K_h[i]
V_h[i] = m_dot_h[i]/(rho_h[i]*A_h)
Re_h[i] = 4 * m_dot_h[i] / (vis_h[i] * pi * D_HX_s)

if Re_h[i] < 100:
    C = 1/1.25
    n = -0.694
    h_h[i] = C * Re_h[i]**n * cp_h[i] / \
    Pr_h[i] ** (2/3) * vis_h[i] / (D_HX_h) * \
    Re_h[i] * (vis_h[i] / vis_w[i]) ** 0.14

elif Re_h[i] > 100 and Re_h [i]<1000:
    C = 0.717/1.25
    n = -0.574
    h_h[i] = C * Re_h[i]**n * cp_h[i] / \

```

```

Pr_h[i] ** (2/3) * vis_h[i] / (D_HX_h) * \
Re_h[i] * (vis_h[i] / vis_w[i]) ** 0.14

if Re_h [i]>1000:
    Ct =0.05
    n = 0.01
    Nu_h [i] = Ct *Re_h[i]**0.8 * Pr_h[i]**0.4 *
(vis_h[i] / vis_w[i]) ** n
    h_h[i] = K_h[i] * Nu_h[i] / (D_HX_h)
    # pressure drop at the hot side:
# DeltaPH[i] = 4*vis_h[i]*V_h[i]*1/(t**2)

# log method
DeltaT1[i] = Thi[i] - Tco[i]
DeltaT2[i] = Tho[i] - Tci[i]
log = math.log(DeltaT1[i] / DeltaT2[i])
DeltaTlog[i] = (DeltaT1[i] - DeltaT2[i]) / (log)
U[i] = 1 / (1 / h_h[i] + 1 / h_c[i])
q_UA[i] = U[i] * A[i] * DeltaTlog[i]

if q_UA[i] < P[i] + 0.005 * P[i] and q_UA[i] > P[i] -
0.005 * P[i]:
    print(Thi[i] - 273.15, P[i])

    break

if q_UA[i] != P[i]:
    Tci[i] = Tci[i] + 0.01

```

```

print(q_UA, Re_c, Re_h, Tci, Tco, Thi, Tho)

UA_deltaT= -(Tho-Tci-Thi+Tco)/log
UA_deltaT = P/UA_deltaT
print(Thi, U*A, q_UA, " Done!")

data = np.array([q_UA, Thi - 273.15, Tho - 273.15, Thi-Tho,
Tci - 273.15, Tco - 273.15, Tco - Tci, m_dot_c, m_dot_h,
                DeltaT1, DeltaT2, DeltaTlog, U*A, Re_c, Re_h,
vis_c, vis_h, K_c, K_h, V_c, V_h, vis_w, Pr_h, h_h*D_HX_s/K_h,
UA_deltaT])

Transposed_data = data.T

df = pd.DataFrame(data.T, columns=['q(w)', 'Thi(C)', 'Tho(C)',
'DeltaTh', 'Tci(C)', 'Tco(C)', 'DeltaTc',
                                'mc (Lpm)', 'mh (Lpm)',
'DeltaT1', 'DeltaT2', 'DeltaTlog',
                                'UA(w/k)', 'Re_c', 'Re_h',
'vis_c', 'vis_h', 'k_c', 'k_h', 'Vc', 'Vh', 'vis_w', 'prh',
'Nu_h', 'UA_DeltaT'])

df.to_excel('HeatTransfer.xlsx', index=False)

```


A.5. CODE FOR TEMPERATURE PROFILE OF WATER TANK

```
# find the temperature profile of the water Tank:
```

```
import CoolProp.CoolProp as CP
import numpy as np
import math
from decimal import Decimal
import matplotlib.pyplot as plt
from HeatTransferAnslsis import TWi
from HeatTransferAnslsis import Two
from HeatTransferAnslsis import h_w
from HeatTransferAnslsis import M_w as m_w
from HeatTransferAnslsis import size
from scipy import integrate
from matplotlib import pyplot as plt
from mpl_toolkits.mplot3d import Axes3D
from matplotlib import cm
import pandas as pd
print (TWi, Two)
pi = math.pi

c1 = np.zeros (size)
c2 =np.zeros (size)

fluid_1 = "water"
L_Tank = 1.5
```

```

z = np.linspace(0, L_Tank, 6)
T = np.zeros(6)
Ts = TWi[1] + 273.15

D_T = 0.6 # m Tank dia.

for j in range (size):

    for i in range(6):
        print (Two[j])
        K = CP.PropsSI('L', 'T', Ts, 'Q', 0, fluid_1)
        h = 2.5 * K / D_T
        m = math.sqrt (4 * h / K * D_T)
        c1 [j] = (Two [j] - TWi [j]-273.15) / (math.exp
(m*L_Tank) - math.exp (-m*L_Tank))
        c2[j] =-c1[j]

        T[i] = c1[j] * math.exp(m * z[i]) + c2[j] * math.exp(-
m * z[i]) + TWi [j] + 273.15
        print(T-273.15, z, c1 , c2)

data = np.array([T-273.15, z])
Tansposed_data= data.T

df = pd.DataFrame(data.T, columns=['T (C)', 'Z(m)'])

df.to_excel('TemperatureDis.xlsx', index=False)

```

```

T = T - 273.15
# Data for the cylinder chart
heights = np.linspace(0, 1.5, 6) # Heights of each section

# Increase meshgrid resolution for finer details
theta = np.linspace(0, 2 * np.pi, 200) # Higher resolution
angular coordinate
H, Theta = np.meshgrid(np.linspace(0, 1.5, 300), theta) #
Finer height and angle meshgrid

# Cylindrical coordinates
X = np.cos(Theta)
Y = np.sin(Theta)
Z = H

# CFD-like colormap (similar to Jet)
cfd_cmap = plt.cm.jet # Jet colormap is often used in CFD
visualizations

# Interpolate the temperature data over the finer grid
T_interp = np.interp(H, heights, T) # Interpolate temperature
data over the height
colors = cfd_cmap((T_interp - T.min()) / (T.max() - T.min()))
# Apply CFD-like colormap

# Plotting the cylinder
fig = plt.figure()
ax = fig.add_subplot(111, projection='3d')

```

```
# Plot the surface with the CFD-like colormap
ax.plot_surface(X, Y, Z, facecolors=colors, shade=False,
               rstride=1, cstride=1)

# Adjust plot aesthetics

ax.set_zlim([0, 1.5])
ax.set_xlabel('X')
ax.set_ylabel('Y')
ax.set_zlabel('Height (m)')

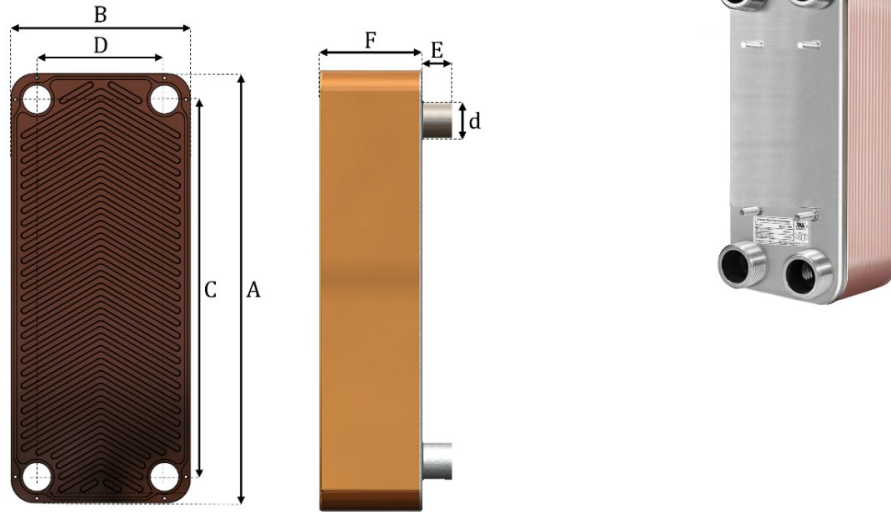
# Optional: remove the axis grid for a cleaner look
ax.grid(False)

# Show colorbar with the CFD-like colormap
mappable = plt.cm.ScalarMappable(cmap=cfd_cmap)
mappable.set_array(T)
plt.colorbar(mappable, ax=ax, label='Temperature (°C)')

plt.show()
```

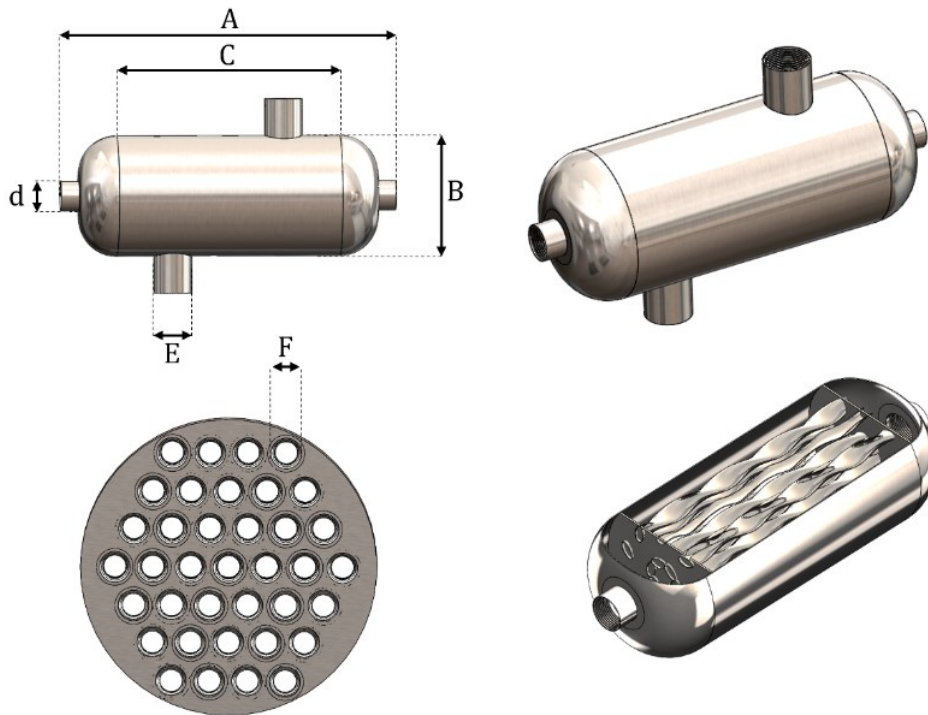
APPENDIX B.

B.1. BRAZED PLATE



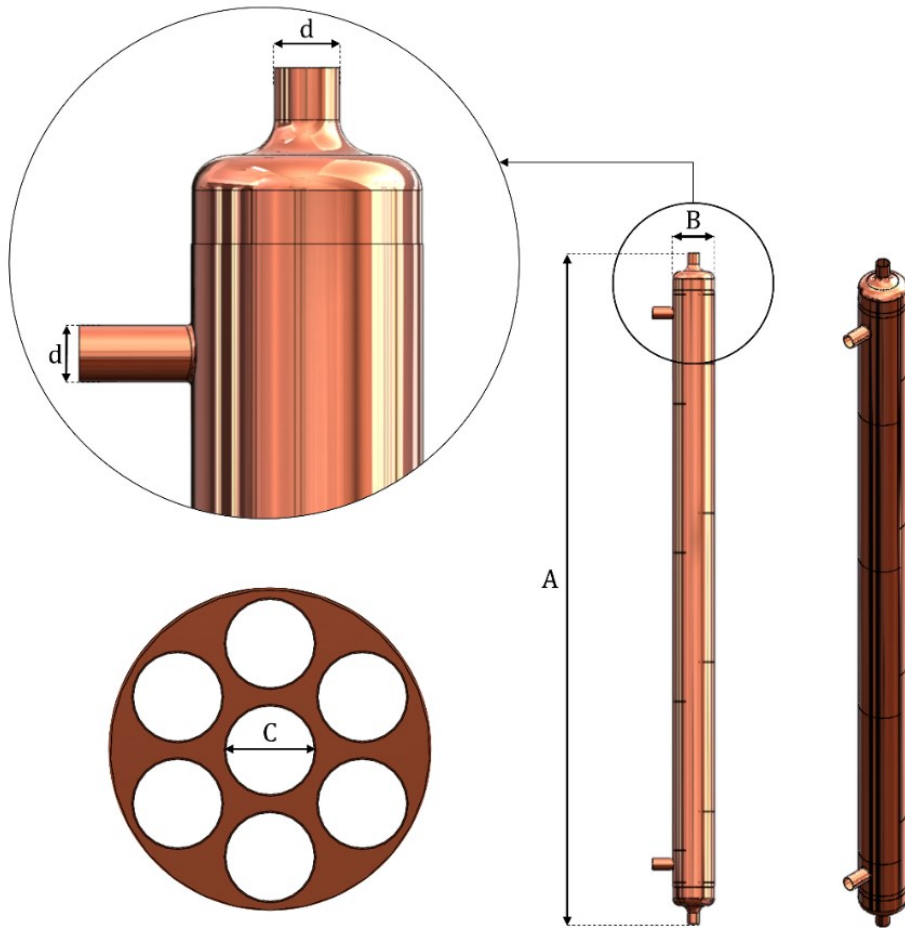
	A	B	C	D	E	F	Np	d
Dim(in)	7.6	3.1	6.1	1.6	3/4	.36+0.09np	12	3/4"
Dim(mm)	193	79	155	40.6	19			NPT

B.2. SHELL AND TWISTED TUBE



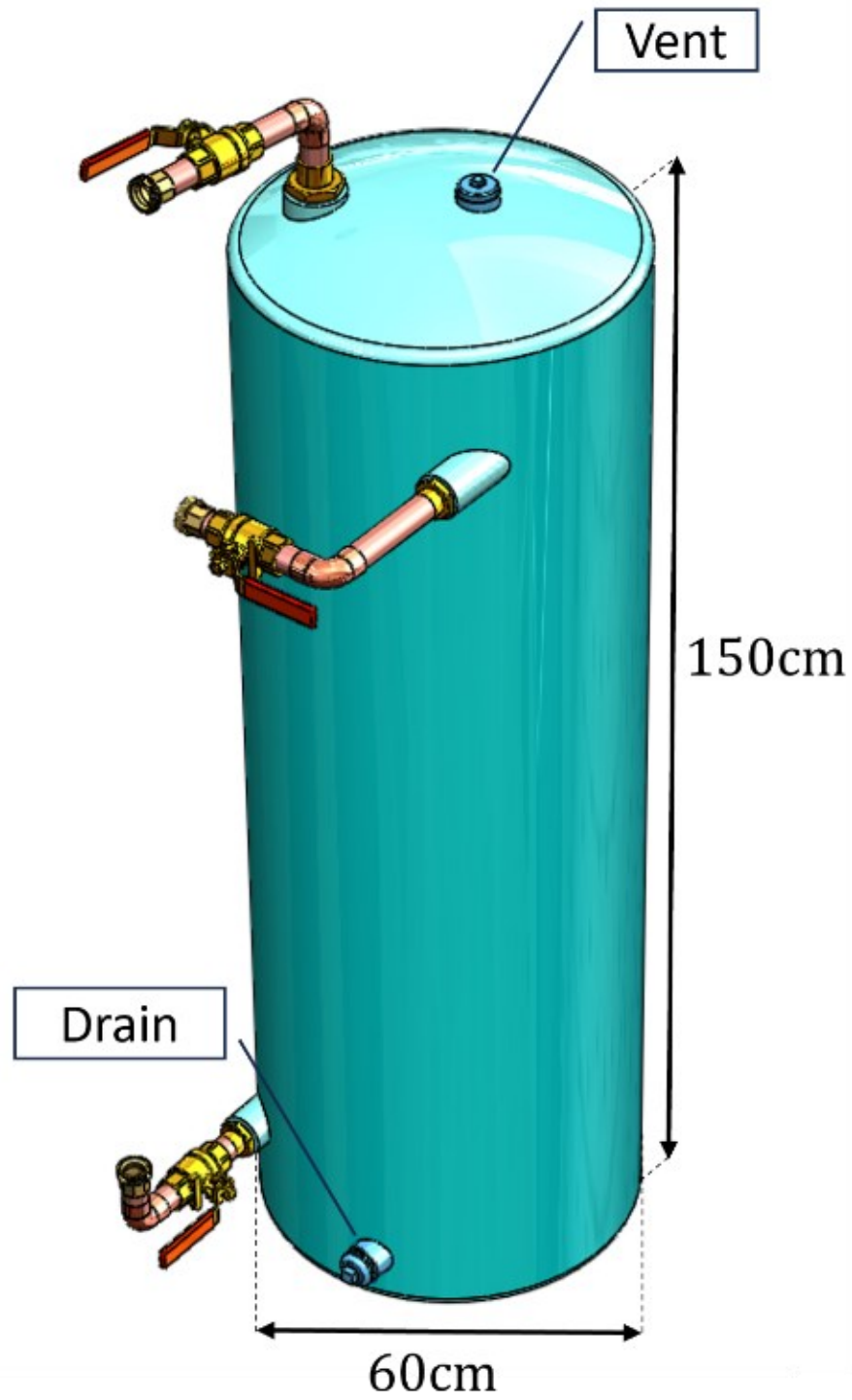
	A	B	C	D	E	F	d
Dim(in)	12	3.15	6	1.6	1" NPT	0.23	¾"
Dim(mm)	305	80	152	40.6	19	6	NPT

B.3. SHELL AND TUBE



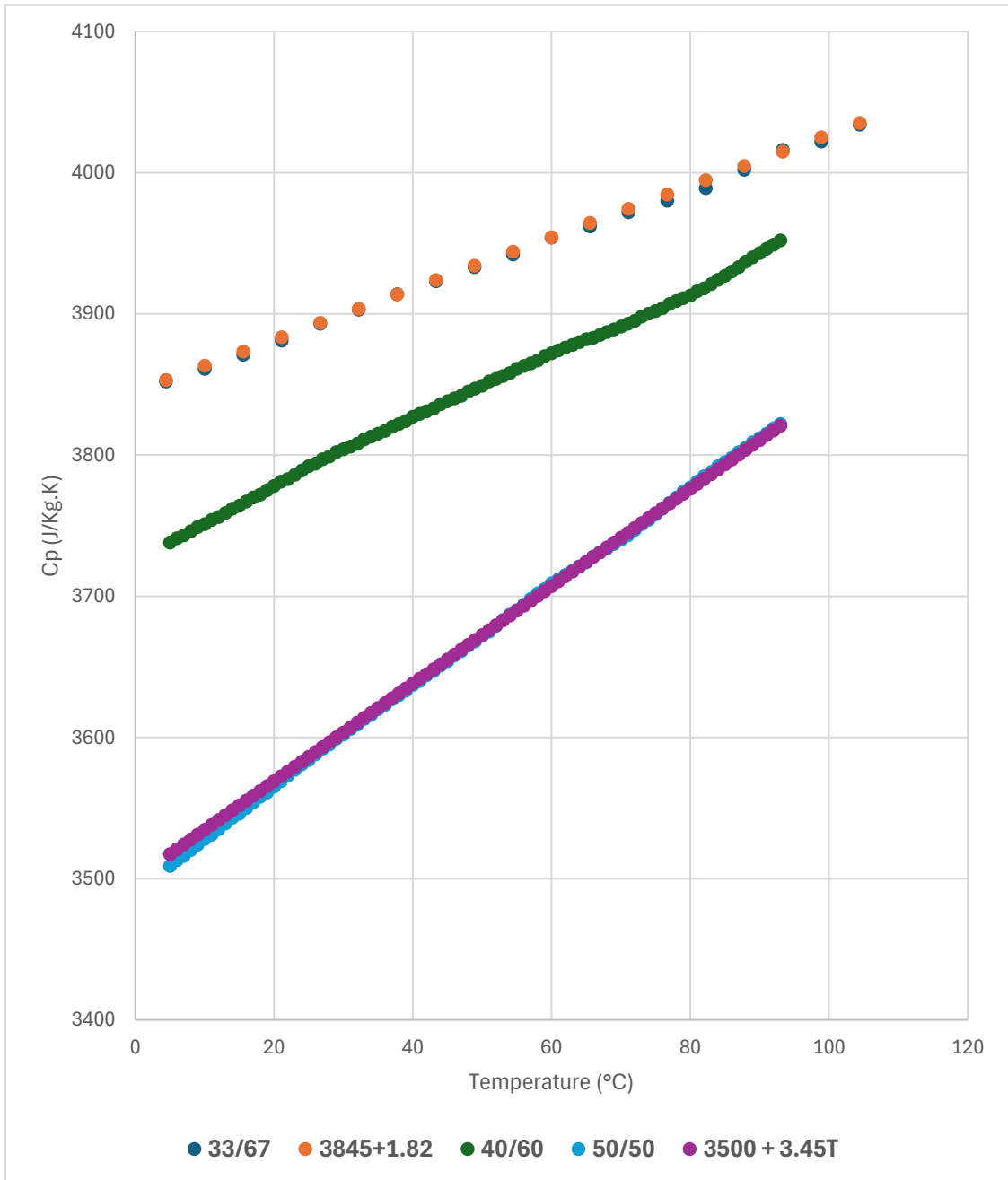
	A	B	C	d
Dim(in)	52	2	1/2"	3/4"
Dim(mm)	305	51	13	19

B.4. WATER TANK

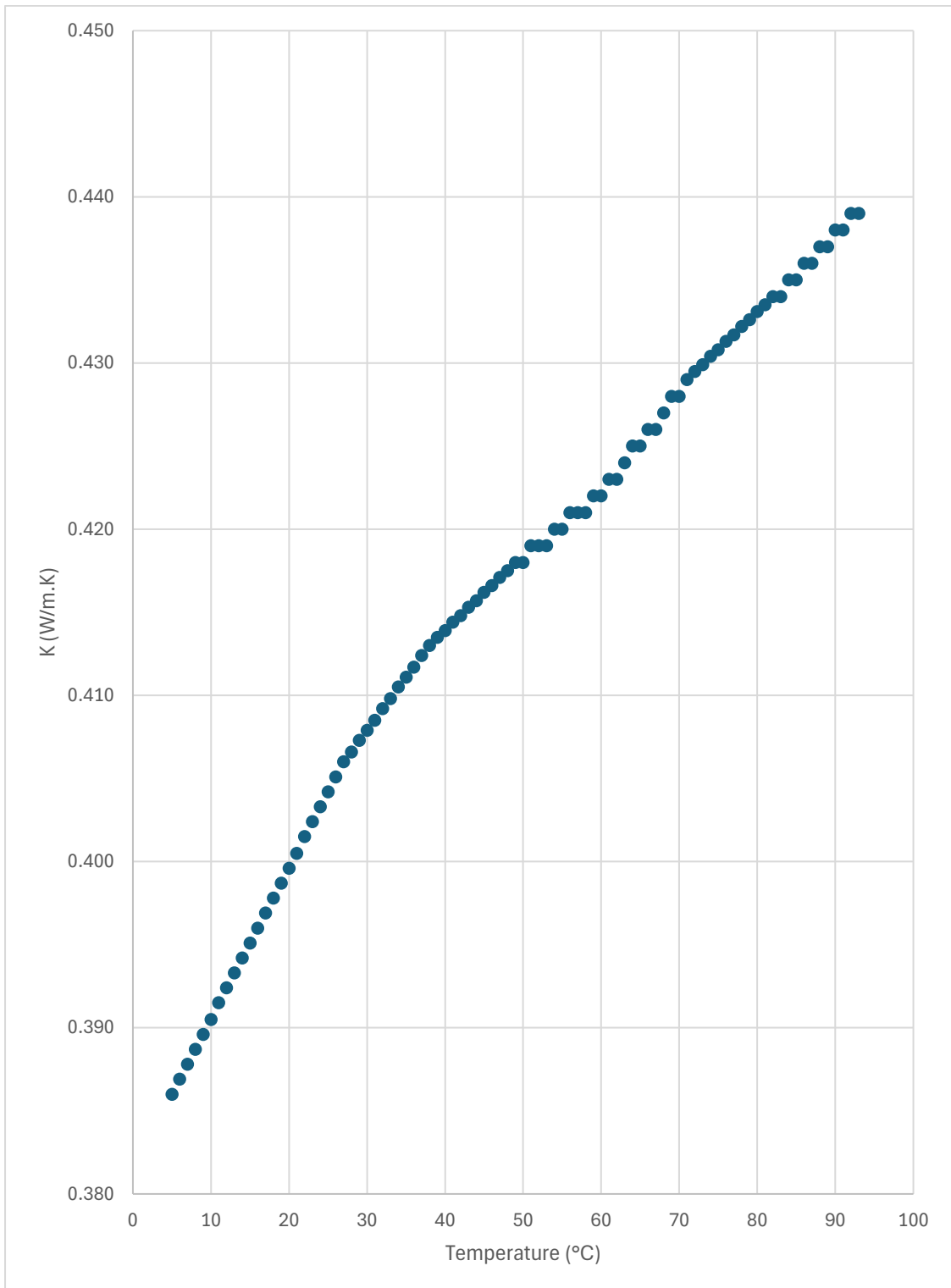


APPENDIX C.

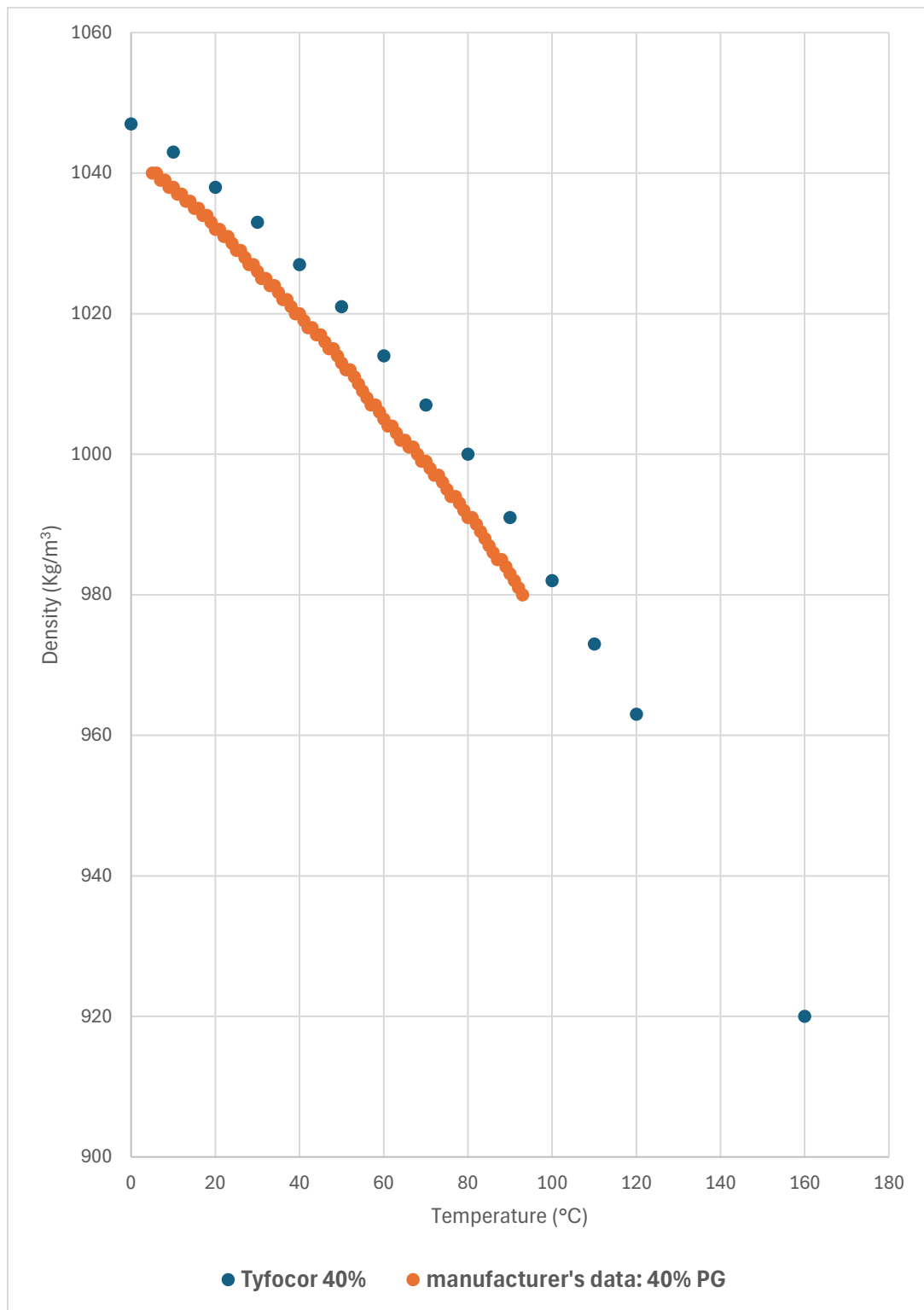
C.1. SPECIFIC HEAT OF PROPYLENE GLYCOL (40%)



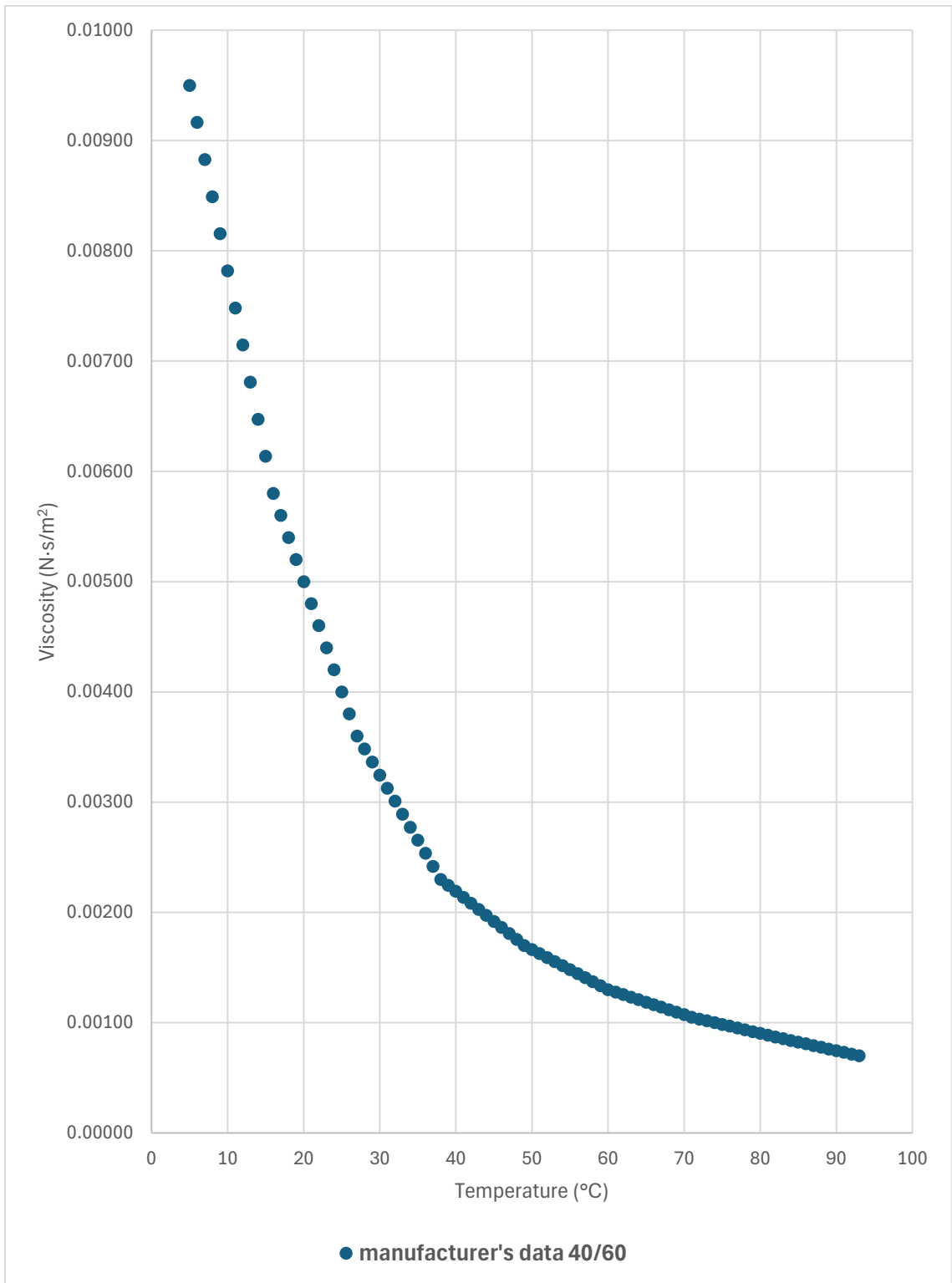
C.2. THERMAL CONDUCTIVITY OF PROPYLENE GLYCOL (40%)



C.3. DENSITY OF PROPYLENE GLYCOL (40%)



C.4. DYNAMIC VISCOSITY OF PROPYLENE GLYCOL (40/60)



APPENDIX D.

D.1. PL HEAT EXCHANGER'S PERFORMANCE BY SEC LTD.

Heat Exchanger Type	Nominal Capacity		Hot Water			Cold Water			Heat Transfer Surface	
			Flow	Pressure drop		Flow	Pressure drop		m ²	ft ²
	kW	Btu/hr	l/min	kPa	psig	l/min	kPa	psig		
PL/PLT 45	13	45,000	23	6.2	0.90	150	7.4	1.07	0.150	1.62
PL/PLT 70	20	70,000	25	7.5	1.09	170	9.2	1.33	0.246	2.64
PL/PLT 130	38	130,000	27	8.1	1.17	200	11.4	1.65	0.339	3.64
PL/PLT 180	53	180,000	30	2.7	0.40	210	7.5	1.1	0.440	4.70
PL/PLT 250	73	250,000	35	4.2	0.60	270	12.0	1.7	0.630	6.80
PL/PLT 300	88	300,000	40	6.4	0.90	300	17.0	2.5	0.840	9.00
PL/PLT 500	146	500,000	55	9.2	1.30	360	22.0	3.2	1.560	16.80
PL/PLT 1000	293	1,000,000	95	16.2	2.35	705	29.1	4.22	1.970	21.21

Nominal values are based on 60°C temperature between incoming heating and heated water.

D.2. M14A HEAT EXCHANGER'S PERFORMANCE BY SEC LTD.

Domestic Hot Water Performance Chart for SEC Brazed Plate Heat Exchangers															
Water Flow GPM	Water Inlet Temp	Water Outlet Temp	Boiler Flow GPM	Boiler Inlet Temp	Boiler Outlet Temp	Btu/hr	Model M14	PSI Hot Side	PSI Cold Side	Model M31	PSI Hot Side	PSI Cold Side	Model M110	PSI Hot Side	PSI Cold Side
0.40	40F	140F	2.03	180F	160F	20,000	M14-6	1.91	0.09						
0.60	40F	140F	3.05	180F	160F	30,000	M14-6	4.17	0.20						
0.80	40F	140F	4.07	180F	160F	40,000	M14-10	2.73	0.13						
1.00	40F	140F	5.08	180F	160F	50,000	M14-10	4.21	0.20						
1.20	40F	140F	6.10	180F	160F	60,000	M14-20	1.63	0.07						
1.40	40F	140F	7.11	180F	160F	70,000	M14-20	2.19	0.10	M31-20	1.73	0.09			
1.60	40F	140F	8.13	180F	160F	80,000	M14-20	2.84	0.13	M31-20	2.23	0.11			
1.80	40F	140F	9.15	180F	160F	90,000	M14-20	3.56	0.17	M31-20	2.79	0.14			
2.00	40F	140F	10.17	180F	160F	100,000	M14-20	4.37	0.21	M31-20	3.41	0.17			
2.50	40F	140F	12.70	180F	160F	125,000	M14-30	3.26	0.15	M31-20	5.20	0.27			
2.80	40F	140F	14.23	180F	160F	140,000	M14-30	4.06	0.19	M31-30	3.02	0.15			
3.00	40F	140F	15.25	180F	160F	150,000	M14-30	4.65	0.22	M31-30	3.45	0.18	M110-20	1.53	0.09